Tesis Doctoral

Modelling and experimental investigation on the processes involved in the indirect solar drying of Granny Smith apples

Autora
Lucía Blanco Cano

Director
Ulpiano Ruiz-Rivas Hernando
Co-director
Antonio Soria Verdugo

DEPARTAMENTO DE INGENIERÍA TÉRMICA Y DE FLUIDOS

Leganés (Madrid), Junio 2016

Tesis doctoral

Modelling and experimental investigation on the processes involved in the indirect solar drying of Granny Smith apples

Autora: Lucía Blanco Cano

Director de Tesis: Ulpiano Ruiz-Rivas Hernando

Co-director de Tesis: Antonio Soria Verdugo

Firma del Tribunal Calificador:

Firma

Presidenta: Dra. Dña. Mercedes de Vega Blázquez

Secretaria: Dra. Dña. María Teresa Miranda García Cuevas

Vocal: Dra. Dña. Verónica Tricio Gómez

Suplente: Dr. D. José Antonio Almendros Ibáñez

Calificación:

Leganés (Madrid), 23 de Junio de 2016

DEPARTAMENTO DE INGENIERÍA TÉRMICA Y DE FLUIDOS
Escuela Politécnica Superior

Modelling and experimental investigation on the processes involved in the indirect solar drying of Granny Smith apples

Autora
Lucía Blanco Cano

Director de Tesis
Ulpiano Ruiz-Rivas Hernando
Co-director de Tesis
Antonio Soria Verdugo

Leganés (Madrid), Junio 2016

A mis padres,
a Jorge y a Juan

Agradecimientos

Llegado el final de esta tesis y de esta etapa, quería recoger una serie de agradecimientos a las muchas personas que han contribuido en este trabajo, tanto directamente, como creando un contexto favorable a su desarrollo.

En primer lugar quería dar las gracias a mis directores, Ulpiano y Antonio. Por sus grandes ideas, por su dedicación, y por enseñarme y acompañarme todo este tiempo.

Asimismo, me gustaría mostrar un agradecimiento muy especial a Luismi, por su gran generosidad y su grado de implicación en esta tesis. También quiero agradecer la valiosa ayuda que me ha aportado Reyes, y que siempre me ha ofrecido con gran disposición. Y por supuesto, al resto de compañeros y compañeras del Departamento, con quienes he pasado muchísimas horas y que han hecho de este tiempo una etapa inolvidable. A Cristina, por las gestiones eficaces. A Fer, Javi, y María, por compartir los ratos de entrenamiento. A Jesús, por tolerar mis extremas temperaturas de confort en el despacho. Y a todos los que han mostrado interés, tanto a nivel técnico como personal, por la tesis y por su autora.

A todo el grupo de Tecnologías Apropiadas, por incluirme, y por valorar estas líneas de investigación y hacer que sean valoradas. Y a Miriam, por además ser amiga.

A Javi y a Fernando, de Demede, por la asistencia técnica. A Ernesto y Guillermo, por evitar que se queme la instalación. A Ben, por ayudarme a elegir entre *in* y *at*. Al mejor entrenador del mundo, J.A. Reyes. A la gente de la Universidad de Oriente, de Santiago de Cuba, por acogerme.

Finalmente quiero agradecer a todas las personas importantes que están a mi lado, por ser maravillosas. A mis padres, mi hermano y mis primas, por el valor que le dan al conocimiento y, sobre todo, por ese gran sentido del humor. A mi padre además por la foto de la portada. A Juan, mi compañero de viaje. Y a mis incondicionales: Mihai, Juanjo, Laura, Jaime, Cris, Lucía, Nuria, Sonsoles, Ana, Sara, Myriam, Pilara y Esther. Por ser un apoyo permanente. Y por muchísimos momentos.

Resumen

Tradicionalmente, el secado de alimentos para su conservación se ha realizado mediante el calor generado en la combustión de biomasa o combustibles fósiles, o bien exponiendo los productos directamente al sol. Ambos métodos presentan ciertas desventajas: la combustión implica dependencia de recursos primarios y emisión de contaminantes a la atmósfera, mientras que exponer los productos directamente al sol conlleva un proceso de secado lento y posibles pérdidas de producto. Como alternativa para evitar dichas desventajas, los secaderos solares se conciben como una tecnología apropiada para operaciones de secado a pequeña escala, contando además con un gran potencial para proporcionar acceso, tanto a la energía como a la tecnología, a sociedades empobrecidas de zonas rurales del planeta. Pese a las ventajas que aporta la tecnología de secado solar y a la enorme cantidad de trabajo de investigación desarrollado en esta materia, los secaderos solares aún están lejos de reemplazar a los métodos tradicionales. La razón fundamental es la inmensa dispersión característica de los resultados de investigación en este campo, provocada tanto por la gran cantidad de parámetros que influyen en el proceso de secado, como por la compleja interacción entre ellos. El diseño de los secaderos solares engloba un amplio espectro de configuraciones y dimensiones, ya que el proceso de secado solar depende sustancialmente del producto a secar, estando además notablemente influido por el clima existente durante la operación. Estos hechos complican la unificación de los estudios de secado solar y, por tanto, la replicabilidad de los trabajos.

El objetivo de esta tesis doctoral es desarrollar un análisis general de los diferentes procesos implicados en las operaciones de secado solar, y estudiar su efecto en el funcionamiento global de un secadero solar indirecto. El estudio busca simplificar los modelos que predicen los complejos procesos de transferencia de calor y masa asociados al secado solar, con el fin de contribuir a la sistematización y unificación de la metodología de evaluación de esta tecnología.

Los secaderos solares constan de un sistema de calentamiento de aire basado en energía solar térmica, una cámara de secado y un sistema de circulación de aire, bien inducida por convección natural o bien forzada por un ventilador. En un secadero solar indirecto, el proceso de calentamiento de aire se lleva a cabo

en el colector solar y el proceso de secado sucede en la cámara de secado. De este modo, ambos procesos ocurren en serie y, por tanto, se pueden estudiar por separado, simplificando el problema. El trabajo desarrollado ha consistido en la realización de medidas experimentales en laboratorio, combinándolas con la modelización teórica de los citados procesos, pudiéndose desglosar en tres vertientes: la puesta en marcha de una instalación experimental, un estudio teórico de los procesos involucrados en el secado solar, para un caso general, y por último la modelización de los citados procesos, empleando manzana de tipo Granny Smith como aplicación y para la validación experimental de los modelos.

En primer lugar, se ha diseñado, construido y caracterizado un prototipo de secadero solar a escala de laboratorio, capaz de reproducir procesos de secado llevados a cabo bajo diferentes condiciones climáticas. La intención es replicar el proceso de secado que tendría lugar en campo en las condiciones controladas del laboratorio, pudiendo particularizarlo para cualquier clima y localización. Además el prototipo permite controlar de manera independiente los diferentes parámetros que influyen en el proceso de secado, lo que permite estudiar su efecto.

La segunda parte consiste en un estudio teórico, que viene motivado por el hecho de que la mayor parte del trabajo desarrollado en la literatura es específico para un secadero y un producto concretos. El trabajo consiste en analizar la capacidad evaporativa que se podría obtener en un secadero solar de tipo indirecto para un caso general. El estudio se basa en la evaporación de agua libre, como indicador general del potencial del secadero solar independientemente del producto, identificando los parámetros más relevantes del proceso y analizando su efecto. La validez del análisis engloba diferentes dimensiones de secaderos solares, dentro de las típicas en aplicaciones de pequeña escala. A partir de una simulación numérica del proceso de evaporacion de agua en la cámara, se deriva un modelo simplificado que calcula la capacidad evaporativa del secadero, basado en un número reducido de parámetros, del que se pueden extraer criterios de diseño y operación generales.

La tercera parte consiste en la modelización de los procesos que tienen lugar en el secadero y su posterior validación experimental. Esta parte comprende tanto el estudio del proceso de calentamiento de aire en el colector solar como el proceso de secado en la cámara. Para los experimentos se emplean las manzanas Granny Smith, identificando un clima característico de su época de recolección y reproduciéndolo en el laboratorio como clima de referencia.

Para el estudio del proceso de calentamiento de aire en el colector solar, que es el que establece las condiciones a la entrada de la cámara de secado y determina las condiciones de operación de la misma, se modelizan matemáticamente los mecanismos de transferencia de calor involucrados, tanto en estado estacionario como en transitorio, obteniéndose las temperaturas de los componentes del colector solar, así como la temperatura del aire a la salida de éste. Los resultados del modelo se validan con medidas experimentales obtenidas en el prototipo. Adicionalmente, se realiza una caracterización del colector solar del secadero de laboratorio, con el fin de evaluar su funcionamiento en el clima de referencia, determinando las condiciones de secado en las que operaría el sistema.

Para el estudio del proceso de secado se desarrolla un modelo capaz de predecir la curva de secado que se obtendría en condiciones variables de temperatura, características de un proceso solar, a partir de la cinética obtenida con condiciones constantes, que es el método más extendido en la literatura. El objetivo del modelo es enlazar los trabajos en cinética de secado con los de secado solar. La cinética de secado de las manzanas Granny Smith se determina empleando un analizador termogravimétrico (TGA) a temperatura constante. A partir del modelo se predice la curva que se obtendría a las condiciones de secado establecidas por el colector. El modelo se valida experimentalmente con medidas efectuadas tanto en la TGA como en el prototipo de secadero solar.

Abstract

Drying of food for its preservation is traditionally carried out using the heat produced by burning fossil fuels or biomass in a furnace, or directly by open-air sun drying. These two methods present several disadvantages. Burning fuel entails dependence on such resources and implies pollution. Exposing the products directly to the sun results in slow processes and product losses. As an alternative to avoid the inconveniences of these two traditional methods, solar dryers are considered as an Appropriate Technology for small-scale drying operations. Moreover, they have a great potential to bring access to energy and technology to impoverished societies in rural areas of the planet. Despite of the advantages of solar drying technology and the high amount of research work developed on this topic, solar dryers are still far from replacing the traditional methods. This may be attributed to the high dispersion of the investigation results, caused by the high amount of parameters affecting the drying process, and the complex interaction between them. Solar dryers are designed in a wide variety of configurations and dimensions. A solar drying process depends substantially on the product to be dried and, furthermore, it is highly affected by the climate during the operation. These facts complicate the unification of studies on solar drying, and thus the replicability of the works.

The objective of this PhD thesis is to develop a comprehensive analysis of the different processes involved in indirect solar drying operations, and to study their effect on the global performance of an indirect solar dryer. The study is an attempt to simplify the models to predict the complex heat and mass transfer processes involved in solar drying. This could contribute to the systematization and unification of the methodology of evaluation of solar drying processes.

Solar dryers consist mainly on air circulating (by natural convection or impelled by a fan) through an air heating system, based on solar thermal energy, and a drying chamber. In an indirect solar dryer, the air heating process takes place in the solar collector and the drying process is carried out in the drying chamber, and thus both processes occur in series. Hence, they can be studied separately, simplifying the problem. The work developed in this thesis is based on laboratory experiments combined with the theoretical modelling of the processes involved in the indirect solar dryer operation. The study is outlined in three main parts: i) the experimental set-up, design and characterization, ii) a

theoretical study of the processes involved in solar drying, for a general case, and iii) the mathematical modelling of such processes, using Granny Smith apples as an application, and for the experimental validation of the models.

In the first part, a lab-scale indirect solar dryer has been designed, constructed and characterized in order to reproduce solar drying processes at a wide range of climates. The aim is to replicate the processes that would take place on site, for any particular location and climate, and under laboratory-controlled conditions. Additionally, the installation can control independently the different parameters that affect the drying process, enabling to study their effect.

In the second part, motivated by the fact that most of the research work is specific for a dryer and a product, a theoretical study on the maximum evaporation rate that can be obtained in indirect solar dryers of small-scale is presented. The processes are modelled for a general case rather than a specific one. The study is based on the evaporation of free water, as a generalized indicator of the potential of the solar dryer, independently of the product. The study is valid for different solar dryer dimensions, within the typical range of small-scale operations. A numerical simulation of the process of free water evaporation in the drying chamber is developed, selecting the most affecting parameters. From the results, a simplified model for the calculation of the maximum evaporation rate is derived, based on a reduced number of parameters, enabling to study their effect and to extract design and operation criteria for indirect solar dryers.

In the third part, the modelling of the processes involved in an indirect solar drying operation are presented: a model of the air heating process to determine the drying conditions, and a model to predict the drying curve in the drying chamber at such conditions. The models are experimentally validated using the results obtained in the drying of Granny Smith apples. A climate characteristic of the harvest season of such variety of apples is identified and reproduced in the laboratory.

For the study of the air heating process, the heat transfer mechanisms in the solar collector are mathematically modelled, for both steady state and transient conditions. The model predicts the temperatures of the components of the solar collector, and the temperature of the airflow at the outlet of the collector, i.e. the temperature at which the drying process begins. The model results are validated with the experimental measurements conducted in the lab-scale indirect solar dryer. Additionally, the solar collector of the lab-scale solar dryer is characterized, in order to asses its thermal performance under the reference

climate, and to determine the drying conditions at which the drying process would take place.

For the study of the drying process, a model to predict the drying curve in the drying chamber at the conditions established by the solar collector is presented. The model is based on the drying kinetics of the product, determined at constant temperature, which is the most extended method in the literature. The aim of this model is to apply the works on drying kinetics obtained at isothermal conditions, to the solar drying process, characterized by variable drying conditions. The drying kinetics of slices of Granny Smith apples is determined in a thermogravimetric analyser (TGA) and in the lab-scale solar dryer, based on the thin-layer equations, at isothermal conditions. The drying curve that would be obtained in a solar dryer at variable drying conditions is estimated using the model developed. The results are validated with experimental measurements carried out in both the TGA and the solar dryer.

Contents

List of Figures

List of Tables

CHAPTER

ONE

Introduction

Contents

1.1 Introduction

Drying agricultural products enhances their storage life, minimises losses during storage, and saves transportation costs (Leon *et al.*, 2002). The drying processes of such products generally demand a relative low thermal power, extended for long time periods. Hence, solar thermal energy is applicable for drying purposes (Vijaya *et al.*, 2012).

The first known drying installation was a solar dryer, located in France and dated at 8000 BC. Similar installations have been found in many places in the world, dated between 7000 BC and 3000 BC. They typically combined solar radiation and natural air circulation, mainly for drying of food. Drying in furnaces burning wood is a more recent technique. The industry of conventional drying started at the 18^{th} century, together with the industries associated with other methods of food preservation (Belessiotis & Delyannis, 2011). Nowadays, drying by burning wood or fossil fuels in furnaces or open-air sun drying (i.e. exposing the product directly to the sun) are still the most extended methods for small-scale drying of food.

The development of Appropriate Technology for food drying, based on solar thermal energy, presents several advantages over these two methods. On one side, using solar thermal energy instead of burning wood or fossil fuels reduces the dependence on those resources and contribute to the reduction of pollution. On the other side, using solar dryers instead of open-air sun drying, prevents product losses and enhances the product quality, since open-air sun drying is a relatively slow process and the product is uncovered, and thus considerable losses and reduction of the product quality occur (Vijaya *et al.*, 2012).

Therefore, solar drying is a widely investigated method for preservation or processing of a wide variety of products; such as agricultural (Kumar *et al.*, 2016), marine (Fudholi *et al.*, 2010), biomass by-products (Montero *et al.*, 2010, 2015), wood (Pirasteh *et al.*, 2014), herbs (Panchariya *et al.*, 2002), cereals (Zomorodian *et al.*, 2007) or fruits (Al-Juamily *et al.*, 2007). Solar drying of fruits is specifically relevant. Many experimental works have been reported in the literature in the last few years on a variety of products such as grapes (Elkhadraoui *et al.*, 2015), tomatoes (Ringeisen *et al.*, 2014), mangos (Dissa *et al.*, 2011), or strawberries (El-Beltagy *et al.*, 2007), among others. Despite the amount of research work available, most of it, and particularly when developed in small-scale dryers, is specific for a dryer and a product.

The use of solar drying is feasible under many different climates. Several works of solar dryers operating under different climates have been reported in the literature, such as tropical (Koua *et al.*, 2009), temperate (Rosselló *et al.*, 1990), dry (Boughali *et al.*, 2009), or continental (Romano *et al.*, 2009). The performance of any solar dryer is strongly dependent on the climate (Singh & Kumar, 2012).

The majority of the solar dryers are based on small-scale equipments, rather than in large-scale facilities for industrial production. Solar drying has not been widely commercialized yet, and thus most of the solar dryers are generally based on empirical data rather than in theoretical designs (Belessiotis & Delyannis, 2011). Many attempts to define standard procedures to test the performance of solar dryers and to compare one solar dryer to another have been done in literature (Jannot & Coulibaly, 1998; Leon *et al.*, 2002; Singh & Kumar, 2012; Altobelli *et al.*, 2014). From the literature review, it can be concluded that there is a lack of unification and standardization in the evaluation of the performance of solar dryers. This can be attributed to the great amount of parameters affecting the drying process, and the complex interaction among them.

When drying a specific product, it is important to know the behaviour of

such product under the particular drying conditions at which it is dried, in terms of the rate at which moisture is extracted from the product. This behaviour is defined by the drying kinetics of the product. Since the drying kinetics is strongly dependent on the drying conditions, it is generally determined at constant drying conditions (Akpinar, 2006; Doymaz, 2009). However, a solar drying process is characterized by variable drying conditions. When the drying kinetics determined at constant conditions is applied to solar drying process, it is by means of simulations of the process in the drying chamber (Karim & Hawlader, 2005; Janjai *et al.*, 2009). Since simultaneous heat and mass transfer occur, those simulations are highly complex. Hence, a relation between the drying kinetics determined at constant conditions and the solar drying performed at variable conditions could contribute to apply the results obtained from the works on drying kinetics to solar drying.

Apples are selected as the test product in this thesis since they are an important raw material produced all around the world (Kaya *et al.*, 2007). Dried apples can be consumed directly or treated as a secondary raw material (Velić *et al.*, 2004). Apples are dried using different methods, such as convective drying (Zlatanović *et al.*, 2013), microwave drying (Contreras *et al.*, 2008), infra-red drying (Toğrul, 2005), fluidized bed (Kaleta *et al.*, 2013), or solar drying (El-Sebaii *et al.*, 2002). The variety of apples named Granny Smith is characterized by growing in areas with climates relatively warm (Vega-Galvez *et al.*, 2012) which makes this variety suitable for solar drying. Solar drying of different varieties of apples has been reported in literature; such as red Jonathan (Romano *et al.*, 2009) or Jonagold (Lamnatou *et al.*, 2012). However, no experiences on Granny Smith have been found.

This PhD thesis presents theoretical and laboratory-based experimental studies on the processes involved in the indirect solar drying of agricultural products. A lab-scale solar dryer was designed, constructed and tested, to reproduce solar drying processes for different climates, under the controlled conditions of a laboratory. As an application, the solar drying process of Granny Smith apples is analysed, replicating the climate characteristic of the harvest season of this variety of apples.

1.2 Fundamentals

The main concepts related to the work developed in this thesis are summarized in this section. An overview of the drying principles and the solar drying

technology is presented.

1.2.1 Drying principles

Drying is the operation of reducing the moisture contained in a product. Drying involves simultaneous heat and mass transfer processes. The heat is transferred from the surrounding air to the product surface, and from the surface to the inside of the product. The mass (water) transfer occurs by means of two mechanisms: the diffusion of moisture from the interior of the product to its surface, and the convection of the moisture from the surface of the product to the drying airflow. Since drying involves evaporation, it is an operation that demands a relative high amount of energy.

The water contained in a product can be unbounded (free water) or bounded (trapped inside the product). The products that only contain unbounded water are called non-hygroscopic, whereas the product containing bounded water, or both, are known as hygroscopic. Agricultural products are typically hygroscopic (Belessiotis & Delyannis, 2011), and thus the mass transfer mechanism governing the process is the diffusion of the moisture in the interior of the product (Panchariya *et al.*, 2002).

When drying a product at constant drying conditions, the process occurs in two differentiated phases: i) the constant rate drying period and ii) the falling rate drying period. Prior to the constant rate period, an initial adjustment might exist since the surface and the air may not be at thermal equilibrium. However, this initial period is too short and it is normally ignored (Treybal, 1980). Then, the constant rate begins, consisting of the evaporation of the free superficial water covering the product. When the diffusion of moisture through the product is not rapid enough to replace the water evaporated from the surface, which becomes unsaturated, the falling rate period begins. The falling rate period is governed by the diffusion mechanisms within the product. The whole drying process of agricultural products typically occurs in the falling rate period (Ahmad-Qasem *et al.*, 2013; Montero, 2005; Evin, 2012; Panchariya *et al.*, 2002), and thus the drying kinetics of each specific product needs to be individually determined.

1.2.2 Solar drying technology

Solar drying may be performed employing many different types of solar dryers, with different geometries, dimensions and configurations, depending on the

application. A recent review was presented by Vijaya *et al.* (2012). Solar dryers normally consist of an airflow circulating (by means of a fan or by natural convection) through an air heating system and a drying chamber.

The main classification of solar dryers divides them into active or passive on one side, and direct, indirect or mixed on the other side (Ekechukwu & Norton, 1999). The distinction between active or passive relies on the nature of the airflow motion. Passive dryers are based on natural convection, whereas active dryers use a fan to induce the air circulation. The classification in direct, indirect or mixed mode is carried out regarding whether the product is directly exposed to the sun radiation or not. In direct solar dryers, the product is located in a drying chamber that has, at least, one transparent wall, and so the product is exposed to solar radiation while drying. In indirect solar dryers, the air is preheated in a solar collector, and the drying chamber is opaque to solar radiation. Mixed mode solar dryers combine both types, preheating the air in a solar collector but also exposing the product in the drying chamber to solar radiation.

Active and indirect solar dryers are selected in this work among the different types of solar dryers due to the following. In indirect solar dryers the product is protected against deterioration caused by the direct exposure to the solar radiation. Regarding active or passive solar dryers, it is agreed that active solar dryers are more effective and more controllable than passive solar dryers (Weiss & Buchinger, 2004).

1.3 Appropriate Technology

The solar drying technology has a potential to improve the access to energy systems of the rural poor areas. It is also a disruptive technology that may replace other available technological solutions addressing the same problem, thus making significant changes to the society, for those and other regions. In this two senses it is very linked to the Appropriate Technology movements. In this section, a briefing of such movements, that have acted in the last 50 years is given, in order to locate the investigation on small-scale solar dryers inside a broad technology movement with proposals, methods, procedures and lessons learned.

The term Appropriate Technology (AT) is commonly used to refer to a technology that considers in its design the socio-economic, cultural or environmental context of the location where it is going to be used, especially in

developing areas. There is a large variety of individual efforts and even organized movements that have focused on the problem of technology design, from the early 1970's up to now. The AT movement includes different philosophies, action plans and even different rules of technology design. Although the problem of designing for the poor is, of course, far to be solved, the AT movement has had a relevant impact in developing countries.

The movement has its basis on several theoretical proposals published in the early 1970s, including E.F. Schumacher's *Small is Beautiful* (Shumacher, 1973). The large repercussion of this publication enabled the creation of several large AT organizations, such as Intermediate Technology (now Practical Actions) in UK, Appropriate Technology International in USA, People Science Movement in India, or German Appropriate Technology Exchange in Germany. These groups performed relevant work in the last decades of the 20th century, and some of them are still working.

Within the target technology of these initiatives, solar thermal equipment is included, and in particular solar dryers, which has resulted in many different reports and handbooks about solar drying. Practical Action has published several books, handbooks and technical briefs. Some examples are the technical brief *Solar Drying* (Swetman, 2007) or the book *Drying: Food Cycle Technology* (ITDG & UNIFEM, 1995). The encyclopedic Appropriate Technology Sourcebook, compiled by Ken Darrow and Mike Saxenian, includes more than 20 books related to solar drying. The development of solar drying technology is also in the Agenda of the main international organisms such as FAO, which has a specific platform for developing of post-harvest technologies, including solar drying (FAO, 2006); or UNESCO, which has also developed technical material (Daguenet, 1989). Furthermore, solar drying technology is included within the 50 breakthroughs (in the second position), which are a collection of the main scientific and technological advances needed for sustainable global development (Buluswar *et al.*, 2014).

It is quite complex to resume the findings of the large variety of initiatives revised in this section to come out with definite rules for a technology to be "appropriate" or simply useful. Nevertheless, some characteristics are summarized below. Among them, most apply to the solar thermal technology.

- Sustainable, both environmentally and socially.
- Based on small-scale production.

- Whenever possible, local available materials should be employed for construction.
- Easy to repair by local people that may not have access to high technical training.
- Based on cheap energy, if possible renewable, and clean.
- The production of waste should be minimized, and whenever waste is generated, recycling should be considered.
- Locally accepted, having the possibility to be adapted by the community at its convenience.
- Affordable throughout its life cycle, from its construction costs to its operation and maintenance, and its removal.
- It should be considered in the design whether the system is going to be used by individuals or by a community.
- Respectful with cultural issues.
- Open source, to allow the user intervening in the technology.
- Design of public domain.
- Low complexity of design, operation and maintenance.
- There is a general discussion about the design to be standardized or particular to each situation.

Solar drying technology could be considered as an Appropriate Technology, for the reasons already mentioned and since most of the previous characteristics could be accomplished. Moreover, the solar drying technology has an important role in developing countries for several practical reasons (Mahapatra & Imre, 1990):

- There is a significant reduction of drying time compared to open-air sun drying.
- The quality of the dried product is enhanced, compared to that dried at open air. The farmer has a potential greater income throughout the production of marketable crops.

- The additional costs required for the installation of solar dryers can be recovered since the product may be placed in the market.
- Most of the developing countries are located in the warmest area of the planet, where the irradiation is higher than the world average, and thus there is a high potential for the use of solar dryers.

Therefore, the solar drying technology has a great potential to improve the agricultural sector, and it might create opportunities for small producers to access the local market.

Despite the great amount of material developed on this field and the cited potential and advantages of the solar drying technology, it is still far from being the most extended practice in small-scale drying operations. This may be attributed to the lack of homogenization in the works developed, or to the fact that the high complexity of the processes involved in solar drying requires specific studies for every product and conditions of use, not being a replicable technology under different operating conditions. Solar drying processes are difficult to control in a simple way, and thus the particular characterization of the specific drying operations needs to be done, which complicates the unification of the studies.

This thesis is an attempt to provide with, on one side, a fundamental study of the processes involved in solar drying for a general case, and, on the other side, an experimental study and the mathematical modelling of the processes involved in an indirect solar drying process. The adequation and the appropriation of the technology has been widely treated in all the cited materials and many others and it is not in the scope of this thesis.

1.4 Outline of this thesis

The thesis is composed mainly of a general theoretical study, motivated by the lack of unification reported in the literature, and a laboratory-based experimental study on indirect solar drying processes, combined with mathematical modelling, in which the heating process of airflow and the drying process of the product are studied independently.

For the experimental analysis, a lab-scale indirect solar dryer has been designed, constructed and characterized. The aim of the installation is to simulate the drying conditions on field, but in a controlled manner, enabling to reproduce different drying processes at different climates and locations.

The description and characterization of the lab-scale solar dryer is detailed in Chapter 2. First, a climate corresponding to the harvesting period of the Granny Smith apples (the reference product selected in this thesis) is identified and characterized, to be reproduced in the laboratory. Then, the experimental facility is described, together with the measurement and control systems. The characterization of the control system to assure a stable operation is detailed in a specific section. Some auxiliary laboratory facilities, which have been used to conduct the experiments, are also described in Chapter 2. Finally, a procedure for the determination of the moisture content of the Granny Smith apples is presented.

Chapter 3 is a theoretical study on the maximum evaporation rate that can be obtained in indirect solar dryers, within the typical range of dimensions of small-scale dryers. The study is based on a fundamental study on the drying capacity of the airflow and the pick-up efficiency of the drying process (defined as the actual amount of moisture absorbed compared to the drying capacity), for evaporation of free water. The evaporation of free water would settle the maximum evaporation rate since the constrictions due to the drying kinetics of a product are not considered. The aim is to study the effect of the different affecting parameters on the maximum evaporation rate. A simplified model for the calculation of the maximum evaporation rate is presented, based on a reduced number of parameters to study their effect. The simplified model is derived from a numerical simulation of the evaporation process of free water in the drying chamber.

Chapter 4 presents a study on the air heating process that takes place in the solar collector. A theoretical modelling of the air heating process is presented, and validated with experiments conducted in the laboratory. A characterization of the solar air heater performance is also presented. Finally, the drying conditions characteristic of the solar dryer operating at the reference climate are determined.

Chapter 5 is a study on the drying kinetics of the Granny Smith apples. The drying kinetics are determined using a thermogravimetric analyser (TGA) at isothermal conditions. The drying curves obtained are modelled with thin-layer equations available in the literature. A mathematical model that predicts the drying curve at variable drying conditions is presented and experimentally validated with the TGA. The model is then applied to the solar drying process, predicting the drying curve that would be obtained when drying Granny Smith apples in the solar dryer, for the climate considered. The model is validated with

experimental measurements carried out in the lab-scale indirect solar dryer.

The results of the whole study are summarized in Chapter 6, where the main conclusions are presented.

References

Ahmad-Qasem, M. H., Barrajon-Catalan, E., Micol, V., Cárcel, J. A. & Garcia-Perez, J. V. 2013 Influence of air temperature on drying kinetics and antioxidant potential of olive pomace. *Journal of Food Engineering* 119 (3), 516–524.

Akpinar, E. K. 2006 Determination of suitable thin layer drying curve model for some vegetables. *Journal of Food Engineering* 73 (3), 75–84.

Al-Juamily, K. E. J., Khalifa, A. J. N. & Yassen, T. A. 2007 Testing of the performance of a fruit and vegetable solar drying system in Iraq. *Desalination* 209 (1-3 SPEC. ISS.), 163–170.

Altobelli, F., Condorí, M., Duran, G. & Martinez, C. 2014 Solar dryer efficiency considering the total drying potential. Application of this potential as a resource indicator in north-western Argentina. *Solar Energy* 105, 742–759.

Belessiotis, V. & Delyannis, E. 2011 Solar drying. *Solar Energy* 85 (8), 1665–1691.

Boughali, S., Benmoussa, H., Bouchekima, B., Mennouche, D., Bouguettaia, H. & Bechki, D. 2009 Crop drying by indirect active hybrid solar - Electrical dryer in the eastern Algerian Septentrional Sahara. *Solar Energy* 83 (12), 2223–2232.

Buluswar, S., Friedman, Z., Mehta, P., Mitra, S. & Sathre, R. 2014 *50 breakthroughs-Critical scientific and technological advances needed for sustainable global development*. Institue for Globally Transformative Technologies Lawrence Berkeley National Lab.

Contreras, C., Martín-Esparza, M. E., Chiralt, A. & Martínez-Navarrete, N. 2008 Influence of microwave application on convective drying: Effects on drying kinetics, and optical and mechanical properties of apple and strawberry. *Journal of Food Engineering* 88 (1), 55–64.

Daguenet, M. 1989 Les sechoirs solaires, theorie et practique. *Tech. Rep.*. UNESCO.

Dissa, A. O., Bathiebo, D. J., Desmorieux, H., Coulibaly, O. & Koulidiati, J. 2011 Experimental characterisation and modelling of thin layer direct solar drying of Amelie and Brooks mangoes. *Energy* 36 (5), 2517–2527.

Doymaz, I. 2009 An Experimental Study on Drying of Green Apples. *Drying Technology* 27 (October 2014), 478–485.

Ekechukwu, O. V. & Norton, B. 1999 Review of solar-energy drying systems II: an overview of solar drying technology. *Energy Conversion and Management* 40 (6), 615–655.

El-Beltagy, A., Gamea, G. R. & Essa, A. H. A. 2007 Solar drying characteristics of strawberry. *Journal of Food Engineering* 78 (2), 456–464.

El-Sebaii, A. A., Aboul-Enein, S., Ramadan, M. R. I. & El-Gohary, H. G. 2002 Experimental investigation of an indirect type natural convection solar dryer. *Energy Conversion and Management* 43 (16), 2251–2266.

Elkhadraoui, A., Kooli, S., Hamdi, I. & Farhat, A. 2015 Experimental investigation and economic evaluation of a new mixed-mode solar greenhouse dryer for drying of red pepper and grape. *Renewable Energy* 77, 1–8.

Evin, D. 2012 Thin layer drying kinetics of Gundelia tournefortii L. *Food and Bioproducts Processing* 90 (2), 323–332.

FAO 2006 Dryer construction for solar dried fruit and vegetables production. *Technologies and practices for small agricultural producers* .

Fudholi, A., Sopian, K., Ruslan, M. H., Alghoul, M. A. & Sulaiman, M. Y. 2010 Review of solar dryers for agricultural and marine products. *Renewable and Sustainable Energy Reviews* 14 (1), 1–30.

ITDG & UNIFEM 1995 *Drying. Food Cycle Technology*. London, UK: Intermediate Technology Publications.

Janjai, S., Lamlert, N., Intawee, P., Mahayothee, B., Bala, B. K., Nagle, M. & Müller, J. 2009 Experimental and simulated performance of a PV-ventilated solar greenhouse dryer for drying of peeled longan and banana. *Solar Energy* 83 (9), 1550–1565.

Jannot, Y. & Coulibaly, Y. 1998 The " Evaporative Capacity " As a Performance Index for a solar-drier air-heater. *Solar Energy* 63 (6), 387–391.

Kaleta, A., Gornicki, K., Winiczenko, R. & Chojnacka, A. 2013 Evaluation of drying models of apple (var. Ligol) dried in a fluidized bed dryer. *Energy Conversion and Management* 67, 179–185.

Karim, M. A. & Hawlader, M. N. A. 2005 Mathematical modelling and experimental investigation of tropical fruits drying. *International Journal of Heat and Mass Transfer* 48 (23-24), 4914–4925.

Kaya, A., Aydin, O. & Demirtas, C. 2007 Drying Kinetics of Red Delicious Apple. *Biosystems Engineering* 96 (4), 517–524.

Koua, K. B., Fassinou, W. F., Gbaha, P. & Toure, S. 2009 Mathematical modelling of the thin layer solar drying of banana, mango and cassava. *Energy* 34 (10), 1594–1602.

Kumar, M., Sansaniwal, S. K. & Khatak, P. 2016 Progress in solar dryers for drying various commodities. *Renewable and Sustainable Energy Reviews* 55, 346–360.

Lamnatou, C., Papanicolaou, E., Belessiotis, V. & Kyriakis, N. 2012 Experimental investigation and thermodynamic performance analysis of a solar dryer using an evacuated-tube air collector. *Applied Energy* 94, 232–243.

Leon, M. A., Kumar, S. & Bhattacharya, S. C. 2002 A comprehensive procedure for performance evaluation of solar food dryers. *Renewable and Sustainable Energy Reviews* 6 (4), 367–393.

Mahapatra, A. K. & Imre, L. 1990 Role of solar-agricultural drying in developing countries. *International Journal of Ambient Energy* 11 (4), 205–210.

Montero, I. 2005 Modelado y construcción de un secadero solar híbrido para residuos biomásicos. PhD thesis, Universidad de Extremadura.

Montero, I., Blanco, J., Miranda, T., Rojas, S. & Celma, A. R. 2010 Design, construction and performance testing of a solar dryer for agroindustrial by-products. *Energy Conversion and Management* 51 (7), 1510–1521.

Montero, I., Miranda, T., Sepúlveda, F., Arranz, J., Rojas, C. & Nogales, S. 2015 Solar Dryer Application for Olive Oil Mill Wastes. *Energies* 8 (12), 14049–14063.

Panchariya, P. C., Popovic, D. & Sharma, A. L. 2002 Thin-layer modelling of black tea drying process. *Journal of Food Engineering* 52 (4), 349–357.

Pirasteh, G., Saidur, R., Rahman, S. M. A. & Rahim, N. A. 2014 A review on development of solar drying applications. *Renewable and Sustainable Energy Reviews* 31, 133–148.

Ringeisen, B., Barrett, D. M. & Stroeve, P. 2014 Concentrated solar drying of tomatoes. *Energy for Sustainable Development* 19 (1), 47–55.

Romano, G., Kocsic, L. & Farkas, I. 2009 Analysis of energy and environmental parameters during solar cabinet drying of apple and carrot. *Drying Technology* 27 (4), 574–579.

Rosselló, C., Bema, A. & Mulet, A. 1990 Solar Drying of Fruits in a Mediterranean Climate. *Drying Technology* 8 (2), 305–321.

Shumacher, F. E. 1973 *Small is Beautiful: A study on economics as if people mattered*. Blond & Briggs.

Singh, S. & Kumar, S. 2012 Testing method for thermal performance based rating of various solar dryer designs. *Solar Energy* 86 (1), 87–98.

Swetman, T. 2007 Solar drying. *Tech. Rep.*. Practical Action.

Toğrul, H. 2005 Simple modeling of infrared drying of fresh apple slices. *Journal of Food Engineering* 71 (3), 311–323.

Treybal, R. E. 1980 *Mass-Transfer Operations*, 3rd edn. United States of America: McGraw-hill Book Company.

Vega-Galvez, A., Ah-Hen, K., Chacana, M., Vergara, J., Martinez-Monzo, J., García-Segovia, P., Lemus-Mondaca, R. & Di Scala, K. 2012 Effect of temperature and air velocity on drying kinetics, antioxidant capacity, total phenolic content, colour, texture and microstructure of apple (var. Granny Smith) slices. *Food Chemistry* 132 (1), 51–59.

Velić, D., Planinić, M., Tomas, S. & Bilić, M. 2004 Influence of airflow velocity on kinetics of convection apple drying. *Journal of Food Engineering* 64 (1), 97–102.

Vijaya, S. V. R., Iniyan, S. & Goic, R. 2012 A review of solar drying technologies. *Renewable and Sustainable Energy Reviews* 16 (5), 2652–2670.

Weiss, W. & Buchinger, J. 2004 Establishment of a production, sales and consulting infrastructure for solar thermal plants in Zimbabwe. *Institute for sustainable Technologies* p. 110.

Zlatanović, I., Komatina, M. & Antonijević, D. 2013 Low-temperature convective drying of apple cubes. *Applied Thermal Engineering* 53 (1), 114–123.

Zomorodian, A., Zare, D. & Ghasemkhani, H. 2007 Optimization and evaluation of a semi-continuous solar dryer for cereals (Rice, etc). *Desalination* 209 (1-3 SPEC. ISS.), 129–135.

CHAPTER

TWO

Experimental set-up, measurements and control system

Contents

2.1 Abstract

A lab-scale indirect solar dryer was designed, constructed and characterized to carry out the experiments conducted in this thesis. The experimental facility

reproduces indirect solar drying processes for a wide range of climates and dryer configurations. The installation can also operate at constant conditions to reproduce steady state processes. The lab-scale solar dryer is composed of an artificial solar dryer and an air conditioning system. The solar dryer is composed of an artificial solar collector and a drying chamber. The air conditioning system establishes the temperature and relative humidity required at the inlet of the solar dryer, associated to the simulated climate. The solar irradiance is reproduced in the artificial solar collector by means of an electric heater. A detailed description of the whole installation, the measurement system and the PID controller employed is presented in this chapter. A characterization of the control system is performed in order to assure the stability of the conditions during operation and the proper tracking of the programmed profiles. A brief description of the auxiliary equipments employed for the experiments, such as a drying oven and a thermogravimetric analyser, is also provided. Finally, the procedure to obtain the initial moisture content of the Granny Smith apple samples is detailed.

2.2 Introduction

The experiments performed in this PhD thesis were conducted employing a laboratory facility that recreates indirect solar drying processes at a wide range of conditions, associated with different climates. The experimental facility was constructed in the Laboratory of Appropriate Technology of the University Carlos III of Madrid. The equipment was applied to the solar drying of Granny Smith apples, at a typical climate of the harvest season of these apples, at a location where they are grown. For the tests, fresh Granny Smith apples bought in a local market were used.

In an indirect solar dryer, the air is taken from the ambient, at the ambient air temperature and relative humidity, and heated in the solar collector. Hence, the characteristic parameters of the climate for solar drying applications, neglecting the wind effect, are: the temperature and the relative humidity of ambient air, and the solar irradiance. The experimental facility consist of two main systems: a system for the conditioning of the air from the laboratory conditions to the conditions prescribed by a certain climate, and an artificial solar dryer that reproduces the solar irradiance absorbed by the solar collector using an electric heater. The whole system is controlled by a Proportional-Integral-Derivative (PID) controller. Since the operating conditions of the experimental

facility are controlled, it can be also operated at constant conditions in order to perform experiments at steady state conditions.

Besides this experimental facility, some auxiliary equipments have been also employed. A drying oven and a precision balance were used to obtain the initial water content of the Granny Smith apples, and a thermogravimetric analyser (TGA) was employed for the study of the drying kinetics of samples of Granny Smith apples.

2.3 Identification of the ambient conditions

In order to reproduce the solar drying process of Granny Smith apples, the climate of the harvest season in a region in Spain where Granny Smith apples are cultivated (Lleida, Cataluña) is selected as the reference climate. The temperature and the relative humidity of the ambient air and the solar irradiance characteristic of a typical sunny day in such season are used as inlet conditions during the experiments.

2.3.1 Characterization of the climate

The apples are typically harvested at the end of September or the beginning of October (Iglesias *et al.*, 2009). A typical day representative of such period, at the location where the apples are cultivated, is selected from weather data available on-line (Energy-Plus, 2015). The solar irradiance and the temperature and relative humidity of the ambient air considered are presented in Figure 2.1.

The climate of the region corresponds to a temperate climate. The harvest days are characterized by a cool weather during the first hours of the morning and a warm afternoon. The relation between the relative humidity and the temperature corresponds to an specific humidity along the day that barely varies. For the conditions depicted in Figure 2.1, the specific humidity during the day, based on psychrometric calculations would vary within $\pm$ 3.4% of its average value. The solar irradiance over the horizontal plane is moderate, due to the relatively low solar elevation angle at the latitude of the location ($\Phi = 41.62°$).

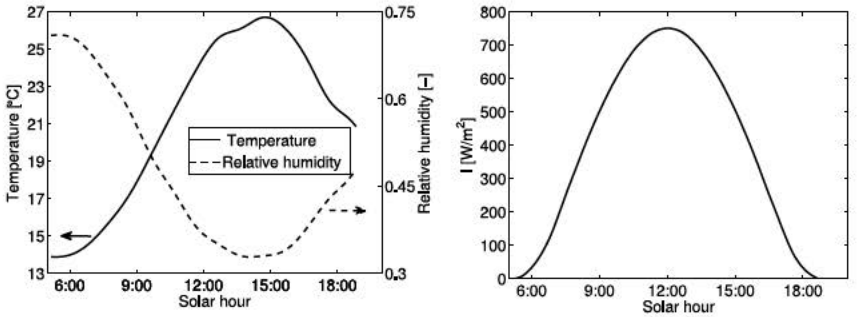

(a) (b)

Figure 2.1: Ambient conditions in the Granny Smith growing area during the harvest season: a) ambient air temperature and relative humidity, b) solar irradiance.

In order to increase the incident solar irradiance on the solar air heater, this is usually tilted a certain angle β. The angle that optimizes the total energy incident along a day $\beta(opt)$ is obtained as (Duffie & Beckman, 2006):

$$\beta(opt) = |\Phi - \delta| \tag{2.1}$$

where Φ is the latitude of the location and δ is the declination corresponding to the day considered. However, the daily optimization of the energy requires the daily readjustment of the collector angle β, which for this application is not feasible, and thus solar dryers of small scale typically operate at a fixed angle β. This angle may also be defined for natural flow reasons, in passive dryers.

In order to obtain the irradiance on the tilted surface of the solar collector, the isotropic diffuse model derived by Liu & Jordan (1963) is used. The model considers the three components of the global radiation: beam I_b, isotropic diffuse I_d and reflected from the ground I_g:

$$I_T = I_b R_b + I_d F_{cs} + I_g F_{cf} \tag{2.2}$$

The view factor from a surface tilted at an angle β to the sky can be calculated as $F_{cs} = (1 + \cos\beta)/2$, whereas the view factor to the ground is $F_{cg} = (1 - \cos\beta)/2$. The reflected irradiance is calculated as the product of the horizontal irradiance and the composite ground reflectance ρ_g. Values of ρ_g for different types of ground were presented by Hunn & Calafell (1977).

$$I_T = I_b R_b + I_d \left(\frac{1 + \cos\beta}{2}\right) + I\rho_g \left(\frac{1 - \cos\beta}{2}\right) \tag{2.3}$$

R_b is the ratio of beam radiation on the tilted surface to that on the horizontal plane, calculated as a function of the latitude Φ , the declination δ, the solar hour angle ω, and the collector angle β as (Duffie & Beckman, 2006):

$$R_b = \frac{\cos(\Phi - \beta)\cos\delta\cos\omega + \sin(\Phi - \beta)\sin\delta}{\cos\Phi\cos\delta\cos\omega + \sin\Phi\sin\delta} \tag{2.4}$$

In order to calculate the diffuse component of the solar irradiance, the correlation of Erbs *et al.* (1982) is used:

$$\frac{I_d}{I} = \begin{cases} 1.0 - 0.09k_T & k_T \leq 0.22 \\ 0.9511 - 0.1604k_T + 4.388k_T^2 - 16.638k_T^3 + 12.336k_T^4 & 0.22 < k_T \leq 0.8 \\ 0.165 & k_T > 0.8 \end{cases} \tag{2.5}$$

where k_T is the clearness index that asses the amount of solar irradiance on the horizontal plane compared to the extraterrestrial irradiance:

$$k_T = \frac{I}{I_o} \tag{2.6}$$

The extraterrestrial irradiance depends on the day of the year n, the latitude of the location Φ, the day declination δ, and the solar hour angle ω:

$$I_o = 1367\left(1 + 0.033\cos\frac{2\pi n}{365}\right)(\cos\Phi\cos\delta\cos\omega + \sin\Phi\sin\delta) \tag{2.7}$$

Only a fraction of the incident solar irradiance on the solar air heater is absorbed by the absorber plate, due to the transmittance of the glass cover and the absorptance of the absorber plate. The solar irradiance absorbed by the absorber plate depends on the effective transmittance-absorptance product $(\tau\alpha)$ (Duffie & Beckman, 2006):

$$S = I_b R_b(\tau\alpha)_b + I_d(\tau\alpha)_d\left(\frac{1 + cos\beta}{2}\right) + \rho_g I(\tau\alpha)_g\left(\frac{1 - cos\beta}{2}\right) \tag{2.8}$$

The effective transmittance-absorptance product can be calculated as follows:

$$(\tau\alpha) = \frac{\tau_c\alpha_p}{1 - (1 - \alpha_p)\rho_c} \tag{2.9}$$

The absorptance of the plate α_p is constant, whereas τ_c, and ρ_c are calculated as:

$$\tau_c = \frac{1}{2}\left(\frac{1 - r_\parallel}{1 + r\parallel} + \frac{1 - r_\perp}{1 + r_\perp}\right)\exp\left(\frac{-K_c t_c}{cos\theta_2}\right) \tag{2.10}$$

$$\rho_c = \left[1 - \frac{1}{2}\left(\frac{1-r_{\parallel}}{1+r_{\parallel}} + \frac{1-r_{\perp}}{1+r_{\perp}}\right)\right] \exp\left(\frac{-K_c t_c}{cos\theta_2}\right] \tag{2.11}$$

being $r_{\parallel}$ and $r_{\perp}$ the parallel and perpendicular components of the unpolarized radiation passing from the air to the glass. K_c is a constant of proportionality that depends on the material, and t_c is the thickness of the material. θ_2 is the angle of the radiation through the glass cover, calculated from the Snell's law. The effective transmittance-absorptance product is specific for every component of the solar irradiance. The angle of incidence considered when applying the Snell's law depends of the component of the solar irradiance for which $(\tau\alpha)$ is calculated. The angle of incidence considered for the beam component $(\tau\alpha)_b$ is the angle of incidence on the tilted collector θ, that can be calculated as:

$$\cos\theta = \cos(\Phi - \beta)\cos\delta\cos\omega + \sin(\Phi - \beta)\sin\delta \tag{2.12}$$

For the diffuse component $(\tau\alpha)_d$, and reflected component $(\tau\alpha)_g$, the angle of incidence is obtained, respectively, as:

$$\theta_d = 59.7 - 0.1388\beta + 0.001497\beta^2 \tag{2.13}$$

$$\theta_g = 90 - 0.5788\beta + 0.002693\beta^2 \tag{2.14}$$

The input parameters considered for the calculations are shown in Table 2.1. Since the incident irradiance on the tilted surface and the irradiance absorbed by the absorber plate depend on the collector angle β, three different values of β are used for comparison: $\beta = 20°$, $\beta = 30°$ and $\beta = 40°$ (this last value approximates the optimal value β_{opt}).

Table 2.1: Input parameters for the calculation of the incident and the absorbed irradiation on the solar air heater.

Parameter	**Symbol**	**Value**
Absorptance of the absorber plate	α_p	0.95
Day of the year	n	265 (22^{nd} Sept)
Latitude	Φ	41.62°
Collector inclination	β	$20°, 30°, 40°$
Ground reflectance	ρ_g	0.2

The results of the solar irradiance on the horizontal plane I, on the tilted surface I_T and the solar irradiance absorbed by the absorber plate S, are presented in Figure 2.2 for different values of β.

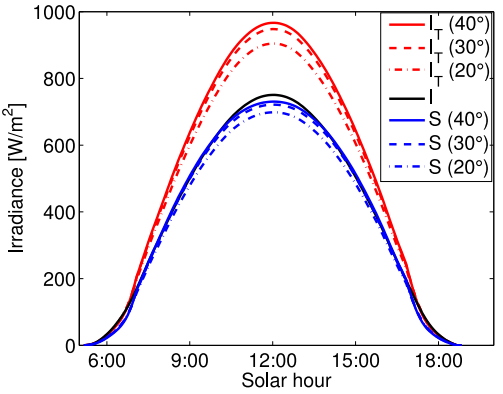

Figure 2.2: Solar irradiance on the solar collector for different collector angles.

The solar irradiance on the horizontal plane in a typical sunny day of the reference climate, together with the irradiance on the tilted collector and the irradiance absorbed by the absorber plate for different collector angles are presented in Figure 2.2. For the days corresponding to the harvest season (declination $\delta \sim 0$), and at the latitude where the apples are cultivated ($\Phi = 41.62°$), a collector angle around $\beta = 40°$ would be the optimal, obtaining higher values of I_T and S for this collector angle; nevertheless the variations for the different angles are not very relevant.

Selection of the solar collector angle

The solar collector angle has two main effects on the air heating process. On one side, if the angle is too large, the buoyancy driven forces may affect the air stream. On the other side, the solar irradiance that would be absorbed, depends on the angle at which the collector is tilted, as shown in Figure 2.2.

The effect of the buoyancy driven forces on the air velocity is of major importance for passive dryers, but becomes negligible for active dryers (in which the air is impelled by a fan) as long as forced convection is guaranteed. In order to assess if such condition is accomplished, the Reynolds and the Grashof numbers should be compared, assuring $\mathrm{Re}^2 \gg \mathrm{Gr}$. The typical air mass flow rates per unit of collector area employed in active solar dryers range from 0.025 kg/m^{2}s to 0.06 kg/m^{2}s (Karim & Hawlader, 2004). These values combined with the typical dimensions of small-scale solar air heaters for drying applications entail large Reynolds numbers, typically operating at non laminar regime (Re>2300),

and thus the condition $\mathrm{Re}^2 \gg \mathrm{Gr}$ is always accomplished. Hence, the effect of the angle on the air stream could be neglected.

Regarding the effect of the angle on the solar irradiance absorbed, if only the particular application of this study is considered, the angle selected for the inclination of the solar collector should be the optimal for those days ($\delta \sim 0°$) at that latitude ($\Phi = 41.62°$), which should be around $\beta \sim 41.62°$. However, the experimental facility is designed to reproduce solar drying processes in any location, at a wide range of climates, and at any period of time in the year, for the harvest of different crops. Moving parts are not desirable in the indirect solar dryer, in order to avoid air leaks and increase the operating life of the equipment, and thus a variable angle is not feasible. Hence, a fixed value of β was selected, to represent a wide range of applications, including passive dryers (although they are outside the scope of this thesis).

The optimal value for this particular application ($\beta \sim 41.62°$) would not suit tropical latitudes during the whole year. However, solar drying in tropical places is probably the most extended application, and thus the selection of an angle $\beta = 40°$ could limit future applications. Typical solar dryers reported in the literature are tilted at angles generally ranging $10° \leq \beta \leq 30°$ operating in locations such as Egypt ($\Phi \sim 30°$, $\beta = 20°$) (El-Beltagy *et al.*, 2007), Singapore ($\Phi \sim 1°$, $\beta = 10°$) (Karim & Hawlader, 2006), Zimbabwe ($\Phi \sim 20°$ south, $\beta = 30°$) (Weiss & Buchinger, 2004) or India ($\Phi \sim 20°$, $\beta = 30°$) (Shanmugam & Natarajan, 2006), among others.

Hence, an angle of $\beta = 20°$ is selected as an intermediate value suitable for different applications. Nevertheless, since the thermal power of the solar irradiance is supplied by a controlled electric heater, as long as the condition $\mathrm{Re}^2 \gg \mathrm{Gr}$ is accomplished, the power programmed could be that calculated for the optimal angle of the application, even though the actual inclination of the collector is $\beta = 20°$.

2.3.2 Determination of the conditions for the tests

The conditions for the tests are determined based on the ambient conditions during the drying process. The thermal power applied to the solar collector is that corresponding to the solar irradiance absorbed by the absorber plate of the solar collector, S. The air temperature and relative humidity at the inlet of the solar collector (T_0 and ϕ_0), are those of the ambient air.

The drying process would not start at the beginning of the day, since the

air temperature and the solar irradiance are low and the air relative humidity is high. As a general procedure, the drying process is considered to begin when the ambient air relative humidity lowers $\phi_0 < 0.6$, which in this case occurs 2.5 hours after the sunrise, and the process ends when the solar altitude angle lowers 10°.

The results of the solar irradiance on the horizontal plane, I and the solar irradiance absorbed by the absorber plate S are presented in Figure 2.3a, for the collector angle selected ($\beta = 20°$). The conditions of the air at the inlet of the solar dryier T_0 and ϕ_0 during the drying process, are presented in Figure 2.3b.

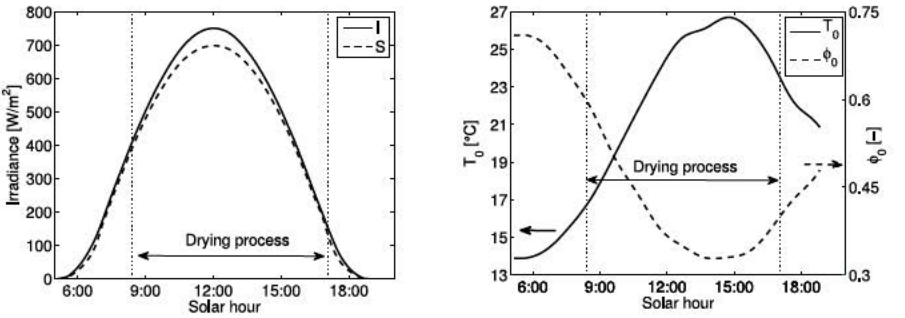

Figure 2.3: Ambient conditions during the drying process. a) Solar irradiance on the solar collector, b) ambient air temperature and relative humidity.

2.4 Experimental facility

The aim of the laboratory installation is to reproduce the drying conditions of the product on field, but in a controlled manner. The main potential of the laboratory solar dryer is that different ambient conditions might be reproduced, so the recreation of drying processes in different climates can be performed at a single location independently of the ambient conditions at that location. The experimental facility has also been designed to permit the operation at constant conditions, in order to perform and analyse steady state processes.

The experimental facility comprises:

- An air intake fed from the pneumatic network of the laboratory to supply the airflow, that acts as the fan of a conventional active solar dryer.

- An air conditioning system to establish a prescribed airflow temperature and relative humidity at the inlet of the solar air heater.

- An artificial indirect solar dryer composed of an electric air heater (that reproduces the performance of a solar collector but with a controlled solar irradiance), and an adiabatic drying chamber.

- The measurement system and the PID controller.

2.4.1 Description of the experimental facility

A schematic of the experimental facility is shown in Figure 2.4. The air is taken from the pneumatic air network available in the laboratory (*1*) through a valve and a pressure regulator (*2*). The air mass flow rate is measured by an air mass flow meter (*3*). The first stage is to establish the conditions of the airflow required at the inlet of the solar collector (T_0, ϕ_0). This process occurs between points *4* and *9* in Figure 2.4. A three-way motorized valve divides the airflow: part of it (*4'*) bubbles through a water column (*5*) in order to increase its relative humidity, and the rest (*4"*) is bypassed. The position of the valve is adjusted by the control system, depending on the required relative humidity at the inlet of the solar collector, ϕ_0. In order to facilitate the humidification of the air during the bubbling process, the water column is heated by an electric heater (*6*). The water column contains a valve with a level sensor to refill the water absorbed by the air. The humid air leaving the water column and the bypassed air are mixed at the entrance of the air heater (*7*), where the airflow is heated with a controlled electric heater (*8*) to obtain the required temperature T_0.

The airflow leaving the air conditioning system enters the plenum (*9*) at temperature T_0 and relative humidity ϕ_0. The plenum is a cylindrical chamber with a diameter of 0.16 m, where the airflow is discharged. At the exit of the plenum, an isolated rectangular duct of 0.2 m long is designed and equipped to act as a flow conditioning section, providing a uniform velocity profile and reducing turbulence and the lateral components of the air velocity. The airflow is directed through the flat-plate solar collector (*10*). An electrical resistance heats the flow, which enters the drying chamber (*11*) at temperature T_1 and relative humidity ϕ_1. The drying chamber contains 13 non-perforated trays, arranged in series to maximize the airflow velocity around the product (*16*). Between the trays, a wired mesh is suspended (*13*), parallel to the trays, to set

the product with the whole surface in contact with the airflow. The first wired mesh (*14*) lays on a balance (*15*), and is used as a reference mesh to register the weight loss during the drying process.

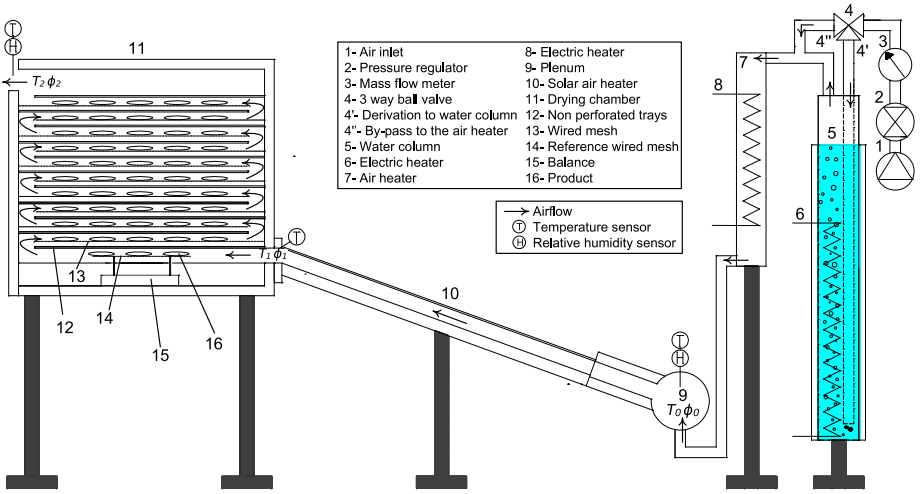

Figure 2.4: Schematic of the experimental facility.

The artificial solar air heater recreates a flat-plate solar collector of upwards type, i.e. the air flows over the absorber plate and under the glass cover. The absorber plate is made of aluminium, with a controlled electric heater wired uniformly along the whole surface, to reproduce the solar irradiance absorbed by the plate for given solar conditions. The collector has a length $L = 1$ m and a width $W = 0.5$ m. The total collector area is $A_c = L \cdot W = 0.5$ m^2 . The airflow circulates between the absorber plate and the glass cover, which are separated a distance $s = 0.045$ m. The walls and the bottom of the solar collector are made of sandwich panel to obtain good insulation. The thickness of the walls and the bottom part are, respectively, 0.03 m and 0.06 m. The drying chamber walls are also made of sandwich panel of 0.03 m of thickness. The inner dimensions of the drying chamber are: width $W = 0.5$ m, length $L_d = 0.75$ m, and a height $H_d = 0.66$ m. The trays are 0.7 m long, leaving 0.05 m between the tray and the end wall for the air circulation. The consecutive trays are separated a distance $s = 0.045$ m. The dimensions are within the typical range for collectors and drying chambers of small-scale indirect solar dryers. For these dimensions, for the typical range of temperatures obtained in solar dryers, operating at a Reynolds number Re > 2300, the condition $\mathrm{Re}^2 \gg \mathrm{Gr}$ is always accomplished, and thus the effect of the collector angle on the air flow can be neglected.

2.4.2 Measurement and control systems

The measurement system consists of several sensors and transducers located at different positions of the experimental facility that are connected to a PC through a Data Acquisition system (DAQ). The software used for the data acquisition and the control is LabView®. The location of the sensors and a schematic of the measurement and control systems are presented in Figure 2.5. The parameters measured are:

- Temperature and relative humidity of the airflow at different locations along the solar dryer. The temperature is measured at the inlet of the collector, at the outlet of the collector (inlet of the drying chamber) and at the outlet of the drying chamber. The relative humidity is measured at the inlet of the collector and at the outlet of the drying chamber.
- Surface temperature at several points of the solar collector: inner and outer surface of the glass cover, upper surface of the absorber plate and inner surface of the insulation. All the measurements are taken at the center of each device.
- Temperature of the ambient, which is the room temperature of the laboratory.
- Temperature of the water contained in the water column.
- Air mass flow rate.
- Weight of the product in the reference mesh measured with a balance.
- Electric power supplied to the electric heater of the artificial solar collector, which is equivalent to the solar irradiance absorbed by the absorber plate multiplied by the collector area.
- Atmospheric pressure.
- Differential pressure at different locations of the solar dryer.

All the signals provided by the transducers are acquired by the DAQ system, connected to the PC. The controller acts on: i) the water heater to set the water column temperature, ii) the power supplied to the solar collector to reproduce the solar irradiance absorbed by the absorber plate, iii) the three-ways valve of the air conditioning system to control the air relative humidity at the inlet

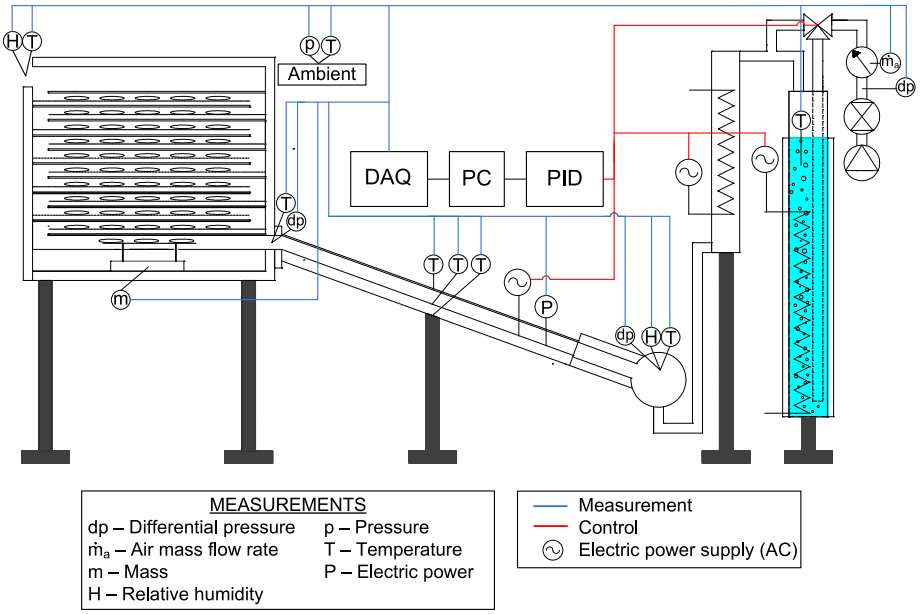

Figure 2.5: Location of the sensors and schematic of the measurement and control systems.

of the collector, and iv) the air heater of the air conditioning to establish the air temperature at the inlet of the collector. In each control system, the data acquired by the DAQ system is compared to the instruction and the controller acts on the corresponding actuator, if necessary. A description of the whole system is detailed below.

Temperature and relative humidity

The temperature of the airflow is measured at three points: at the inlet of the collector T_0, at the outlet of the collector T_1 and at the outlet of the drying chamber T_2. The relative humidity of the airflow is measured at the inlet of the collector ϕ_0 and at the outlet of the drying chamber ϕ_2. T_1 is measured using a Type T thermocouple with an accuracy of ± 1 °C. The temperature and the relative humidity of the airflow at the collector inlet and at the drying chamber outlet are measured using two transmitters DeltaOhm® HD4817T. The temperature is measured by a NTC thermistor of 10 kΩ with an accuracy of ± 0.3 °C and a range of operation from -20 °C to 80 °C. The relative humidity is measured by a capacitive sensor with an accuracy of 1.5% within the range of 0% to 90% and 2% within the range of 90% to 100%. The transducer has an

analogue output of $4-20$ mA.

The temperatures of the ambient air, the absorber plate, the glass cover and the isolation of the solar air heater are also measured using Type T thermocouples with an accuracy of ± 1 °C. The thermocouples employed to measure the absorber plate, the isolation and the glass cover are located at the center of each device.

Air mass flow rate

The air mass flow rate is measured by a mass flow meter SMC® PF2A703H located between the air intake and the air conditioning system. To assure an accurate measurement, the apparatus was located with 1 m of pipe upstream and 1 m of pipe downstream, to provide with proper flow conditions. The air mass flow meter uses a thermal sensor, with an accuracy of $\pm 1.5\%$ full scale, and an analogue output of $4-20$ mA. The time of response is 1 s. The operating range is from $3{\cdot}10^{-3}$ kg/s to $6{\cdot}10^{-2}$ kg/s.

Weight of the product

During the whole drying process the weight of the product located on the reference tray is registered using a balance PCE® PM3T, which has a capacity of 3000 g and an accuracy of ± 1 g. The balance has an analogue output of $4-20$ mA.

Power of the electrical heater of the solar collector

The heat flux in the solar collector is simulated with an electrical resistance of 13 Ω. The power is supplied by a solid state relay Carlo Gavazzi® RM1E and measured with a power transducer Carlo Gavazzi® CPT-DIN. The system operates within the range of the solar power absorbed by a typical absorber plate, from 0 to 1200 W/m^2 with an accuracy of ± 5 W/m^2.

Pressure

The atmospheric pressure is measured with a barometer DeltaOhm® HD9408T with an accuracy of ± 50 Pa. The sensor is a piezoresistive diaphragm. The range of measurement is from 800 mbar to 1100 mbar. The output is analogue, $4-20$ mA. Several drills have been done in the solar dryer to measure the differential pressure between different zones or to the ambient, which corresponds

to the manometric pressure. The apparatus is a low-pressure differential pressure transmitter Sensor Technics® BTEL5005D4A with an analogue output of $4-20$ mA, an accuracy of 0.1% full scale and a range of operation from 0 mbar to 5 mbar.

DAQ modules

The DAQ modules acquire the analogue signals provided by the different transducers, as depicted in Figure 2.5, and convert the signals into digital signals to the PC. The DAQ modules used are: two modules with 8 channels for analogue input ADAM-4017+, one module with 8 channels for thermocouples ADAM-4018+ and one module with 4 channels for analogue input ADAM-4024, that presents 4 more channels for analogue output, employed for the control system. The input channels receive the analogue signals from the sensors and the output channels send analogue signals to the actuators: the heater of the solar collector, the air and the water heaters of the air conditioning system, and the three-ways valve.

Control system

The air conditioning system and the electrical heater of the absorber plate establishes the experimental conditions prescribed for the tests: the temperature T_0 and relative humidity ϕ_0 of the airflow at the entrance of the collector and the solar irradiance absorbed by the plate. The air conditioning system provides air at the simulated ambient conditions: T_0 and ϕ_0. The electrical heater of the solar collector supplies the power equivalent to the solar irradiance absorbed by the absorber plate multiplied by the collector area. In order to get the desired conditions, a control system is employed. The control system is a PID controller that acts on the air conditioning system and on the electrical heater of the collector depending on the data input from the sensors. The signals are provided bye the 4 output channels of the DAQ module ADAM-4024.

2.5 Characterization of the control system

A Proportional-Integral-Derivative controller (PID) has been developed using LabView®. A schematic of the control systems is presented in Figure 2.6

The temperature T_0 and the relative humidity ϕ_0 of the airflow are measured in the plenum, located at the collector inlet. The control of the temperature

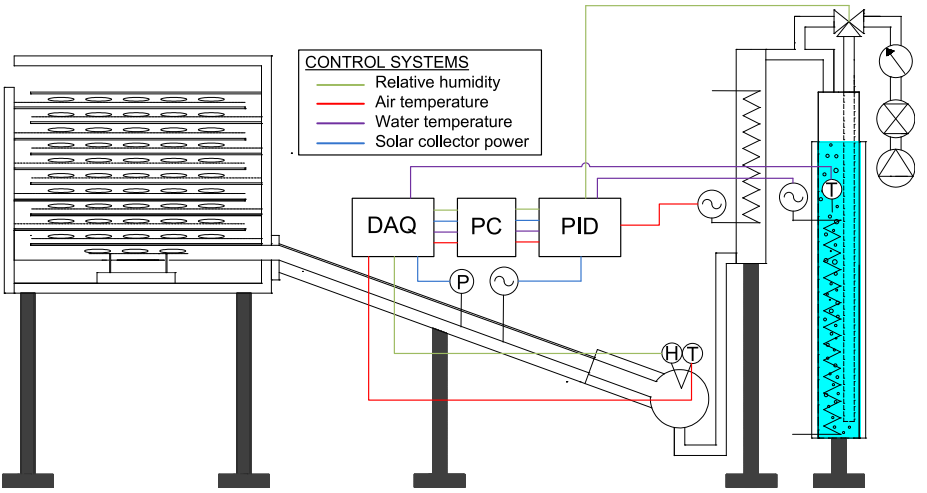

Figure 2.6: Schematic of the control systems of the lab-scale solar dryer.

acts on the power of the air heater of the air conditioning system, while the control of the relative humidity acts on the position of the three-ways valve, which determines the portion of air derived through the water column. In order to enhance the evaporation process in the water column, the water is heated at a certain temperature, which is also controlled by the system. The temperature of the water is measured by a thermocouple, and the control system acts on the electric heater immersed in the water column. The control of the power of the solar air heater acts on the signal that the solid state relay supplies to the electrical resistor of the solar collector. The signal of the power transducer is acquired by the DAQ modules, and it is compared to the instruction corresponding to the solar irradiance absorbed by the absorber plate, modifying the output signal as required.

The experimental facility is designed to operate at two modes: reproducing a solar drying process, with its corresponding variable profiles of temperature, relative humidity and solar irradiance; or at steady state conditions. Therefore, the facility should accomplish two main requirements:

- Be capable of following the profiles of the simulated ambient conditions during a day, when recreating a solar drying process.
- Maintain stable conditions when reproducing steady state operation.

The control of the air temperature and relative humidity is complex due to two main reasons. On one side, both parameters are coupled. To simplify the problem, the control acts on different devices depending on which one has to be settled. Nevertheless, variations in one parameter affects the other, which has to be re-established. On the other side, the system presents inertia. The control acts on the air conditioning system based on the signal provided by the sensors, which are located at the plenum. The thermal capacitance of the elements of the air conditioning system, and of the piping that joins it with the plenum, and the inertia of the humidification process, entail a slow response to the control system.

The characterization of the control of the air relative humidity, the air temperature, and the power of the electric heater of the solar collector are treated separately since they are performed by different systems. The temperature of the water column is an auxiliary parameter to facilitate the humidification process. The control of the water temperature is employed to maintain it constant. Hence, such control system is not studied in detail.

The stabilization process depends on the parameters of the PID controller: proportional gain, integral time and derivative time. The effect of the PID parameters in the response of the control system of the relative humidity, the temperature and the electric power are analysed, and the most suitable PID parameters are selected.

For each control system, several tests with different values of the proportional gain k_p and of the integral time t_i were conducted to evaluate their effect in the stabilization of the process around an instruction. The derivative time is not used in any case since it produces too many sudden changes in the actuators that could reduce their operating life. Based on the results of the PID parameters analysis, the values of k_p and t_i for the subsequent operations in the experimental facility are selected. For the selection, besides the effect of the PID parameters on the approach to the instruction, it is also considered that the installation is planned to operate at steady state conditions, or following a variable profile but with long characteristic times of change characteristic of variables that change slowly during a day.

In order to analyse the stabilization process, three characteristics times are evaluated in every test:

- t_0: Time between the instant when the instruction is given and the instant when the conditions begin to vary.

- t_1: Time between the instant when the instruction is given and the instant when 95% of the variation is reached.

- t_2: Time between the instant when the instruction is given and the instant when the process begins to stabilize, considering stabilization when the peaks of the wave defined by the process oscillates within a certain value. The criteria to select that value is specified in each process.

Once the PID parameters are selected for each control system, the stability of the process at steady state conditions and the response to variable profiles are characterized. For the analysis of the stability at steady state conditions, several tests are conducted in each case, giving instructions within the range of operation of the solar dryer, which are the ambient conditions during a day of reference, presented in Figure 2.3. A time of stabilization is previously left, before the tests begins, until the process is reasonably stable around the instruction (the approaching period is not considered). For the case of variable conditions, a variable profile is programmed consisting of a set of instructions, given at a rate of variation consistent with the characteristic time of change of ambient conditions during a day. A time of stabilization is also left, until the process is stable around the first instruction of the set.

2.5.1 Control of the relative humidity

The control of the relative humidity ϕ_0 acts on the position of the three-ways valve of the air conditioning system (Figure 2.6). The temperature of the water in the water column has a strong effect on the dynamics of the humidification process, since it affects the evaporation rate in the column, and thus, the relative humidity of the airflow. Hence, an analysis of this effect is carried out prior to the study of the PID parameters effect. Two tests at different water column temperatures were conducted: at 45 °C and 60 °C. The stability of the relative humidity of the airflow around three values ($\phi_0 = 0.7$, $\phi_0 = 0.5$ and $\phi_0 = 0.3$) is analysed for each water temperature. The results are shown in Figure 2.7.

The results show the stabilization process of the relative humidity of the airflow, from the relative humidity of the pneumatic network, to three different instructions, for two temperatures of the water column. The wave defined by the process presents a sharp shape. This is due to the dynamics of the humidification process, the slow motion of the valve and the inertia of the process. The valve starts closing slowly, and the process do not react immediately. The

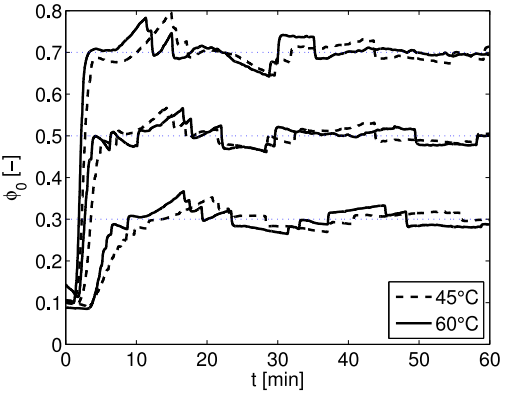

Figure 2.7: Stability of the relative humidity ϕ_0 around the instruction values of $\phi_0 = 0.7$, $\phi_0 = 0.5$ and $\phi_0 = 0.3$, for different temperatures of the water column.

response is sudden and delayed, leading to the stepped shaped profile. Even though the process at 60 °C is a bit faster, the results obtained for both temperatures present minor differences. In order to compare the stability for both temperatures, an statistical analysis of the results is performed. The average and the standard deviation of the process, once the instruction was reached for the first time, are calculated. The results are presented in Table 2.2 for the case of 45 °C and Table 2.3 for the case of 60 °C. In order to evaluate the time of response in each case, the characteristic time t_1 (time between the instant when the instruction is given and the 95% of the variation is reached) is also presented in both tables.

Table 2.2: Analysis of the stability of the relative humidity around the instruction with the water at 45 °C.

Instruction [-]	**Average** [-]	**Standard deviation** [-]	t_1 **[s]**
$\phi_0 = 0.7$	0.70	0.02	221
$\phi_0 = 0.5$	0.50	0.02	301
$\phi_0 = 0.3$	0.30	0.02	705

The results reported in Tables 2.2 and 2.3 show that, the temperature of the water column presents no appreciable effect on the stability, but the process is faster using a temperature of 60 °C. Hence, this will be the value used for the rest of tests.

Table 2.3: Analysis of the stability of the relative humidity around the instruction with the water at 60 °C.

Instruction [-]	**Average** [-]	**Standard deviation** [-]	t_1 [s]
$\phi_0 = 0.7$	0.70	0.02	165
$\phi_0 = 0.5$	0.50	0.02	227
$\phi_0 = 0.3$	0.30	0.02	527

In order to study the effect of the PID parameters on the humidification process, several tests using different PID parameters are studied, maintaining the water column at 60 °C. The nominal case is defined by a proportional gain $k_p = 0.003$ and an integral time $t_i = 0.15$ min, which are varied in the rest of the tests, keeping constant one parameter and varying the other. The tests consist on the humidification of the airflow, from the conditions of the pneumatic network (around $\phi = 0.1$), to an instruction of $\phi_0 = 0.5$.

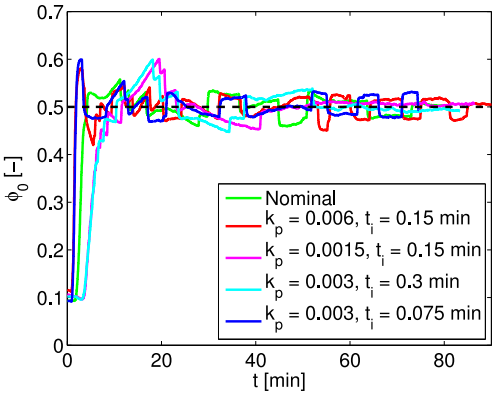

Figure 2.8: Effect of the PID paramaters on the relative humidity ϕ_0 in a humidification process, with an instruction of $\phi_0 = 0.5$.

The results presented in Figure 2.8 show that increasing the proportional gain k_p or decreasing the integral time t_i, the process is faster, but less stable. The values of the characteristics times t_0, t_1, t_2, defined above, are presented in Table 2.4. t_2 is the time until the process oscillates within the instruction $\phi = 0.50 \pm 0.06$.

The parameters presented in Table 2.4 are specific for the particular humidification process shown in Figure 2.8, since they depend on the initial value, the

Table 2.4: Characteristic times and maximum difference between the instruction and the process in the control of ϕ_0.

PID parameter	t_0 [s]	t_1 [s]	t_2 [s]
$k_p = 0.003$, $t_i = 0.15$ min	90	247	291
$k_p = 0.006$, $t_i = 0.15$ min	50	104	352
$k_p = 0.0015$, $t_i = 0.15$ min	190	518	1242
$k_p = 0.003$, $t_i = 0.3$ min	180	620	1174
$k_p = 0.003$, $t_i = 0.075$ min	53	109	196

ongoing process and the instruction given.

In general, to maintain stable conditions low values of k_p and high t_i are required, but to follow profiles that are changing, higher values of k_p and low t_i are more appropriate. Intermediate values of $k_p = 0.003$ and $t_i = 0.15$ min are selected for the PID controller of the relative humidity. For such value, the stability of a steady state process and the response to a variable profile is evaluated.

Stability at steady state conditions

For the selected PID paramters, the analysis of stability during time at steady state conditions is carried out for the instructions $\phi_0 = 0.35$, $\phi_0 = 0.45$, $\phi_0 = 0.55$ and $\phi_0 = 0.65$, covering the range of the relative humidities used for the rests of the tests (Figure 2.3b). In order to assure a stable operation at steady state conditions, a stabilization time is left before the beginning of the tests. The test begins after the approaching phase has ended.

The results, shown in Figure 2.9a, present the same stepped behaviour characteristic of the relative humidity control. The average and the standard deviation of the processes are depicted in Figure 2.9b. It can be observed that the average coincides with the instruction and the standard deviation is relatively low.

Response to variable profiles

For the operation at variable conditions, an stabilization time is left before the beginning of the tests, as in the case of steady state conditions, around the instruction corresponding to the first value of the profile.

The profiles programmed consist of a set of variable instructions of the air

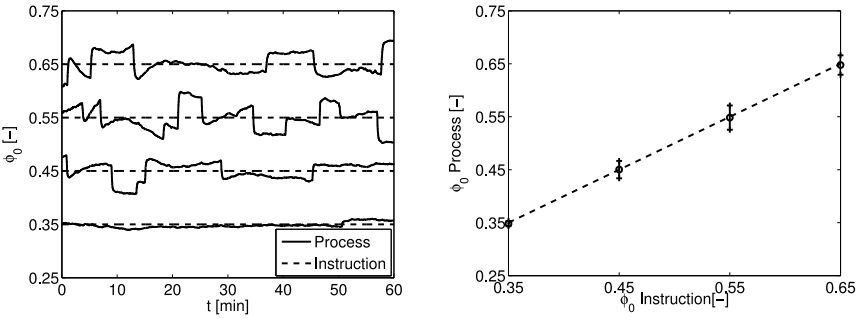

(a) (b)

Figure 2.9: Stability of the relative humidity ϕ_0 at steady state conditions for the instructions $\phi_0 = 0.35$, $\phi_0 = 0.45$, $\phi_0 = 0.55$ and $\phi_0 = 0.65$ a) as a function of time and b) statistical analysis.

relative humidity, given every 5 min during 90 min, and at the rate of variation characteristic of a day. The process is presented in Figure 2.10a as a function of time, including the moving average of the process, centred in a period of 10 min, depicted in dashed line. The solid black line represents the profile of variable instructions. Since the instruction changes every 5 min, the curve presents a stepped shape. The average and the standard deviation within the 5 min interval is presented in Figure 2.10b

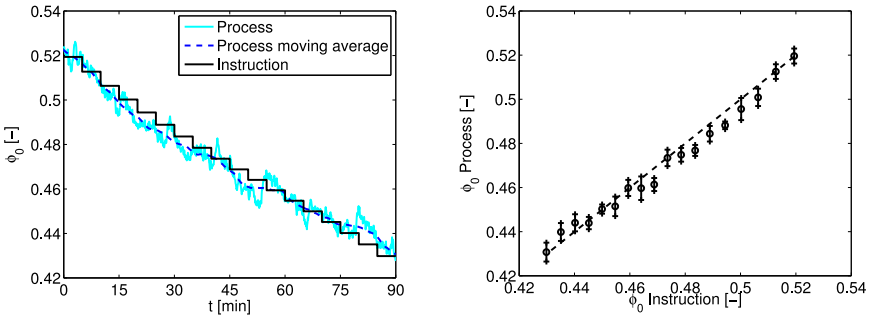

(a) (b)

Figure 2.10: a) Response of the control of the air relative humidity to a variable profile. b) Process response as a function of the instruction given.

Figure 2.10 shows a proper response of the air relative humidity at the inlet of the collector ϕ_0 to a variable relative humidity of the ambient air, for a rate of change characteristic of the ambient air during a day. The deviations shown in Figure 2.10b show the effect of the inertia but are on the range of those of Figure 2.9b.

2.5.2 Control of the air temperature

The PID controller of the air temperature T_0 acts on the electric heater of the air conditioning system (Figure 2.6). The same procedure followed for the characterization of the control of the relative humidity is employed for the air temperature. The values of the proportional gain and the integral time for the nominal case are $k_p = 0.1$ and $t_i = 2$ min. In each test, the initial temperature was the room temperature (around 18 °C) and the instruction was $T_0 = 22$ °C. The results of the tests are depicted in Figure 2.11.

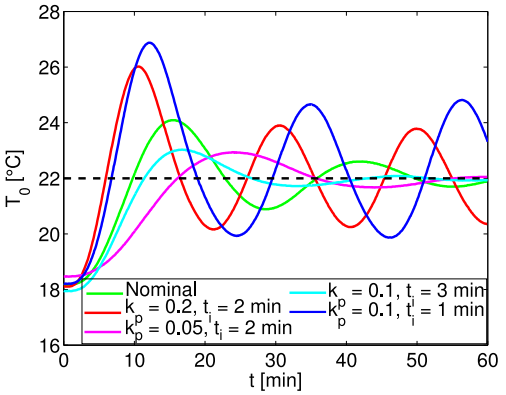

Figure 2.11: Effect of the PID parameters on the temperature T_0 in a heating process.

Figure 2.11 shows the stabilization process of the temperature T_0 as a function of time, from room temperature to an instruction of $T_0 = 22$ °C, for different values of the proportional gain, k_p, and the integral time, t_i. It can be observed that increasing the proportional gain or reducing the integral time, faster approaches are obtained; however, a strong overpass occurs. The processes are slow, which is a characteristic pattern of systems of hight inertia. The values of the characteristic times t_0, t_1, t_2 are presented in Table 2.5. t_2 is the time until the process oscillates within the instruction $T_0 = 22.0 \pm 0.5$ °C. In

the case of the control of temperature, it is important to assess the maximum difference obtained between the process and the instruction in the first peak of the modulated wave defined by the process, since strong overpasses might be produced. Hence, this temperature difference $\Delta T_{0\max}$ is also representative of the stabilization process, and it is presented in all cases, together with the time when it occurs, $t(\Delta T_{0\max})$.

Table 2.5: Characteristic times and maximum difference between the instruction and the process in the control of T_0.

PID Parameter	t_0 [s]	t_1 [s]	t_2 [s]	$\Delta T_{0\max}$ [°C]	$t(\Delta T_{0\max})$ [s]
$k_p = 0.1$, $t_i = 2$ min	100	570	3300	2.1	910
$k_p = 0.2$, $t_i = 2$ min	80	350	–	4.0	630
$k_p = 0.05$, $t_i = 2$ min	125	925	2655	0.9	1430
$k_p = 0.1$, $t_i = 3$ min	115	660	1970	1.0	1000
$k_p = 0.1$, $t_i = 1$ min	85	400	–	4.9	720

As in the case of the air relative humidity, in order to obtain a stable air temperature, higher integral times or lower proportional gain are desirable, even though the approach is very slow. For the mode of operation of the experimental facility, the values selected are $k_p = 0.1$ and $t_i = 3$ min, considering a moderate overpassing and an intermediate characteristic time.

Stability at steady state

To analyse the stability at steady state conditions of the temperature T_0, tests at 22 °C, 25 °C and 28 °C were conducted. The results, presented in Figure 2.12a, with the average and standard deviation depicted in Figure 2.12b, show a very stable operation under steady state conditions.

Response to variable profiles

In order to asses the response to variable profiles, a similar test to that of the air relative humidity is conducted. The profile programmed is consistent with the reference climate, modifying the instruction, as in the previous case, every 5 min during 90 min. The results are presented in Figure 2.13.

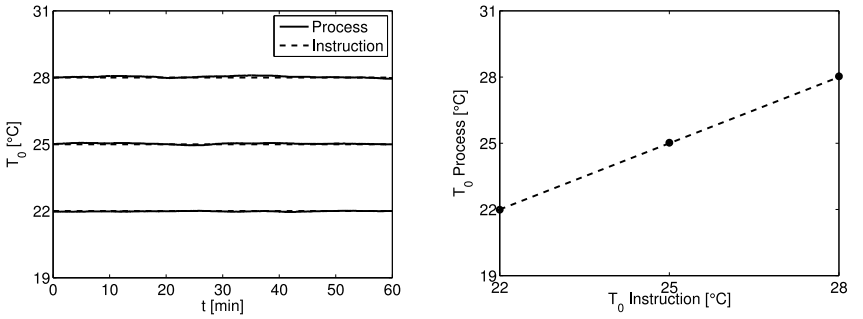

(a) (b)

Figure 2.12: Stability of the temperature T_0 at steady state conditions for the instructions $T_0 = 22$ °C, $T_0 = 25$ °C and $T_0 = 28$ °C a) as a function of time and b) statistical analysis.

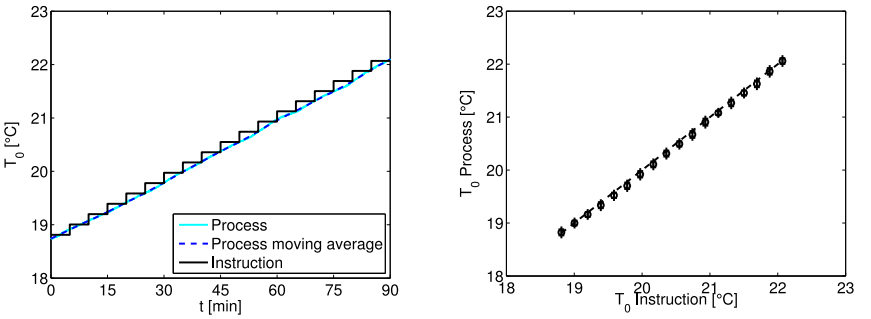

(a) (b)

Figure 2.13: a) Response of the control of the air temperature to a variable profile. b) Process response as a function of the instruction given.

The results show a precise tracking of the variable instruction, with a slight effect of the inertia. However, since the stabilization processes are slow, in every test conducted, a time of stabilization around the first value of the variable profile is necessary prior to the beginning of the test, as in the case of the control of the air relative humidity.

2.5.3 Power of the electric heater of the solar collector

The control of the power of the electric heater of the solar collector is used to reproduce the solar irradiance absorbed by the absorber plate of the solar air heater. The PID controller acts on the signal supplied by the solid state relay, and thus acts directly on the power, based on the measurement provided by the power transducer, as established in Figure 2.6.

The results of the tests to evaluate the effect of the PID parameters are presented in Figure 2.14. The nominal case is defined by a proportional gain $k_p = 1 \cdot 10^{-4}$ and an integral time $t_i = 0.1$ min. As in the previous cases, these values are varied independently to see their effect.

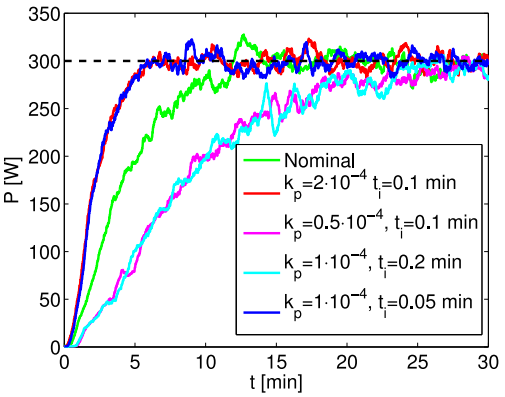

Figure 2.14: Effect of the PID parameters on the power of the electric heater for an instruction of 300 W.

The control of the power of the absorber plate is much faster than the control of the conditions of the airflow. This is because the control acts directly on the power of the electric heater, which is the signal measured, and thus, the inertia is very low. However, the signal presents high ripple, caused by the indented wave supplied by the relay. It can be observed in Figure 2.14 that doubling the proportional gain or reducing the integral time to half the nominal value, a very similar response is obtained. The three characteristic times t_0, t_1 and t_2 are presented in Table 2.6. t_2 is the time until the instruction is reached for the first time, since afterwards it stays stable and overpasses barely happen.

Table 2.6: Characteristic times in the control of the power of the electric solar air heater.

PID Parameter	t_0 [s]	t_1 [s]	t_2 [s]
$k_p = 1 \cdot 10^{-4}$, $t_i = 0.1$ min	23	602	719
$k_p = 2 \cdot 10^{-4}$, $t_i = 0.1$ min	9	298	360
$k_p = 0.5 \cdot 10^{-4}$, $t_i = 0.1$ min	46	1161	1684
$k_p = 1 \cdot 10^{-4}$, $t_i = 0.2$ min	37	1137	1564
$k_p = 1 \cdot 10^{-4}$, $t_i = 0.05$ min	12	317	350

In the case of the control of the power, it is difficult to appreciate the differences in the stability of the different cases, once the instruction is reached. Hence, an statistical analysis has been carried out. The average and the standard deviation of every cases are presented in Table 2.7.

Table 2.7: Statistic analysis of the stability of the power of the electric solar air heater over the instruction.

PID Parameter	Average [W]	Standard deviation [W]
$k_p = 1 \cdot 10^{-4}$, $t_i = 0.1$ min	297.3	11.2
$k_p = 2 \cdot 10^{-4}$, $t_i = 0.1$ min	299.4	7.7
$k_p = 0.5 \cdot 10^{-4}$, $t_i = 0.1$ min	284.9	8.1
$k_p = 1 \cdot 10^{-4}$, $t_i = 0.2$ min	286.8	11.0
$k_p = 1 \cdot 10^{-4}$, $t_i = 0.05$ min	299.2	7.7

The processes that present higher stability (average closer to the instruction and lower standard deviation) are the process that has double proportional gain than the nominal case, and the process with half of the nominal integral time, which moreover, are the fastest processes, and thus any of them could be selected. Among them, the values $k_p = 2 \cdot 10^{-4}$ and $t_i = 0.1$ min are selected for the PID controller.

Stability at steady state

For the evaluation of the stability of the power of the absorber plate around a constant instruction, tests at 200 W, 240 W and 280 W were conducted, corresponding to solar irradiances absorbed by the collector of 400 W/m^2, 480 W/m^2 and 560 W/m^2, respectively. The results are shown in Figure 2.15.

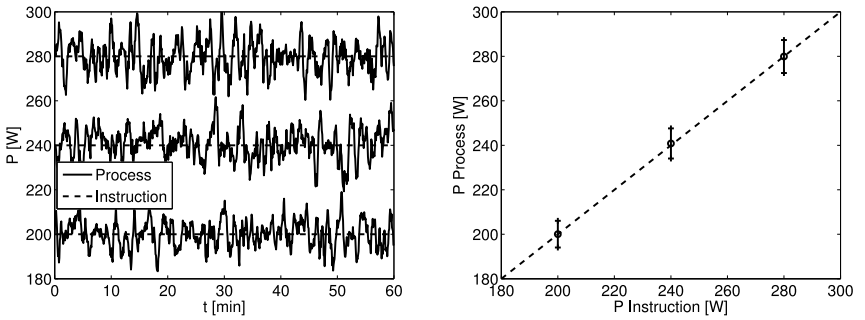

(a) (b)

Figure 2.15: Stability of the power of the solar air heater at steady state conditions for the instructions $P = 200$ W, $P = 240$ W and $P = 280$ W a) as a function of time and b) statistical analysis.

Figure 2.15a shows the power of the absorber plate obtained in the tests as a function of time. The power of the absorber plate presents a high ripple, caused by the indented wave supplied by the relay. Figure 2.15b shows the average value for each instruction and the standard deviation. The results show a proper behaviour of the mean values, despite of the ripple. The standard deviation is within the range of the accuracy of the acquisition system, which for the type of the signal provided by the relay is ± 10 W.

Response to variable profiles

The response to a variable instruction is presented in Figure 2.16, for a programmed profile corresponding to a variation of the absorber solar irradiance S multiplied by the collector area A_c, during 90 min, in intervals of 5 min.

Despite of the ripple of the signal, and specially considering the moving average, a good response of the control tracking a variable instruction can be observed. Figure 2.16b show that the the inertia in the control system is negligible.

2.5.4 Safety during operation

There are several risks associated to the operation of the experimental facility. Since the drying processes take several hours, the laboratory allows the operation in remote, and thus the safety of the whole system must be assured when

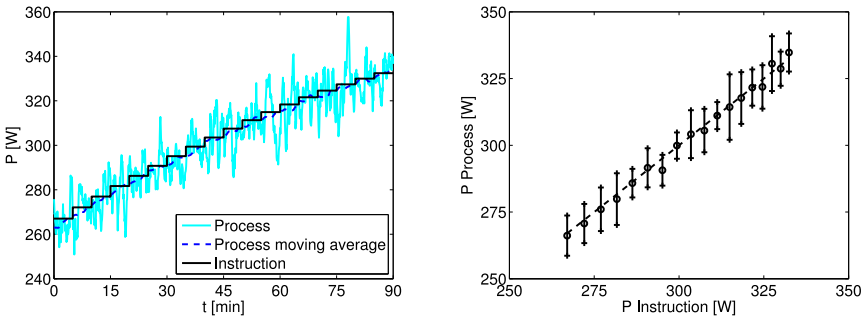

(a) (b)

Figure 2.16: a) Response of power of the electric air heater of the solar collector to a variable profile. b) Process response as a function of the instruction given.

the user is not present. The potential causes and consequences of such risks have been evaluated and actions have been taken to assure a safe operation of the system.

The system operates using electrical resistors of high power: 5000 W for the water heater, and 4000 W and 2500 W for the air heaters. The resistors are connected to the three-phase electrical network of the laboratory, and the whole system employs magneto-thermal breakers according to the standards. The system is designed to operate with air flowing around the air heaters, and with the water heater immersed in water. The airflow is supplied continuously from the pneumatic network available in the laboratory, and the water column is refilled by a float valve system with water supplied by the hydraulic network. However, should the hydraulic or pneumatic networks supplies be cut off, a fire might occur. In order to prevent from fire risk, thermal switches have been included in the parts in contact with the electrical resistors, in order not to exceed a certain temperature. The electrical power would be cut off if the walls of the water column exceeds 80 °C, the air heater of the air conditioning system exceeds 60 °C, or the absorber plate exceeds 150 °C.

In addition, the software has an alarm system that cuts off the power when a failure is detected, but the PC has to be operative and the communication with the DAQ modules has to be effective. If any failure regarding the PC operation or the communication occurs, the DAQ modules have a watchdog system that cuts off the signals sent to the electric heaters.

2.6 Auxiliary experimental facilities

Besides the artificial solar dryer described, some auxiliary equipments have been used for certain tests. For the determination of the initial moisture content of the samples, an electrical oven and a precision balance are employed. For the determination of the drying kinetics of the samples of Granny Smith apples, a thermogravimetric analyser (TGA) is used. These auxiliary experimental facilities are described in this section.

2.6.1 Drying oven

For the determination of the initial moisture content of the fresh apples, the samples are dried in a drying oven Memmert UFE 500. The mass of the samples, before and after the drying process, is determined using a balance Denver Instrument of 1500 g of capacity and 0.01 g of accuracy. The procedure followed for the determination of the moisture content and the results are detailed in section 2.7

2.6.2 Thermogravimetric analyser

A thermogravimetric analyser (TGA) is an equipment capable of measuring with high precision the evolution of the weight of a product as a function of time, for a determined temperature profile. Hence, it is commonly used to study processes involving heat and mass transfer such as pyrolysis of biomass (Damartzis *et al.*, 2011) or drying processes (Cai & Chen, 2008).

A thermogravimetric analyser TGA Q500 TA Instruments is used to obtain the drying kinetics of small portions of Granny Smith apples. The inert gas employed was nitrogen, flowing through the furnace at a rate of 0.06 l/min. The sensitivity in the mass measurements is 0.1 μg. The isothermal temperature accuracy is ± 1 °C and the precision of the thermocouple is ± 0.1 °C. The temperature range of operation is from room temperature to 1000 °C. The range of permissible heating rates is from 0.01 °C/min to 100 °C/min. The method for the temperature calibration is based on the Curie Point of a reference material.

The samples employed in the tests where cylinders of 1 cm in diameter and a thickness of 2.4 mm. The mass of the Granny Smith apples employed in the TGA measurements was around 150 mg. Even though the apple samples do not become oxidized in a nitrogen stream, the samples were submerged in citric

acid to present the same initial conditions as those of the tests in the solar dryer.

Characterization

When a TGA is used to study drying processes, the variation of the temperature is generally programmed at a constant heating rate, which entails a linear increasing of temperature (Madhava *et al.*, 2001; Freire *et al.*, 1999). Some authors have also used the TGA for the determination of drying kinetics at isothermal conditions (Chen *et al.*, 2012; Li & Kobayashi, 2005).

In this work, the TGA is used in two operating modes: at isothermal conditions and following the temperature profile that would be obtained in the inlet of the drying chamber. Since the temperature at the inlet of the chamber does not present a linear increase, the temperature profile that the TGA must follow is programmed in short time intervals, varying the heating rate in every interval. On the other side, when the TGA is used at isothermal conditions, a high heating rate is provided at the beginning, until the temperature of operation is reached (instant when the test begins) and from that instant, it is programmed at constant temperature.

In order to characterize both operation modes, two set of tests are conducted: one at isothermal conditions, at three different temperatures; and the other at non-isothermal conditions, with variable heating rates. In order to conduct the isothermal test, the furnace is pre-heated at a certain temperature in each case. For the non-isothermal tests, a set of different heating rates are programmed, ranging between 0.01 °C/min and 0.08 °C/min. The results are presented in Figure 2.17.

The tests conducted at constant temperatures are depicted in Figure 2.17a, and at variable heating rates in Figure 2.17b. In the case of isothermal conditions, three isothermal processes are conducted at 30 °C, 35 °C, and 40 °C. The heating rates for the non-isothermal test are determined dividing a typical temperature profile at the inlet of the drying chamber in intervals of approximately 10 min. Since in the TGA only positive heating rates can be programmed, only processes in which the temperature increases can be analysed. The results show a very accurate behaviour of the TGA in both cases.

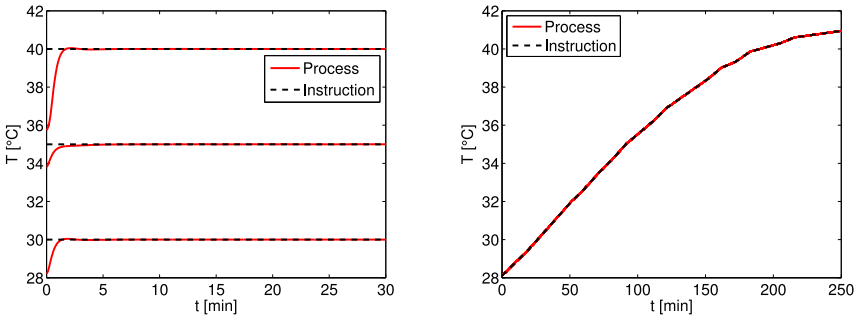

Figure 2.17: a) Stability of the temperature in the TGA at isothermal conditions. b) Response to non-isothermal profiles at variable heating rates.

2.7 Determination of the initial moisture content

Solar drying occurs in a range of air temperatures and relative humidities for which the elimination of all the moisture contained in the product is not feasible. In order to know the amount of moisture eliminated in a drying process, the initial moisture content of the fresh product should be determined.

The initial content of moisture of the fresh product is determined drying several samples in the electrical oven and using a balance.

In order to assess the moisture content two trays are used, as specified in the standard UNE-E-EN 14774-1 (AENOR, 2010). In each test, both trays are weighted empty. The product is then placed on one of the trays, which is weighted again and the initial weight of the product m_0 is determined. Both trays are introduced into the oven. The empty tray is used as a reference to correct the measurement of the weight when they are withdrawn hot from the oven, since the buoyancy effect may affect the measure. The oven is heated using a heating rate of 10 °C/min up to 90 °C, and then maintained constant at 90 °C. The trays are kept inside the oven during four hours at 90 °C. Once the product is dried, both trays are weighted and the weight is corrected based on the measurement obtained in the reference tray. The mass of the dried product m_d is thus obtained. The initial content of moisture is determined, in wet basis, as follows:

$$M_0 = \frac{m_0 - m_d}{m_0} \tag{2.15}$$

following the described procedure, 25 samples of slices of different Granny Smith apples are dried. The initial moisture content obtained in each case is presented in a histogram in Figure 2.18a. The data of all the tests is subjected to a normality test. The data is depicted in a normal plot, presented in Figure 2.18b. The cross symbols represent the cumulative probability of the corresponding moisture content, and the dashed line presented that for a normal distribution.

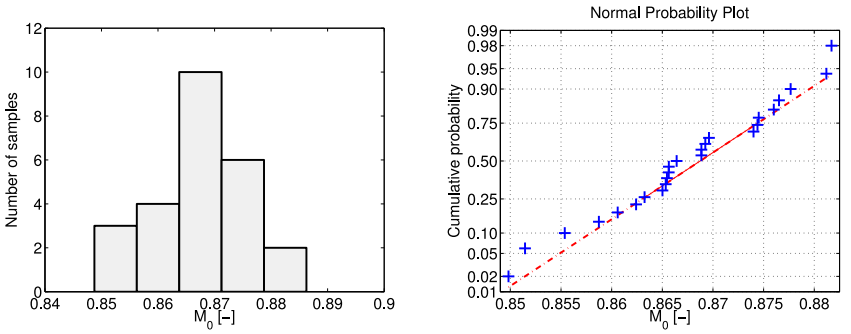

(a) (b)

Figure 2.18: a) Histogram of the moisture content of the 25 samples. b) Comparison of the probability of the moisture content in the samples with a normal distribution.

The data presented in Figure 2.18 shows that the experimental results follow a normal distribution. The average moisture content is $M_0 = 0.867$ kg/kg (wet basis) with a standard deviation of 0.008 kg/kg.

Nomenclature

A_c	Collector area [m^2]
dp	Differential pressure [Pa]
F_{cs}	View factor form the collector to the sky [-]
F_{cG}	View factor form the collector to the ground [-]
H	Relative humidity [-]
H_d	Drying chamber height [m]
I	Solar irradiance on the horizontal plane [W/m^2]
I_b	Beam component of the solar irradiance [W/m^2]
I_d	Diffuse component of the solar irradiance [W/m^2]

I_g Solar irradiance reflected from the ground [W/m^2]
I_o Extraterrestrial solar irradiance [W/m^2]
I_T Solar irradiance on the tilted surface [W/m^2]
K_c Constant of proportionality of the glass cover [s^{-1}]
k_p Proportional gain [-]
k_T Clearness index [-]
L Collector length [m]
L_d Drying chamber length [m]
m Mass [kg]
m_0 Initial product mass [kg]
m_d Mass of the dried product [kg]
M Moisture content [kg/kg]
M_0 Initial moisture content [kg/kg]
n Day of the year [-]
p Pressure [Pa]
P Electrical power of the solar air heater [W]
$r_\parallel$ Parallel component of the unpolarized radiation [-]
$r_\perp$ Perpendicular component of the unpolarized radiation [-]
R_b Ratio of beam radiation on the tilted plane to that on the horizontal plane [-]
s Distance between absorber plate and glass cover; or between the trays [m]
S Solar irradiance absorbed by the absorber plat [W/m^2]
t Time [s]
t_c Thickness of the glass cover [m]
t_i Integral time [min]
t_0 Characteristic time of the stabilization process [s]
t_1 Characteristic time of the stabilization process [s]
t_2 Characteristic time of the stabilization process [s]
T_0 Temperature at the inlet of the collector [°C]
T_1 Temperature at the inlet of the drying chamber [°C]
T_2 Temperature at the outlet of the drying chamber [°C]
W Solar dryer width [m]

Greek letters

α_p Absorptance of the absorber plate [-]

β	Inclination of the solar collector [°]
$\beta(opt)$	Optimal inclination of the solar collector [°]
δ	Declination [°]
θ	Angle of incidence of the solar radiation on the solar collector [°]
θ	Angle of incidence of the solar radiation on the solar collector [°]
θ_d	Equivalent angle of incidence of the diffuse component of the solar radiation on the solar collector [°]
θ_g	Equivalent angle of incidence of the ground reflected component of the solar radiation on the solar collector [°]
ρ_c	Reflectance of the glass cover [-]
ρ_g	Ground reflectance [-]
ϕ_0	Relative humidity at the inlet of the collector [-]
ϕ_1	Relative humidity at the inlet of the drying chamber [-]
ϕ_2	Relative humidity at the outlet of the drying chamber [-]
Φ	Latitude [°]
τ_c	Transmittance of the glass cover [-]
ω	Solar hour angle [°]
$(\tau\alpha)$	Effective transmittance-apsorptance product [-]
$(\tau\alpha)_b$	Beam component of the effective transmittance-apsorptance product [-]
$(\tau\alpha)_d$	Diffuse component of the effective transmittance-apsorptance product [-]
$(\tau\alpha)_g$	Ground reflection component of the effective transmittance-apsorptance product [-]

Abbreviations

ANR	Standard reference atmosphere conditions
DAQ	Data Acquisition
NTC	Negative Temperature Coefficient
PID	Proportional Integral Derevivative controller
RMSE	Root mean square error
TGA	Thermogravimetric analyser

References

AENOR 2010 Biocombustibles sólidos. Determinación del contenido de humedad. Método de secado en estufa. Parte 1: Humedad total. Método de referencia.

Cai, J. M. & Chen, S. Y. 2008 Determination of Drying Kinetics for Biomass by Thermogravimetric Analysis under Nonisothermal Condition. *Drying Technology* 26 (12), 1464–1468.

Chen, D., Zheng, Y. & Zhu, X. 2012 Determination of effective moisture diffusivity and drying kinetics for poplar sawdust by thermogravimetric analysis under isothermal condition. *Bioresource Technology* 107, 451–455.

Damartzis, T., Vamvuka, D., Sfakiotakis, S. & Zabaniotou, A. 2011 Thermal degradation studies and kinetic modeling of cardoon (Cynara cardunculus) pyrolysis using thermogravimetric analysis (TGA). *Bioresource Technology* 102 (10), 6230–6238.

Duffie, J. A. & Beckman, W. A. 2006 *Solar Engineering of Thermal processes*, 3rd edn. Hoboken, New Jersey: John Wiley and Sons.

El-Beltagy, A., Gamea, G. R. & Essa, A. H. A. 2007 Solar drying characteristics of strawberry. *Journal of Food Engineering* 78 (2), 456–464.

Energy-Plus 2015 http://energyplus.net/weather, accessed: may 2015.

Erbs, D. G., Klein, S. A. & Duffie, J. A. 1982 Estimation of the diffuse radiation fraction for hourly, daily and monthly-average global radiation. *Solar Energy* 28 (4), 293–302.

Freire, F., Figuredo, A. & Ferrão, P. 1999 Thermal Analysis and Drying Kinetics of Olive Bagasse. *Drying Technology* 17 (4-5), 895–907.

Hunn, B. D. & Calafell, D. O. 1977 Determination of average ground reflectivity for solar collectors. *Solar Energy* 19 (1), 87–89.

Iglesias, I., Carbó, J., Bonany, J. & Montserrat, R. 2009 Varietal Innovation in apples. *Revista de Fruticultura* pp. 13–25.

Karim, M. A. & Hawlader, M. N. A. 2004 Development of solar air collectors for drying applications. *Energy Conversion and Management* 45 (3), 329–344.

Karim, M. A. & Hawlader, M. N. A. 2006 Performance evaluation of a v-groove solar air collector for drying applications. *Applied Thermal Engineering* 26 (1), 121–130.

Li, Z. Y. & Kobayashi, N. 2005 Determination of moisture diffusivity by thermo-gravimetric analysis under non-isothermal condition. *Drying Technology* 23 (6), 1331–1342.

Liu, B. Y. H. & Jordan, R. C. 1963 The Long-Term Average Performance of Flat-Plate Solar Energy Collectors. *Solar Energy* 7 (2), 53–74.

Madhava, M., Rao, P. Srinivasa & Goswami, T. K. 2001 Drying Kinectics of Paddy Using Thermogravimetric Analysis. *Drying Technology* 19 (6), 1201–1210.

Shanmugam, V. & Natarajan, E. 2006 Experimental investigation of forced convection and desiccant integrated solar dryer. *Renewable Energy* 31 (8), 1239–1251.

Weiss, W. & Buchinger, J. 2004 Establishment of a production, sales and consulting infrastructure for solar thermal plants in Zimbabwe. *Institute for sustainable Technologies* p. 110.

CHAPTER

THREE

Evaluation of the maximum evaporation rate

Contents

3.1 Abstract

A theoretical study on the maximum evaporation rate obtainable in a small-scale indirect solar dryer is presented, considering evaporation of free water. The study considers general cases instead of a specific one. A mathematical model of the evolution of the temperature and the specific humidity of the airflow along the drying chamber is developed. Based on the results, some simplifications are proposed and justified in order to calculate the maximum evaporation rate as a function of a reduced number of parameters, to study their effect. The results show that the effect of the air mass flow rate on the maximum evaporation rate, which is the major effect, is affected by the aspect ratio of the drying chamber, defined as the ratio of the total drying area to the cross section in the drying chamber. Design and operation criteria can be extracted from the results.

3.2 Introduction

In indirect solar dryers, the air heating process and the drying process occur in series, and thus they can be studied separately. The global performance of the solar dryer relies on the interaction of the solar collector performance, the drying chamber performance, and the drying characteristics of the product. The drying capacity of the airflow, i.e., the total amount of vapour that the airflow can absorb before saturation, depends on the temperature and relative humidity of the airflow at the inlet of the chamber, and thus on the heating process in the collector. The ratio of the actual amount of vapour absorbed by the airflow over its drying capacity is the pick-up efficiency (Leon *et al.*, 2002), which depends on the drying process.

The flat-plate solar air heaters, single-glazed, with the air flowing between the absorber plate and the cover (upwards type) suit small-scale drying applications (Ekechukwu & Norton, 1999). Mathematical models for this type of air heaters were compiled by Duffie & Beckman (2006), based on the collector efficiency factor F', and the collector heat loss coefficient U_L. In active solar dryers, the temperature increment in the air heater is clearly affected by the air mass flow rate induced by the fan. Industrial dryers typically regulate the air mass flow rate to control the temperature (Şevik, 2014). The application of small-scale dryers is the rural sector, where control systems are less feasible. In such dryers, an air mass flow rate is normally set, and the drying temperature varies with the ambient conditions (Sreekumar *et al.*, 2008). The usage of an air heater improves the intrinsic drying capacity of the air at ambient conditions.

The drying process occurs in two stages: the constant rate period and the falling rate period (Sokhansanj & Jayas, 2006). During the constant rate period, the evaporation of unbounded superficial water occurs. During the falling rate period, the mechanisms of diffusivity inside the product govern the process, which is strongly dependent on the product (Belessiotis & Delyannis, 2011). Large-scale industrial dryers typically operate for a specific product, for which the drying process is optimized. Unlike large-scale solar dryers, the small-scale dryers are typically used for multipurpose applications (Pangavhane *et al.*, 2002; El-Sebaii *et al.*, 2002; Tiris & Dincer, 1995).

Many authors have reported the lack of unification on the methodology to evaluate the operation of a solar dryer (Singh & Kumar, 2012; Leon *et al.*, 2002). Among the different methods employed in the literature, Passamai & Saravia (1997) and Altobelli *et al.* (2014) proposed to evaluate the actual potential of

the solar dryer based on the evaporation of free water. The interest of this method is that the potential of the dryer is evaluated without the dependence of the product. The rate of evaporation of free water establishes the maximum vapour mass flow rate that can be absorbed by the airflow. It depends only on the interactions between the airflow and the wet surface of the product. Hence, assessing the pick-up efficiency considering evaporation of free water, allows the evaluation of the drying chamber without the dependence of the product, and for the maximum evaporation rate permissible for the drying conditions.

This chapter presents a theoretical study on the performance of indirect solar dryers of small-scale. The study is based on the heat and mass transfer processes occurring during the constant rate period, considering the evaporation of free superficial water. The work is divided in three parts: i) the evaluation of the solar air heater performance, ii) the evaluation of the drying chamber performance and iii) the evaluation of the global system performance. The first part addresses the determination of the drying capacity of the airflow in terms of the capacity acquired in the collector. The second part studies the pick-up efficiency obtainable during the evaporation of free water in the constant rate period, in the drying chamber. For the calculation of the pick-up efficiency, a mathematical model of the heat and mass transfer processes in the drying chamber is presented. Based on the results of the model, some simplifications in the calculation of the pick-up efficiency are proposed and justified. The third part determines the maximum evaporation rate that can be obtained in the dryer depending on the interaction of the solar collector and the drying chamber. The aim is to express the maximum evaporation rate as a function of a reduced number of parameters, to study their effect and to extract design and operation criteria.

3.3 Theoretical modelling

This section presents a mathematical model of the processes occurring in an active indirect solar dryer, during the evaporation of free water. Heat losses from the drying chamber to the ambient are neglected and steady state is assumed. A schematic of an indirect solar dryer is presented in Figure 3.1a. A schematic of a possible process taking place in the indirect solar dryer is represented in the psychrometric chart of Figure 3.1b.

The state 0 corresponds to the conditions at the inlet of the collector, which for this application are the ambient air conditions. The state 1 corresponds to

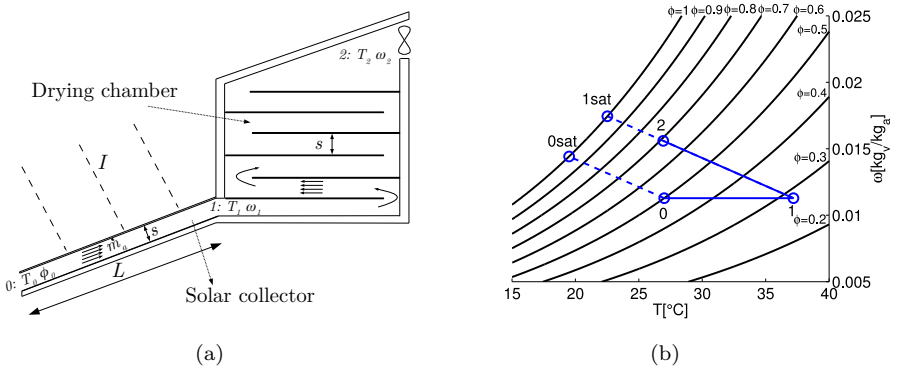

Figure 3.1: a) Schematic of an indirect solar dryer with the configuration considered in this chapter and b) typical air heating and drying processes presented in a psychrometric chart.

the outlet of the collector, which coincides with the inlet of the drying chamber. The state 2 describes the conditions at the outlet of the drying chamber. The air enters the solar collector at temperature T_0 and relative humidity ϕ_0. The heating process occurs along the solar air heater at constant specific humidity, $\omega_1 = \omega_0$. The airflow leaving the solar collector (T_1, ω_1), flows along the adiabatic drying chamber, over the trays arranged in series, absorbing water until the chamber exit (T_2, ω_2), following and adiabatic saturation process (an assumption only valid for indirect solar dryers). In Figure 3.1b two more states appear: 0sat and 1sat. They correspond to the adiabatic saturation conditions of states 0 and 1. The drying capacity of the air is the amount of vapour that the airflow can absorb until saturation. Therefore, the drying capacity of the airflow entering the collector is defined by points 0 and 0sat, while the capacity of the heated airflow at the inlet of the drying chamber is defined by points 1 and 1sat. The pick-up efficiency compares the actual amount of vapour absorbed between states 1 and 2 with the drying capacity of the heated airflow.

The dimensions and operating conditions considered in this study are selected based on typical small-scale solar dryers from the literature (Karim & Hawlader, 2004; Oztop *et al.*, 2013). The dimensions considered are: collector lengths L from 1 m to 3 m, with a width to length ratio W/L from 0.5 to 1 and a plate spacing s from 0.02 to 0.08 m. The width of the drying chamber is the same as that of the solar collector, W. The separation between trays is the same as the separation between the absorber plate and the glass cover,

s, maintaining the same airflow velocity in both devices. The cross section $A_s = W \cdot s$ is the same in both collector and chamber. The total drying area is $A_d = W \cdot L_d$, being L_d the total drying path length. The range of the aspect ratio of the drying chamber studied is from $A_d/A_s = 5$ to $A_d/A_s = 500$, and the range of the air mass flow rate per unit of collector area is $\dot{m}_a/A_c$ from 0.025 kg/m^{2}s to 0.07 kg/m^{2}s, being $A_c = W \cdot L$ the collector area.

3.3.1 Determination of the drying capacity

The drying capacity, defined as the total amount of vapour that the airflow leaving the solar collector can absorb before saturation, depends exclusively on the inlet conditions of the airflow and on the air heating process in the collector.

Duffie & Beckman (2006) presented a model for the calculation of the temperature at the outlet of a flat-plate collector T_1 as a function of the collector heat loss coefficient U_L, and the collector efficiency factor F'. U_L and F' depend only on the design of the solar collector (Hottel & Whillier, 1958).

$$T_1 = T_{amb} + \frac{I(\tau\alpha)}{U_L} - \left[\frac{I(\tau\alpha)}{U_L} - (T_0 - T_{amb})\right] \exp\left(\frac{-F'U_L A_c}{\dot{m}_a c_p}\right) \tag{3.1}$$

This chapter considers that the air enters the solar collector at ambient temperature $T_0 = T_{amb}$. The increment of temperature in the collector divided by the solar irradiance can be aggregated in a single parameter:

$$\frac{T_1 - T_0}{I} = \frac{(\tau\alpha)}{U_L}\left(1 - \exp\frac{-F'U_L A_c}{\dot{m}_a c_{p_a}}\right) \tag{3.2}$$

The values $U_L = 7$ W/m^{2}K and $F' = 0.85$ are representative for the whole range of parameters analysed, and could be obtained in any flat-plate collector with a proper design. The temperature increment in the solar collector divided by the solar irradiance calculated for such values of U_L and F' is presented in Figure 3.2.

The results in Figure 3.2 are shown as a function of the air mass flow rate per unit of collector area, aggregating the variations in both $\dot{m}_a$ and A_c. The results show that lower air mass flow rates entail larger increments of temperature since the air velocity in the solar air heater is lower, and thus the residence time in the collector for a certain length is greater.

The drying capacity $\dot{m}_{v_{DC}}$ is :

$$\dot{m}_{v_{DC}} = \dot{m}_a \left(\omega_{1\text{sat}} - \omega_1\right) \tag{3.3}$$

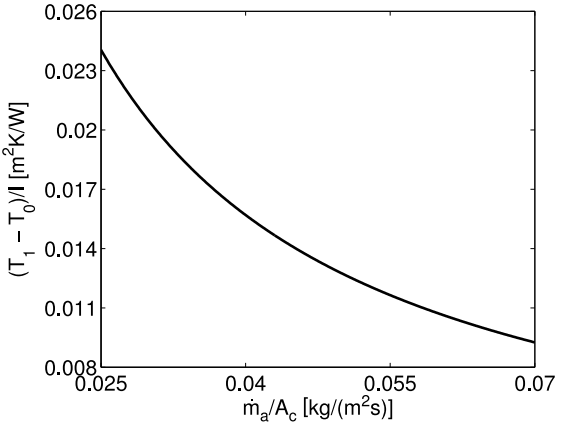

Figure 3.2: Temperature increment divided by the solar irradiance absorbed by the solar collector, for $U_L = 7$ W/m^{2}K and $F' = 0.85$, as a function of the air mass flow rate per unit of collector area.

where $\omega_1 = \omega_0$ and $\omega_{1\text{sat}}$ is obtained using the following psychrometric relations, considering an adiabatic saturation process starting at state 1:

$$\omega_{1\text{sat}} = 0.622 \frac{p_{\text{sat}}(T_{1\text{sat}})}{p_a - p_{\text{sat}}(T_{1\text{sat}})} \tag{3.4}$$

$$T_{1\text{sat}} - T_{(0°C)} = \frac{\omega_{1\text{sat}} h_{v_{(0°C)}} - \omega_1 \left[h_{v_{(0°C)}} + c_{p_v} \left(T_1 - T_{(0°C)} \right) \right]}{\omega_{1\text{sat}} (c_{p_w} - c_{p_v}) - \omega_1 c_{p_w} - c_{p_a}} - \\ - \frac{c_{p_a} \left(T_1 - T_{(0°C)} \right)}{\omega_{1\text{sat}} (c_{p_w} - c_{p_v}) - \omega_1 c_{p_w} - c_{p_a}} \tag{3.5}$$

The results obtained from equations (3.3) to (3.5) are shown in Figure 3.3, for a nominal case defined by an air ambient temperature $T_0 = 27$ °C, a relative humidity $\phi_0 = 0.5$ and a solar irradiance $I = 800$ W/m^2. The case for unheated air is also presented for comparison. The case of unheated air considers that the drying process begins at ambient conditions, corresponding to the process 0 to 0sat in Figure 3.1b, whereas the drying process after the air heating process corresponds to the process 1 to 1sat.

The maximum increment in the specific humidity that can be obtained in the processes 0 to 0sat and 1 to 1sat is presented in Figure 3.3a for the nominal case. The corresponding drying capacity, calculated with equation (3.3), is presented in Figure 3.3b. The results are presented as a function of the air mass flow rate per unit of collector area, consistently with the results in Figure 3.2. For the

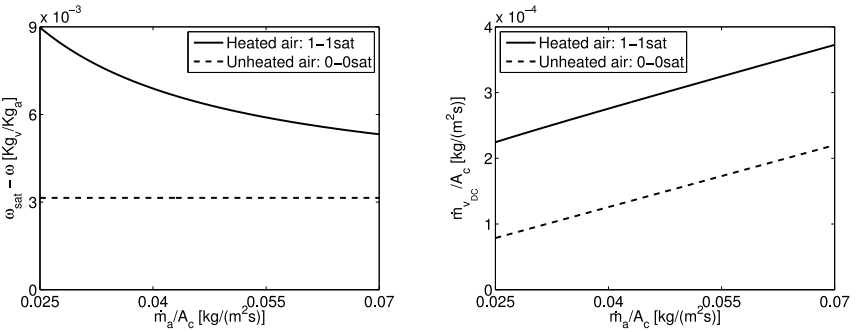

Figure 3.3: a) Increment in the specific humidity in an adiabatic saturation process and b) drying capacity as a function of the air mass flow rate per unit of collector area.

case of heated air (1 to 1sat), an increase of the air mass flow rate per unit of collector area presents two opposite effects: increasing the vapour that can be extracted $\dot{m}_{v_{DC}}$ and decreasing the increment in specific humidity $\omega_{1\text{sat}} - \omega_1$. The effect on the increment of specific humidity is due to the effect of the air mass flow rate on the temperature increment. Lower T_1 entails lower $\omega_{1\text{sat}}$. The effect on the drying capacity shows that the multiplicative effect of the air mass flow rate on the drying capacity (equation (3.3)) counteracts the descent of $\omega_{1\text{sat}} - \omega_1$. Comparing the curves of heated and unheated processes, it can be observed that the heating process loses effect, in terms of increment of specific humidity (Figure 3.3a), as the air mass flow rate per unit of collector area increases. Doubling the air mass flow rate, the difference between the increment in specific humidity of heated and unheated air (difference between solid and dashed lines) is reduced to the half, approximately. However, this effect is mitigated when considering the drying capacity. The differences between the heated and unheated processes in Figure 3.3b are almost constant in the whole range considered ($\dot{m}_{v_{DC}}$(heated) - $\dot{m}_{v_{DC}}$(unheated) $\sim 1.45{\cdot}10^{-4}$ kg/m^{2}s), which entail that the increment in specific humidity in Figure 3.3a (solid line) presents a hyperbolic decay.

The results in Figure 3.3 correspond to the nominal case defined by $\phi_0 = 0.5$, $T_0 = 27$ °C and $I = 800$ W/m^2. Variations in these parameters modify the drying capacity. A ratio R is defined to asses such effect, comparing the drying capacity obtained for the different values of T_0, ϕ_0 and I to that obtained for

the nominal values:

$$R = \frac{\dot{m}_{v_{DC}}}{\dot{m}_{v_{DC}}(nom)} \tag{3.6}$$

The analysis considers variations of 20 °C $\leq T_0 \leq$ 35 °C, 0.3 $\leq \phi_0 \leq$ 0.9 and 300 W/m^2 $\leq I \leq$ 1000 W/m^2. The results are presented in Figure 3.4. In every case, two parameters are kept constant and equal to the nominal value, and the third one is varied.

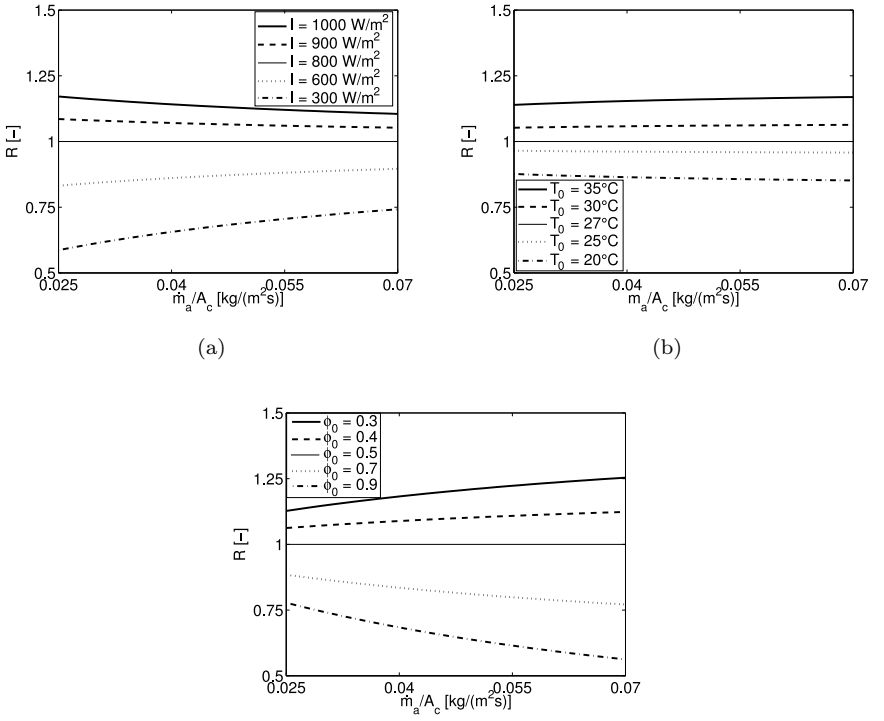

Figure 3.4: Ratio of variation of the drying capacity over the nominal case: a) effect of solar irradiance absorbed by the solar collector, b) effect of the ambient air temperature and c) effect of the ambient air relative humidity.

The nominal case corresponds to a multiplying factor $R = 1$. As may be expected, high irradiance (Figure 3.4a) and an ambient air with high temperature (Figure 3.4b) and low humidity (Figure 3.4c) are conditions more propitious for drying. It can be observed in the graphs that the effect on R of varying I, T_0 or ϕ_0 at a determined $\dot{m}_a/A_c$ is quasilinear. But the quantitative effect of I,

T_0 or ϕ_0 on R depends on $\dot{m}_a/A_c$. The effect of the solar radiation is reduced for higher air mass flow rates per unit of collector area, since the temperature increment is lower. The effect of T_0 on R increases slightly whereas the effect of ϕ_0 on R increases notably when the air mass flow rate per unit of collector area is increased.

3.3.2 Modelling of the process in the drying chamber

The process considered for the modelling of the drying chamber is the evaporation of free water. The control volume analyzed is shown in Figure 3.5.

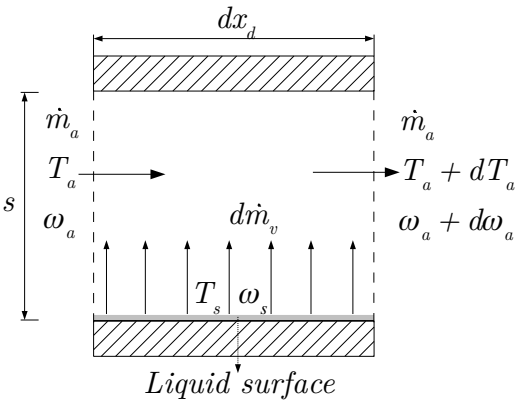

Figure 3.5: Control volume analyzed in the drying chamber.

The mass and energy balances in the control volume of the drying chamber are:

$$\dot{m}_a d\omega_a = d\dot{m}_v = n_v W dx_d \tag{3.7}$$

$$n_v h_w W dx_d = \dot{m}_a (c_{p_a} + \omega_a c_{p_v}) dT_a + \dot{m}_a \left[h_{v_{(0^\circ C)}} + c_{p_v} \left(T_a - T_{(0^\circ C)} \right) \right] d\omega_a \tag{3.8}$$

with the boundary conditions:

$$x_d = 0 \longrightarrow \begin{cases} T_a = T_1 \\ \omega_a = \omega_1 \end{cases} \tag{3.9}$$

n_v is the rate at which moisture evaporates from the surface, defined by the convective mass transfer coefficient K and the difference in specific humidity

between the saturated air layer over the liquid surface, ω_s, and the bulk air, ω_a:

$$n_v = K(\omega_s - \omega_a) \tag{3.10}$$

The energy balance on the liquid surface, neglecting conduction and radiation terms is:

$$h_c(T_s - T_a) = n_v h_{fg} \tag{3.11}$$

For the configuration shown in Figure 3.5 the convective heat and mass transfer coefficients, h_c and K respectively, can be calculated using the correlation proposed by Treybal (1980):

$$\frac{h_c}{\rho_a u c_{p_a}} \mathrm{Pr}^{2/3} = \frac{K}{\rho_a u} \mathrm{Sc}^{2/3} = 0.11 \mathrm{Re}^{-0.29} \qquad 2600 \leq \mathrm{Re} \leq 22000 \tag{3.12}$$

The range of application of this study, described in section 3.3 entails Reynolds numbers within the range $2600 \leq \mathrm{Re} \leq 22000$, and thus equation (3.12) is applicable in the whole range considered. The characteristic length in the Reynolds number is the hydraulic diameter. Equations (3.7) to (3.12) were numerically solved in MatLab® using the finite differences method. The input parameters of the model are: the solar irradiance I, the air temperature and relative humidity at the collector inlet T_0 and ϕ_0, the collector and the drying chamber dimensions, and the air mass flow rate $\dot{m}_a$. The input parameters employed in the model as a nominal case are: $T_0 = 27$ °C, $\phi_0 = 0.5$, $I = 800$ W/m^2, $L = 1$ m, $W = 0.5$ m, $s = 0.04$ m, and $\dot{m}_a = 0.025$ kg/s. The distribution of the temperature and the specific humidity of the air and the liquid surface along the drying path are shown in Figure 3.6 for the nominal case.

The evolution of the temperatures is shown in Figure 3.6a and that of the specific humidities in Figure 3.6b. For the hypotheses assumed (adiabatic process at steady state), the surface is at the wet bulb conditions, which are the conditions corresponding to the thermal equilibrium with the bulk air. As the air flows along the dryer, it losses heat used to evaporate the water on the product surface, decreasing its temperature and increasing its specific humidity, until saturation is reached. The wet bulb conditions increase slightly towards saturation conditions, $T_{1\mathrm{sat}}$ and $\omega_{1\mathrm{sat}}$. Figure 3.6 shows that the conditions of the surface ω_s and T_s, barely vary along x_d and are very close to saturation conditions, and thus they could be considered constant, $T_s = T_{1\mathrm{sat}}$ and $\omega_s = \omega_{1\mathrm{sat}}$.

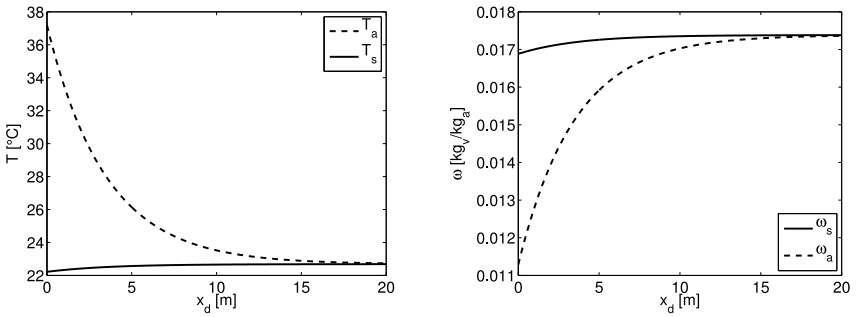

(a) (b)

Figure 3.6: Evolution of a) temperature and b) specific humidity of the air and the liquid surface along the drying chamber.

Due to dimensional restrictions (shorter lengths of the drying path) saturation may not be reached. The pick-up efficiency assesses the percentage of the saturation process covered in the drying chamber.

3.3.3 Determination of the pick-up efficiency

The pick-up efficiency is defined as the ratio of the actual amount of vapour absorbed by the airflow over its drying capacity.

$$\eta_{pu} = \frac{\omega_2 - \omega_1}{\omega_{1\text{sat}} - \omega_1} \tag{3.13}$$

The specific humidity of the air at the outlet of the drying chamber, $x_d = L_d$, can be calculated combining equation (3.7) and equation (3.10):

$$\int_{\omega_a=\omega_1}^{\omega_a=\omega_2} \dot{m}_a d\omega_a = \int_{x_d=0}^{x_d=L_d} K(\omega_s - \omega_a) W dx_d \tag{3.14}$$

As shown in Figure 3.6, ω_s can be assumed to be constant, $\omega_s = \omega_{1\text{sat}}$. Variations in K along the drying path are due to the variations of the thermal properties with the temperature and thus, it can also be assumed to be constant, $\bar{K}$, calculated for the average temperature between T_1 and $T_{1\text{sat}}$. With such simplifications, the specific humidity at the outlet of the chamber can be calculated as:

$$\omega_2 = \omega_{1\text{sat}} - (\omega_{1\text{sat}} - \omega_1) \exp\left(-\frac{\bar{K}}{\dot{m}_a} A_d\right) \tag{3.15}$$

Combining equations (3.13) and (3.15), a simple expression can be obtained for the pick-up efficiency:

$$\eta_{pu} = 1 - \exp\left(-\frac{\bar{K}}{\dot{m}_a} A_d\right) \tag{3.16}$$

In order to validate the simplification of considering $\bar{K}$ and $\omega_s = \omega_{1\text{sat}}$ as constants, the variations of K and ω_s along x_d were calculated for the whole range of dryer dimensions and air mass flow rates with the model presented in section 3.3.2. The analysis showed variations lower than 3.5% for K and 7% for ω_s in all cases. The resulting maximum absolute error in the pick-up efficiency was 0.07 for the whole range of configurations. Hence, calculating the pick-up efficiency with equation (3.16) can be considered accurate for small-scale indirect solar dryers, with the configuration presented in Figure 3.1a.

3.4 Calculation of the maximum evaporation rate

This section presents the maximum evaporation rate, $\dot{m}_v$, that can be obtained in a small-scale indirect solar dryer, considering the coupling between the solar collector and the drying chamber, for the evaporation of free water. The maximum evaporation rate results from the multiplication of the pick-up efficiency (equation (3.16)) and the drying capacity (equation (3.3)). Introducing the definition of K (equation (3.12)) in the exponent of the pick-up efficiency, and rearranging terms, the maximum evaporation rate $\dot{m}_v$ is obtained. For the calculation of the Reynolds number, the hydraulic diameter is assumed to be $2s$ (assuming $W >> s$).

$$\dot{m}_v = \left\{1 - \exp\left[-0.11 Sc^{-2/3} \frac{A_d}{A_s} \left(\frac{2}{\mu}\frac{\dot{m}_a}{W}\right)^{-0.29}\right]\right\} \dot{m}_a(\omega_{1\text{sat}} - \omega_1) \tag{3.17}$$

Results of equation (3.17), using the ambient conditions and the collector area defined by the nominal case, are shown in Figure 3.7. In Figure 3.7a, the maximum evaporation rate is presented as a function of the air mass flow rate $\dot{m}_a$, for different aspect ratios A_d/A_s. The data is rearranged in Figure 3.7b to clarify the effect of A_d/A_s.

Figure 3.7a shows that the drying capacity (in a blue solid line) and the maximum evaporation rate (for different A_d/A_s) increase with the air mass flow rate. However, the effect of the air mass flow rate on the maximum evaporation rate is more relevant for high values of A_d/A_s while for low values of

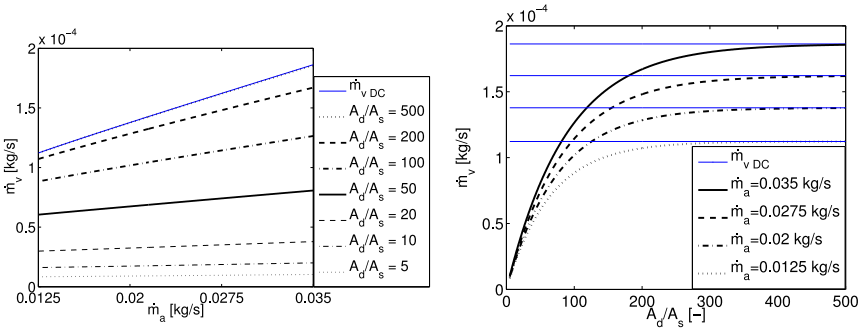

(a) (b)

Figure 3.7: Maximum evaporation rate as a function of a) the air mass flow rate and b) the aspect ratio of the drying chamber.

A_d/A_s the effect of $\dot{m}_a$ on $\dot{m}_v$ becomes negligible. The effect of the aspect ratio of the drying chamber on the maximum evaporation rate can be observed in Figure 3.7b. For low A_d/A_s (below 200 for the nominal case), increasing A_d/A_s, whenever possible, enhances notably the drying process in terms of the maximum evaporation rate obtainable. In the region where A_d/A_s is larger, the maximum evaporation rate presents an asymptotic trend to the drying capacity (blue solid line), and thus increasing A_d/A_s appears to be useless. Design and operation criteria could be extracted from the results. For the range of parameters analysed, A_d/A_s should be between 200 and 300, depending on the air mass flow rate. Within that range, doubling the air mass flow rate entails an increment of around 20% in the maximum evaporation rate obtainable, while below $A_d/A_s = 50$, the effect of increasing the air mass flow rate is slight.

The ambient conditions have a negligible effect on the pick up efficiency calculated with equation 3.16, and thus the effect on the maximum evaporation rate is equivalent to the effect on the drying capacity.

3.5 Conclusions

A study on the maximum evaporation rate obtainable in a small-scale indirect solar dryer is presented, based on the drying capacity that the airflow acquires in the solar collector, and the pick-up efficiency of the drying chamber, evaporating free water. The heat and mass transfer processes occurring in the drying chamber are modelled. Based on the results of the model, a simple expres-

sion for the analytical calculation of the pick-up efficiency is proposed. The maximum absolute error obtained when using the proposed expression instead of the numerical solution of the model is 0.07. The expression is used for the calculation of the maximum evaporation rate of the solar dryer, expressed as a function of a reduced number of parameters: air mass flow rate, collector width and length, aspect ratio in the drying chamber (drying area to cross section) and ambient conditions. The results show that the maximum evaporation rate increases with the air mass flow rate, but with a strong dependence on the aspect ratio of the drying chamber. Hence, a proper selection of the aspect ratio could enhance the drying process. For the nominal case analysed (a collector of 1 m length and 0.5 m width), the drying chamber aspect ratio to obtain a proper evaporation rate should be between 200 and 300, depending on the air mass flow rate.

Nomenclature

A_c	Collector area [m^2]
A_d	Total drying area [m^2]
A_s	Cross section in the drying chamber [m^2]
c_{p_a}	Specific heat of the air [J/kgK]
c_{p_v}	Specific heat of the vapour [J/kgK]
c_{p_w}	Specific heat of the water [J/kgK]
F'	Collector efficiency factor [−]
h_c	Convective coefficient [W/m^2K]
h_{fg}	Specific enthalpy of vaporization [J/Kg]
$h_{v(0°C)}$	Specific enthalpy of saturated vapor at 0 °C [J/kg]
h_w	Specific enthalpy of water [J/kg]
I	Solar irradiance [W/m^2]
K	Convective mass transfer coefficient [kg/m^2s]
$\bar{K}$	Constant convective mass transfer coefficient [kg/m^2s]
L	Collector length [m]
L_d	Drying path length [m]
$\dot{m}_a$	Air mass flow rate [kg/s]
$\dot{m}_v$	Maximum evaporation rate [kg/s]
$\dot{m}_{v_{DC}}$	Drying capacity [kg/s]
n_v	Rate of evaporation of moisture per unit of surface [kg/m^2s]
p_a	Absolute pressure [Pa]

p_{sat}	Saturation pressure [Pa]
Pr	Prandtl number [−]
Re	Reynolds number [−]
R	Ratio of variation of the drying capacity over the nominal case [−]
s	Plate spacing (collector) and tray spacing (drying chamber) [m]
Sc	Schmidt number [−]
T	Temperature [°C]
T_a	Temperature of the air in the drying chamber [°C]
T_{amb}	Temperature of the ambient air [°C]
T_s	Temperature of the surface of the liquid [°C]
T_0	Temperature at the inlet of the solar collector [°C]
T_1	Temperature at the outlet of the solar collector or inlet of the drying chamber [°C]
$T_{1\text{sat}}$	Temperature at adiabatic saturation conditions [°C]
T_2	Temperature at the outlet of the drying chamber [°C]
$T_{(0°C)}$	Temperature at 0 °C [°C]
u	Airflow velocity [m/s]
U_L	Collector heat loss coefficient [W/m^{2}K]
W	Width of the dryer [m]
x_d	Coordinate of the drying chamber in the fluid flow direction [m]

Greek letters

η_{pu}	Pick-up efficiency [−]
μ	Dynamic viscosity of the air [kg/ms]
ρ_a	Density of the air [kg/m^3]
ϕ_0	Relative humidity at the inlet of the collector [−]
ω	Specific humidity [kg/kg]
ω_s	Specific humidity over the liquid surface [kg/kg]
ω_{sat}	Specific humidity at adiabatic saturation condition [kg/kg]
ω_0	Specific humidity at the inlet of the collector [kg/kg]
ω_1	Specific humidity at the inlet of the drying chamber [kg/kg]
$\omega_{1\text{sat}}$	Specific humidity at adiabatic saturation conditions at the inlet of the drying chamber [kg/kg]
ω_2	Specific humidity at the outlet of the drying chamber [kg/kg]
$(\tau\alpha)$	Effective transmittance-absorptance product [−]

References

Altobelli, F., Condorí, M., Duran, G. & Martinez, C. 2014 Solar dryer efficiency considering the total drying potential. Application of this potential as a resource indicator in north-western Argentina. *Solar Energy* 105, 742–759.

Belessiotis, V. & Delyannis, E. 2011 Solar drying. *Solar Energy* 85 (8), 1665–1691.

Duffie, J. A. & Beckman, W. A. 2006 *Solar Engineering of Thermal processes*, 3rd edn. Hoboken, New Jersey: John Wiley and Sons.

Ekechukwu, O. V. & Norton, B. 1999 Review of solar-energy drying systems III: low temperature air-heating solar collectors for crop drying applications. *Energy Conversion and Management* 40 (6), 657–667.

El-Sebaii, A. A., Aboul-Enein, S., Ramadan, M. R. I. & El-Gohary, H. G. 2002 Experimental investigation of an indirect type natural convection solar dryer. *Energy Conversion and Management* 43 (16), 2251–2266.

Hottel, H. C. & Whillier, A. 1958 Evaluation of flat-plate solar-collector performance. *Transactions of the Conference on Use of Solar Energy* 54 (1), 19–41.

Karim, M. A. & Hawlader, M. N. A. 2004 Development of solar air collectors for drying applications. *Energy Conversion and Management* 45 (3), 329–344.

Leon, M. A., Kumar, S. & Bhattacharya, S. C. 2002 A comprehensive procedure for performance evaluation of solar food dryers. *Renewable and Sustainable Energy Reviews* 6 (4), 367–393.

Oztop, H. F., Bayrak, F. & Hepbasli, A. 2013 Energetic and exergetic aspects of solar air heating (solar collector) systems. *Renewable and Sustainable Energy Reviews* 21, 59–83.

Pangavhane, D. R., Sawhney, R. L. & Sarsavadia, P. N. 2002 Design, development and performance testing of a new natural convection solar dryer. *Energy* 27 (6), 579–590.

Passamai, V. & Saravia, L. 1997 Relationship Between a Solar Drying Model of Red Pepper and the Kinetics of Pure Water Evaporation (I). *Drying Technology* 15 (5), 1419–1432.

Singh, S. & Kumar, S. 2012 Testing method for thermal performance based rating of various solar dryer designs. *Solar Energy* 86 (1), 87–98.

Sokhansanj, S. & Jayas, D. S. 2006 Drying of Foodstuffs. In *Handbook of Industrial Drying*, 3rd edn. (ed. A.S Mujumdar), chap. 21, pp. 522–545. Taylor and Francis Group, CRC Press.

Sreekumar, A., Manikantan, P. E. & Vijayakumar, K. P. 2008 Performance of indirect solar cabinet dryer. *Energy Conversion and Management* 49 (6), 1388–1395.

Tiris, C. & Dincer, I. 1995 Investigation of the thermal efficiencies of a solars dryer. *Energy Conservation and Management* 36 (3), 205–212.

Treybal, R. E. 1980 *Mass-Transfer Operations*, 3rd edn. United States of America: McGraw-hill Book Company.

Şevik, S. 2014 Experimental investigation of a new design solar-heat pump dryer under the different climatic conditions and drying behavior of selected products. *Solar Energy* 105, 190–205.

CHAPTER

FOUR

Mathematical modelling and experimental analysis of a solar air heater

Contents

4.1 Abstract

In indirect solar drying, the air heating process in the collector precedes the drying process in the drying chamber, thus establishing the drying conditions. This chapter presents a study on the solar air heating process occurring in the

solar collector, as a part of the indirect solar dryer. First, a theoretical modelling of the heat transfer mechanism, that calculates the temperatures of the glass cover, the absorber plate and the airflow at the outlet of the collector, for different operating conditions, is presented. The model is firstly developed assuming steady state conditions, and it is based on the theoretical calculations of the collector efficiency factor F' and the collector heat loss coefficient U_L. From the results of the steady state model, a model of the solar collector operating at transient conditions is evolved. Both models are experimentally validated. In addition, an experimental analysis is performed to characterize the operation of the lab-scale solar collector. The thermal performance is obtained in terms of the thermal efficiency and the increment of temperature is obtained as a function of the solar irradiance. Following a standard procedure, the experimental values of F' and U_L are obtained and compared to the values derived from the theoretical model. Finally, the drying conditions obtained for the reference climate defined in Chapter 2, and the associated maximum evaporation rate, are presented and analysed.

4.2 Introduction

The drying conditions at the inlet of the drying chamber are established by the solar collector, and affects the global performance of the solar dryer. Hence, it is important to study the performance of the solar collector at the conditions at which the solar drying is going to operate.

Solar air heaters for drying applications comprise mainly an absorber plate, a glass cover, the channel through which the air flows, and insulation. Many different configurations exist, depending on the shape and disposition of these components. Regarding the shape of the absorber plate, the solar air heaters can be flat-plate type or corrugated. Depending on the disposition of the airflow, the absorber plate and the glass cover, they can be classified as upwards-type, if the air flows above the absorber plate and below the glass cover; downwards-type, if the air flows below the absorber plate and above the insulation, or with two channels, if the air flows on both sides of the absorber plate. This last type can operate with a single pass, if the air flows through both channels in parallel, or double pass if that occurs in series. Solar air heaters have typically one glass cover, although they can be unglazed for low cost applications, or present more than one glass cover if the efficiency is to be enhanced. Among the variety of types of solar air heaters, the flat-plate solar collectors of upwards type with

one glass cover are appropriate for drying applications due to the compromise between simplicity and good performance (Ekechukwu & Norton, 1999), and thus this is the application selected in this thesis.

Many authors have focused on the study of solar air heaters for drying applications. A recent review on the state of the art was presented by Oztop *et al.* (2013). Most of the work consists of experimental analysis or mathematical modelling of the air heating process. The experimental works typically are based on the evaluation of the thermal performance of specific solar air heaters. Kadam & Samuel (2006) assessed the temperature increment obtained in a flat-plate solar collector during several days. Karim & Hawlader (2006) compared the performance of flat-plate, corrugated and finned solar air heaters at different air mass flow rates. Singh & Kumar (2012) obtained different correlations for the Nusselt number from the experimental data obtained in a lab-scale solar air heater operating at steady state.

Regarding the mathematical modelling, a review of the different models available in the literature was presented by Tchinda (2009). Most of the theoretical works are based on the calculation of the removal factor F_R, the collector efficiency factor F' and the collector heat loss coefficient U_L, parameters derived by Hottel & Whillier (1958) that depend only on the solar collector design.

The thermal performance of the solar air heaters is generally assessed (both experimentally and numerically) by means of the thermal efficiency, defined as the ratio of useful heat to available solar irradiance (Akpinar & Koçyigit, 2010; Alta *et al.*, 2010; Montero *et al.*, 2010). Evidently, the thermal performance of a solar air heater is highly dependent on the dimensions, materials and configuration, and on the ambient conditions during the operation.

In Chapter 3, a theoretical study on the effect of the solar air heating process on the drying capacity of the airflow was presented. The aim of the study was to identify the most affecting parameters and to analyse their effect on the global process. In order to reduce the number of parameters, several simplifications were done. This chapter presents a more detailed study on the solar air heating process, specific for the solar air heater employed in the experimental facility.

This Chapter includes, firstly, a mathematical modelling of the air heating process, based on a model proposed by Duffie & Beckman (2006) for flat-plate solar air heaters. The model is validated with experimental results obtained in the solar collector of the lab-scale solar dryer described in Chapter 2. Then, a detailed experimental analysis is presented, in order to characterize the lab-scale solar air heater and to determine the drying conditions.

4.3 Theoretical modelling of the solar air heater

A schematic of a solar air heater of the upwards type (i.e. the air flows above the absorber plate and below the glass cover) and the heat fluxes considered is depicted in Figure 4.1.

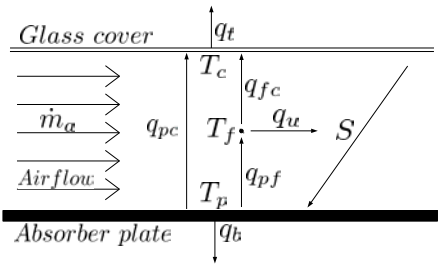

Figure 4.1: Schematic of the heat fluxes in the solar air heater.

As a major hypothesis, the heat fluxes per unit of collector area represented in Figure 4.1 are assumed to be constant in the whole surface and referred to the average temperatures of the absorber plate T_p, the glass cover T_c, and the airflow T_f. S is the solar irradiance absorbed by the absorber plate of the solar air heater, calculated in equation (2.8) in Chapter 2. The solar irradiance absorbed by the glass cover is neglected since the absorptance of glass is typically low. q_{pf} and q_{pc} are the heat fluxes from the absorber plate to the airflow (convection) and to the glass cover (radiation), respectively. q_{fc} is the heat transferred from the airflow to the glass cover. q_b and q_t are the heat losses from the absorber plate and the glass cover to the ambient air, respectively. The heat losses through the lateral walls are neglected. q_u is the useful heat gained by the airflow.

The heat balances on the airflow, the absorber plate and the glass cover are:

$$q_u = q_{pf} - q_{fc} \tag{4.1}$$

$$m_p c_p \frac{dT_p}{dt} = S - q_b - q_{pf} - q_{pc} \tag{4.2}$$

$$m_c c_c \frac{dT_c}{dt} = q_{pc} + q_{fc} - q_t \tag{4.3}$$

The capacitive term of the airflow is neglected since it is small compared to that of the glass cover and the absorber plate.

The heat transferred from the absorber plate to the fluid and from the fluid

to the cover, neglecting radiation, are calculated as:

$$q_{pf} = h_{c_{pf}}(T_p - T_f) \tag{4.4}$$

$$q_{fc} = h_{c_{fc}}(T_f - T_c) \tag{4.5}$$

The heat transfer coefficients are obtained from the correlation for the Nusselt number proposed by Singh & Kumar (2012). This correlation is specific for solar air heaters of indirect solar dryers with upwards airflow, for a Reynolds number based on the hydraulic diameter ranging $3000 < \mathrm{Re} < 9000$:

$$\mathrm{Nu} = \frac{h_c d_h}{k_a} = 0.707\mathrm{Re}^{0.477}\mathrm{Pr}^{0.4} \tag{4.6}$$

The heat transferred between the plate and the cover by radiation is calculated as:

$$q_{pc} = \frac{\sigma(T_p^4 - T_c^4)}{\epsilon_c^{-1} + \epsilon_p^{-1} - 1} \tag{4.7}$$

In order to express the heat flux by radiation in the form of equations (4.4) and (4.5), an equivalent coefficient $h_{r_{pc}}$ is used:

$$q_{pc} = h_{r_{pc}}(T_p - T_c) \tag{4.8}$$

Substituting into equation (4.7):

$$h_{r_{pc}} = \frac{\sigma(T_p^2 + T_c^2)(T_p + T_c)}{\epsilon_c^{-1} + \epsilon_p^{-1} - 1} \tag{4.9}$$

The heat losses from the absorber plate to the ambient through the bottom of the collector are expressed in terms of the bottom heat loss coefficient, U_b, that considers conduction through the insulation and convection to the ambient:

$$q_b = U_b(T_p - T_{amb}) \tag{4.10}$$

$$U_b = \left(\frac{t_i}{k_i} + \frac{1}{h_{c_{ia}}}\right)^{-1} \tag{4.11}$$

The heat losses from the inner surface of the glass cover are expressed in terms of the top heat loss coefficient U_t:

$$q_t = U_t(T_c - T_{amb}) \tag{4.12}$$

U_t is calculated considering conduction through the glass cover, and convection and radiation to the ambient from the glass cover upper surface:

$$U_t = \left(\frac{1}{h_{c_{ca}} + h_{r_{ca}}} + \frac{t_c}{k_c}\right)^{-1} \tag{4.13}$$

The correlation used for the Nusselt on the upper surface of the glass cover is that recommended by Incropera & Dewitt (1990) for natural convection, based on the characteristic length $l_c = A_c/2(W + L)$:

$$\mathrm{Nu} = \frac{h_c l_c}{k_a} = 0.54\mathrm{Ra}^{1/4} \tag{4.14}$$

The correlation is valid for a range of Rayleigh numbers of $10^4 \leq \mathrm{Ra} \leq 10^7$. The effect of the wind and of the angle of inclination of the solar collector are neglected. The radiation coefficient $h_{r_{ca}}$ is calculated as:

$$h_{r_{ca}} = \sigma \epsilon_c (T_c^2 + T_{amb}^2)(T_c + T_{amb}) \tag{4.15}$$

4.3.1 Operation at steady state conditions

In this section, the modelling of the solar air heater assuming steady state conditions is presented. The numerical results are compared with the experimental measurements obtained in the laboratory facility. The experimental validation is shown in section 4.4.

Under steady state conditions, the previous equations for the energy balance yield:

- For the absorber plate:

$$S - U_b(T_p - T_{amb}) - h_{c_{pf}}(T_p - T_f) - h_{r_{pc}}(T_p - T_c) = 0 \tag{4.16}$$

- For the glass cover:

$$h_{r_{pc}}(T_p - T_c) + h_{c_{fc}}(T_f - T_c) - U_t(T_c - T_{amb}) = 0 \tag{4.17}$$

- For the airflow:

$$q_u = h_{c_{pf}}(T_p - T_f) - h_{c_{fc}}(T_f - T_c) \tag{4.18}$$

Operating at steady state conditions, the useful heat can be expressed as a function of the collector efficiency factor F' and the collector heat loss coefficient U_L, parameters that depend only on the design of the solar collector (Hottel & Whillier, 1958):

$$q_u = F' \left[S - U_L(T_f - T_{amb}) \right] \tag{4.19}$$

Combining equations (4.16) to (4.19), F' and U_L can be obtained:

$$F' = \frac{h_{c_{pf}} h_{r_{pc}} + h_{c_{pf}} U_t + h_{r_{pc}} h_{c_{fc}} + h_{c_{pf}} h_{c_{fc}}}{(U_t + h_{r_{pc}} + h_{c_{fc}})(U_b + h_{r_{pc}} + h_{c_{pf}}) - h_{r_{pc}}^2} \tag{4.20}$$

$$U_L = \frac{(U_b + U_t)(h_{c_{pf}} h_{c_{fc}} + h_{c_{pf}} h_{r_{pc}} + h_{c_{fc}} h_{r_{pc}}) + U_b U_t (h_{c_{pf}} + h_{c_{fc}})}{h_{c_{pf}} h_{r_{pc}} + h_{c_{pf}} U_t + h_{r_{pc}} h_{c_{fc}} + h_{c_{pf}} h_{c_{fc}}} \tag{4.21}$$

The energy balance in a control volume of the solar collector, such as that represented in Figure 4.2, is:

$$\dot{m}_a c_{p_a} dT_a = F' \left[S - U_L (T_a - T_{amb}) \right] W dx \tag{4.22}$$

where T_a is the temperature of the airflow along the solar collector direction.

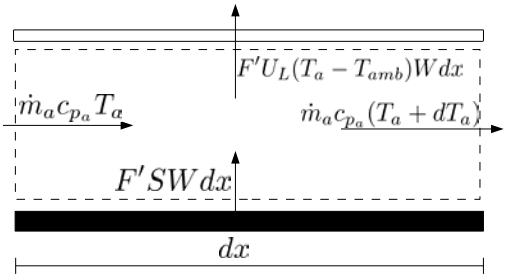

Figure 4.2: Control volume in the solar collector.

F' and U_L can be considered constant along the coordinate x in the direction of the collector length (Duffie & Beckman, 2006) and thus equation (4.22) can be integrated to obtain the distribution of the temperature of the fluid along the collector $T_a(x)$, with the airflow entering at temperature T_0:

$$T_a(x) = T_{amb} + \frac{S}{U_L} - \left[\frac{S}{U_L} - (T_0 - T_{amb}) \right] \exp\left(-\frac{F' U_L W x}{\dot{m}_a c_{p_a}} \right) \tag{4.23}$$

The temperature at the outlet of the collector T_1 can be obtained from equation (4.22), for $x = L$:

$$T_1 = T_{amb} + \frac{S}{U_L} - \left[-\frac{S}{U_L} - (T_0 - T_{amb}) \right] \exp\left(-\frac{F' U_L A_c}{\dot{m}_a c_{p_a}} \right) \tag{4.24}$$

The average fluid temperature can be calculated as:

$$T_f = \frac{1}{L}\int_0^L T_a(x)dx = \\ = T_{amb} + \frac{S}{U_L} - \left[\frac{S}{U_L} - (T_0 - T_{amb})\right]\frac{\dot{m}_a c_{p_a}}{F'U_L A_c}\left[1 - \exp\left(-\frac{F'U_L A_c}{\dot{m}_a c_{p_a}}\right)\right] \tag{4.25}$$

Equations (4.16) and (4.17) can be rearranged to determine the temperatures of the absorber plate and the glass cover as a function of the average fluid temperature as:

$$T_p = T_f + \\ + \frac{S(U_t + h_{r_{pc}} + h_{c_{fc}}) - (T_f - T_{amb})(U_t h_{r_{pc}} + U_t U_b + U_b h_{r_{pc}} + U_b h_{c_{fc}})}{(U_t + h_{r_{pc}} + h_{c_{fc}})(U_b + h_{r_{pc}} + h_{c_{pf}}) - h_{r_{pc}}^2} \tag{4.26}$$

$$T_c = T_f + \frac{Sh_{r_{pc}} - (T_f - T_{amb})(U_t h_{c_{pf}} + U_t U_b + U_b hr_{pc} + U_t h_{r_{pc}})}{(U_t + h_{r_{pc}} + h_{c_{fc}})(U_b + h_{r_{pc}} + h_{c_{pf}}) - h_{r_{pc}}^2} \tag{4.27}$$

The equations system (4.16) to (4.27) was numerically solved using Matlab® following the procedure presented in Figure 4.3. The results and the experimental validation are presented in section 4.4.

4.3.2 Operation at transient conditions

The energy balances for the absorber plate, the glass cover and the fluid, under transient conditions, obtained from equations (4.1) to (4.3), with the simplifications defined in equations (4.4) to (4.15), are:

$$S - U_b(T_p - T_{amb}) - h_{c_{pf}}(T_p - T_f) - h_{r_{pc}}(T_p - T_c) = \rho_p V_p c_p \frac{dT_p}{dt} \tag{4.28}$$

$$h_{r_{pc}}(T_p - T_c) + h_{c_{fc}}(T_f - T_c) - U_t(T_c - T_{amb}) = \rho_c V_c c_c \frac{dT_c}{dt} \tag{4.29}$$

$$h_{c_{pf}}(T_p - T_f) - h_{c_{fc}}(T_f - T_c) = \dot{m}_a c_{p_a}(T_1 - T_0) \tag{4.30}$$

The heat capacitance of the airflow is neglected since it is small compared to that of the absorber plate and the glass cover. The initial conditions are:

$$t = 0 \longrightarrow \begin{cases} T_p = T_{amb} \\ T_c = T_{amb} \end{cases} \tag{4.31}$$

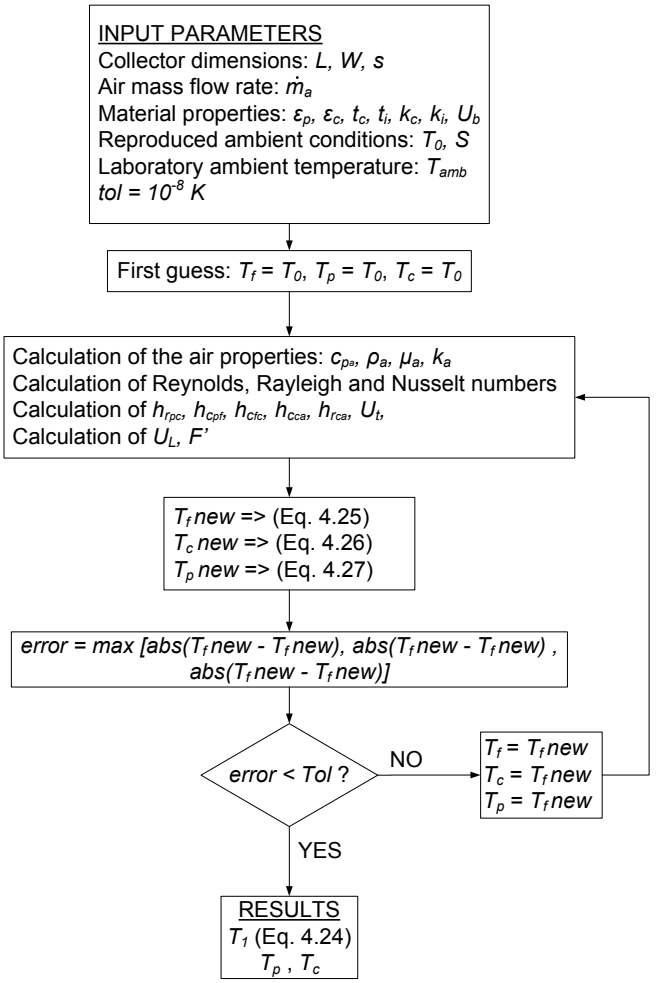

Figure 4.3: Numerical procedure to solve the steady state model.

The parameters F' and U_L were obtained using equations (4.20) and (4.21), which are derived from the energy balance in the solar collector (equations (4.16) to (4.18)) assuming steady state conditions. Hence, they cannot be used for the mathematical modelling of the solar air heater considering the capacitive terms characteristic of the transient conditions. F' and U_L were used in the calculation of the temperature distribution of the airflow along the collector (equation (4.23)), in order to obtain the average temperature T_f. However, equation (4.23) is not valid if the capacitive terms associated to transient conditions are

considered, since it is obtained assuming steady state conditions. To obtain T_f for transient conditions, the average fluid temperature is here assumed to coincide with the average of a linear temperature distribution of the airflow along the collector, and thus the average value would be:

$$T_f = \frac{T_0 + T_1}{2} \tag{4.32}$$

With this assumption, equations (4.28) to (4.30) were solved in MatLab® using the finite difference method. The results and the experimental validation are presented in section 4.4.

4.4 Experimental validation of the model

A mathematical modelling of the air heating process occurring at steady state and at transient conditions was presented in sections 4.3.1 and 4.3.2 respectively. Several tests were conducted in order to validate these models.

In the case of the steady state operation, the tests consisted of giving an instruction of constant temperature at the inlet of the collector and a constant electric power to the lab-scale solar air heater, corresponding to different values obtainable within the reference climate.

For the test at transient conditions, the profile corresponding to the solar irradiance and the temperature at the inlet of the collector, determined in section 2.3.2 and presented in Figure 2.3, is programmed in the laboratory facility.

In every test, the temperature at the outlet of the solar air heater, the temperature of the absorber plate and the temperature of the glass cover, measured at the center of each device, were registered at a frequency of 0.2 Hz by the data acqusition system, as described in section 2.4.2.

4.4.1 Experimental validation of the model at steady state conditions

A particular case of the input parameters to the steady state model is presented in this section, and compared to the experimental results obtained in the laboratory facility.

The geometric parameters and the physical properties of the materials used as input parameters for the model are presented in Table 4.1, based on typical values for the present application.

Table 4.1: Input parameters of the model.

Parameter	Symbol	Value
Air mass flow rate	$\dot{m}_a$	0.015 kg/s
Collector length	L	1 m
Collector width	W	0.5 m
Air passage height	s	0.045 m
Absorber plate emisivity	ϵ_p	0.03
Glass cover emisivity	ϵ_c	0.88
Glass thickness	t_c	0.005 m
Glass thermal conductivity	k_c	1.4 W/mK
Bottom heat loss coefficient	U_b	1.5 W/m^{2}K

For the experiments, 26 tests at different solar irradiances and temperatures at the inlet of the collector were performed. The power supplied to the air heater was that corresponding to a solar irradiance absorbed by the absorber plate within the range of $S = 100$ W/m^2 and $S = 700$ W/m^2. The values of the temperature at the inlet of the solar collector T_0 were within the range of variation of the ambient temperature of the reference climate (between 16 °C and 26.5 °C), described in section 2.3.2. During the tests, the laboratory (ambient) temperature was constant, at values ranging between $T_{amb} = 11$ °C and $T_{amb} = 16$ °C.

Figure 4.4 shows the experimental temperatures obtained at the outlet of the collector (a), the average absorber plate temperature (b) and the average inner surface of the glass cover (c) versus the predicted temperatures using the model, for different values of T_0, T_{amb} and S, and the input parameters shown in Table 4.1. The experimental results are depicted including the range of accuracy of the sensor.

Figure 4.4 shows a good agreement between the prediction of the model and the experimental result for T_1 and T_c, whereas the model underestimate T_p in the whole range, with an error ranging between 5.3 °C and 7.7 °C. The reason for the higher experimental temperature obtained in the absorber might be attributed to the fact that the model calculates the average temperature of the components, whereas the measurement is taken at the middle of the component. In addition, the fact that the artificial absorber plate consists of an electrical resistance, where the temperature differs in different locations may contribute to the error, since the model assumes an uniform distribution of the

temperature. The mean errors obtained were negligible ($\sim$ 0.0 °C) for T_1, -6.6 °C for T_p and 0.75 °C for T_c. The maximum errors were -0.7 °C for T_1, -7.7 °C for T_p and 2.0 °C for T_c.

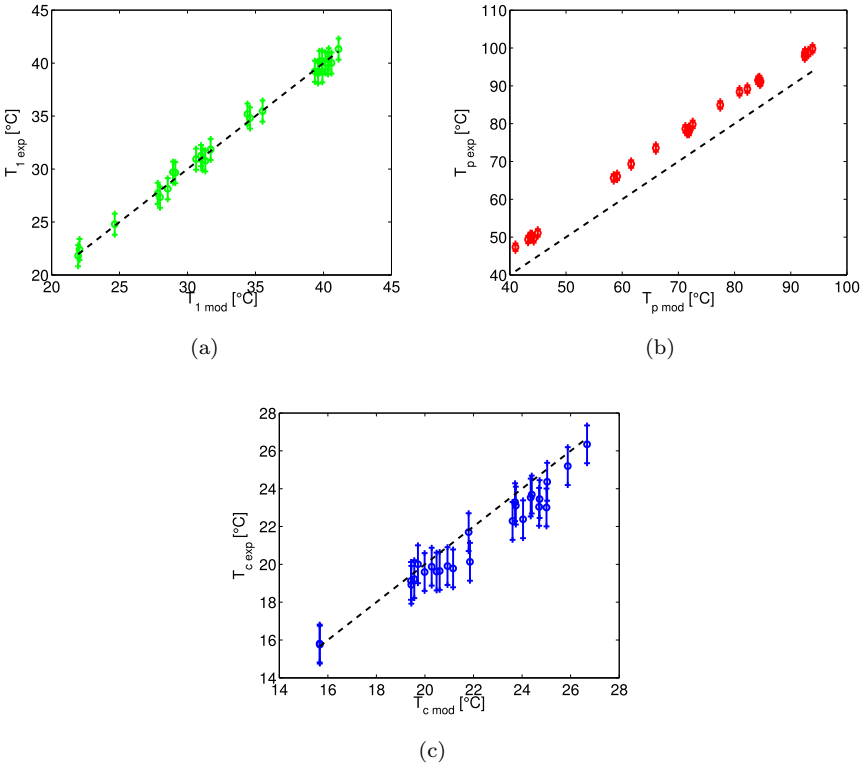

Figure 4.4: Experimental temperatures versus the model prediction of a) the airflow at the outlet of the collector, b) the average absorber plate temperature and c) the average glass cover temperature.

4.4.2 Experimental validation of the model at transient conditions

The model at transient conditions considers the average temperature calculated as the mean value between the inlet and the outlet (equation (4.32)) to coincide with the average fluid temperature obtained for the distribution of the temperature of the airflow along the solar collector length (equation (4.25)). In order to validate such hypothesis, the experimental results of the 26 tests presented

in the previous section, obtained at steady state conditions, are employed. The average temperature of the fluid is calculated with equations (4.32) and (4.25), and compared. The results showed an average error of 0.17 °C with a standard deviation of 0.06 °C. Hence, equation (4.32) can be applied.

For the resolution of the transient model, the input parameters are the same as those presented in Table 4.1, adding those related to capacitive terms, based on typical values of the materials. These values are presented in Table 4.2.

Table 4.2: Input parameters of the model for the transient operation of the solar air heater.

Parameter	Symbol	Value
Density of the absorber plate	ρ_p	2700 kg/m^3
Volume of the absorber plate	V_p	10^{-3} m^3
Specific heat of the absorber plate	c_p	880 J/kgK
Density of the glass cover	ρ_p	2500 kg/m^3
Volume of the glass cover	V_c	$2.5 \cdot 10^{-3}$ m^3
Specific heat of the glass cover	c_c	840 J/kgK

The results are shown in Figure 4.5. Figure 4.5a shows the temperatures of the absorber plate (in red), the fluid at the outlet of the collector (in green) and the glass cover (in blue) obtained with the model (solid lines), and the experimental temperature measured for each part (dashed lines). Figure 4.5b shows the errors obtained when comparing the experimental and the theoretical results.

It can be observed in Figure 4.5 that the model predicts properly the temperature at the outlet of the collector, but the errors are higher in the prediction of the glass cover temperature, and specially, in the absorber plate temperature. The errors are consistent with those obtained with the steady state model.

4.5 Experimental characterization of the lab-scale solar air heater

Several tests were conducted in order to characterize the performance of the solar air heater of the laboratory facility. The tests were conducted at steady state, based on the ASHRAE Standard 93−77 (Hill *et al.*, 1979). In order to analyse the time of response of the solar collector to reach the steady state,

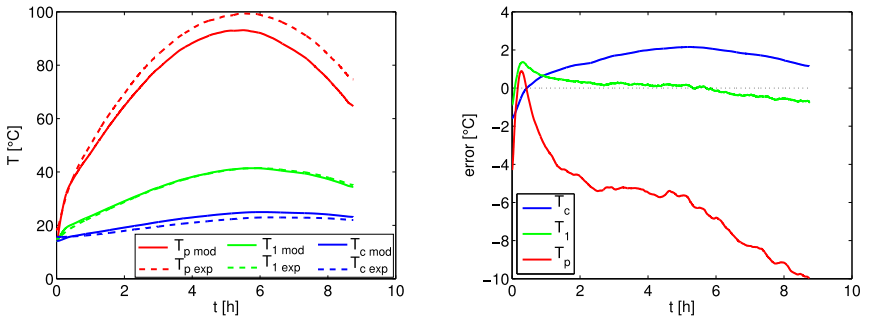

(a) (b)

Figure 4.5: a) Temperatures of the absorber plate, the airflow at the outlet of the collector and the glass cover during time, obtained experimentally and with the model. b) Error of the model compared to the experimental results.

the characteristic time is previously studied. The performance of the solar air heater is evaluated in terms of the thermal efficiency and the increment of temperature obtainable.

4.5.1 Characteristic time of the solar air heater

To evaluate the inertia of the air heater, the evolution with time of the temperature of the absorber plate is studied, from ambient conditions to the steady state, for a heating process at constant power, and from that temperature to ambient temperature during a cooling process with the power switched off.

The energy balance on the absorber plate of the solar collector during the heating process, referring all the heat losses to a global heat loss coefficient U_p would be:

$$m_p c_p \frac{dT_p}{dt} = SA_c - U_p A_c (T_p - T_{amb}) \tag{4.33}$$

with the initial condition $t = 0 \longrightarrow T_{p_i} = T_{amb}$. When the steady state is reached, equation (4.33) yields:

$$\frac{S}{U_p} = (T_{p_f} - T_{amb}) \tag{4.34}$$

The temperature T_{p_f} is the value of the temperature when the process is stable, and thus it is assumed to be the temperature at steady state. Therefore,

the heating process is described by the solution of equation (4.33) as a function of time:

$$\frac{T_p - T_{p_i}}{T_{p_f} - T_{p_i}} = 1 - \exp\left(-t\frac{U_p A_c}{m_p c_p}\right) \tag{4.35}$$

The first term in equation (4.35) is a single dimensionless parameter Θ_h. The factor multiplying the time in the exponent of the exponential function is the inverse of the characteristic time of the heating process $\tau_h = m_p c_p / U_p A_c$. Hence, the heating process is defined by:

$$\Theta_h = 1 - \exp\left(-\frac{t}{\tau_h}\right) \tag{4.36}$$

Following the same procedure, the cooling process is expressed as:

$$\Theta_c = \frac{T_p - T_{p_f}}{T_{p_i} - T_{p_f}} = \exp\left(-\frac{t}{\tau_c}\right) \tag{4.37}$$

In order to determine the characteristic time of response for the solar collector to reach the steady state, a whole heating process is monitored, from the ambient temperature to the steady state. Afterwards, the power is switched off and a cooling process from the steady state temperature to ambient temperature is registered. Θ_h and Θ_c were calculated in both cases, and the results were fitted to equations (4.36) and (4.37) respectively, to obtain the values of the characteristic times τ_h and τ_c. The results are shown in Figure 4.6. The values obtained respectively were $\tau_h = 981$ s and $\tau_c = 1216$ s.

4.5.2 Performance of the lab-scale solar air heater

The performance of a solar air heater is typically assessed by means of the thermal efficiency, defined as:

$$\eta = \frac{\dot{m}_a c_{p_a}(T_1 - T_0)}{I A_c} \tag{4.38}$$

For a given air mass flow rate $\dot{m}_a$, Hottel & Whillier (1958) proposed to determine the thermal efficiency of solar collectors as a function of the heat removal factor F_R and the heat loss coefficient U_L.

$$\eta = F_R(\tau\alpha) - F_R U_L \left(\frac{T_0 - T_{amb}}{I}\right) \tag{4.39}$$

The expression was originally derived for water solar heaters, but a wide number of authors have applied such expression to solar air heaters, (Yeh & Lin

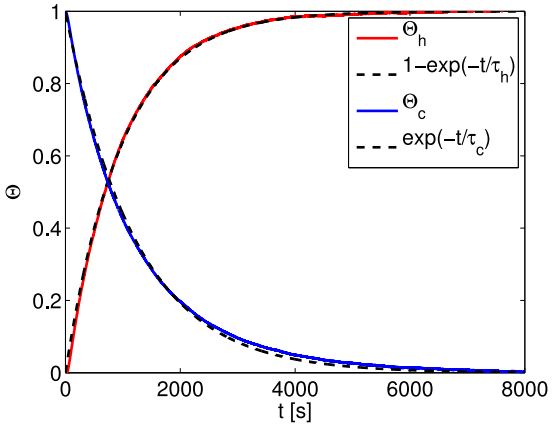

Figure 4.6: Heating and cooling processes expressed as a function of the dimensionless parameters Θ_h and Θ_c and fitting to the equations expressed as a function of the characteristic times τ_h and τ_c.

(1996), Alta *et al.* (2010), among others). The thermal efficiency in equation (4.39) is expressed in terms of the effective transmittance-absorptance product ($\tau\alpha$), which is the effective relation between the solar irradiance absorbed by the solar collector and the solar irradiance on the horizontal plane: $(\tau\alpha) = S/I$. I is extracted from weather data available on-line (Energy-Plus, 2015) for the reference climate, and depicted in Figure 2.1b. S is obtained using equation (2.8), which is composed of several factors multiplying I. Such factors are hardly variable during the day and can be reduced to a single term, named the effective transmittance-absoptance product ($\tau\alpha$). In order to obtain ($\tau\alpha$), S and I are linearized. The relation is shown in Figure 4.7.

The values of S calculated using equation (2.8) are presented with cross symbols as a function of I. The linear relation given by $S = (\tau\alpha) \cdot I$ is presented in dashed line. The effective transmittance-absorptance product obtained was $(\tau\alpha) = 0.94$. This result is not experimental, but an output of the model. Nevertheless, it is necessary for further analysis and thus it is included here.

In order to characterize the solar air heater based on equation (4.39), several tests were conducted at steady state conditions using an air mass flow rate $\dot{m}_a = 0.015$ kg/s. Different values of I and T_0 within their range of variation during the drying process (Figure 2.3), were used for the tests. The results are shown in Figure 4.8.

Considering the mathematical relation shown in equation (4.39), the exper-

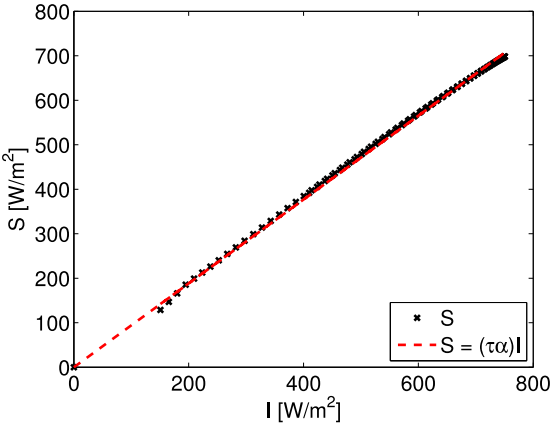

Figure 4.7: Solar irradiance absorbed by the solar collector S as a function of the solar irradiance on the horizontal plane I.

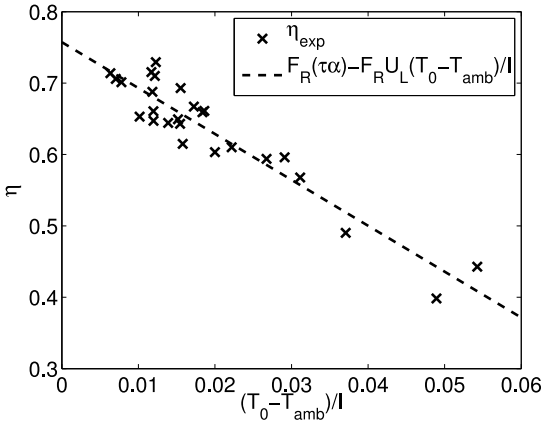

Figure 4.8: Thermal efficiency as a function of the difference between the temperature at the inlet of the collector and the laboratory temperature, divided by the solar irradiance on the horizontal plane.

imental points were fitted to a linear function of $(T_0 - T_{amb})/I$, obtaining a value of $F_R = 0.80$ and $U_L = 8.0$ W/(m^{2}K).

In many applications of solar air heaters, the temperature at the inlet coincides with the ambient temperature, and thus equation (4.39) cannot be directly applied. Hence, it is more extended to refer the thermal efficiency to the collector efficiency factor F' and the collector heat loss factor U_L (Njomo, 1991; Forson *et al.*, 2003; Montero, 2005). Equation (4.40) is based on the average

temperature of the fluid in the solar collector. The thermal efficiency is thus:

$$\eta = F'(\tau\alpha) - F'U_L\left(\frac{T_f - T_{amb}}{I}\right) \tag{4.40}$$

Combining equation (4.39) and (4.40), F' can be calculated as:

$$F' = -\frac{\dot{m}_a c_{p_a}}{A_c U_L}\left[\log\left(1 - \frac{F_R U_L A_c}{\dot{m}_a c_{p_a}}\right)\right] \tag{4.41}$$

The value obtained is $F' = 0.90$.

In the model presented in section 4.3.1, F' and U_L were mathematically modelled, based on a set of hypotheses that yields to equations 4.20 and 4.21. The values obtained from the model were $F'_{mod} = 0.85$ and $U_{L_{mod}} = 6.6$ W/m^{2}K. The experimental determination of F' and U_L based on equations (4.39) to (4.41) yields $F' = 0.90$ and $U_L = 8.0$ W/m^{2}K. The differences are attributed to the hypotheses assumed in the mathematical model, from which expressions for the calculation of F' and U_L are directly derived (section 4.3.1).

The thermal efficiency calculated in equation (4.38) from the experimental measurements obtained for the steady state tests is presented in Figure 4.9 as a function of $(T_f - T_{amb})/I$. T_f is calculated with equation (4.25) for the values of F' and U_L obtained. The thermal efficiency obtained in equation (4.40) with the values of the model ($F'_{mod} = 0.85$ and $U_{L_{mod}} = 6.6$ W/m^{2}K) and with the experimental values ($F'_{exp} = 0.90$ and $U_{L_{exp}} = 8.0$ W/m^{2}K) are also presented in Figure 4.9 in dashed and dotted lines respectively.

The thermal efficiency (equation (4.40)) obtained from the values of F'_{exp} and $U_{L_{exp}}$ calculated in this section fits better the experimental results since they are directly derived from the experimental data. However, the thermal efficiency obtained for F'_{mod} and $U_{L_{mod}}$ is also in agreement with the experimental data, since the deviations between the modelled and the experimental efficiency was relatively low.

The temperature increment obtained in the collector is also an important parameter to analyse, since the drying conditions depend directly on the temperature at the outlet of the collector. Figure 4.10 shows the experimental increment of temperature measured during the tests as a function of the solar irradiance, together with the linear fitting of the data.

The experimental results show a linear increment of the temperature of the airflow with the solar irradiance, which is in accordance with previous studies reported in the literature (Kadam & Samuel, 2006; Karim & Hawlader, 2006; Karsli, 2007; Leon & Kumar, 2007).

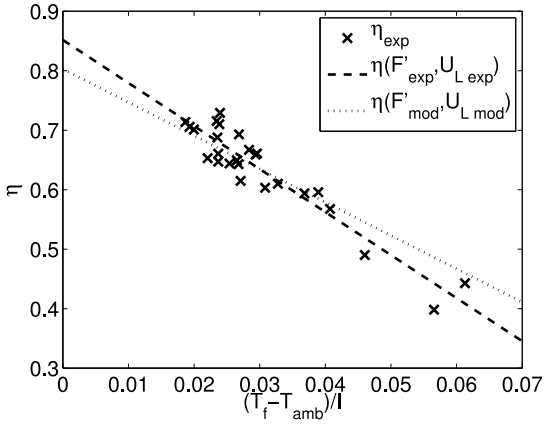

Figure 4.9: Efficiency as function of the difference between the average fluid temperature and the laboratory temperature divided by the solar irradiance on the horizontal plane.

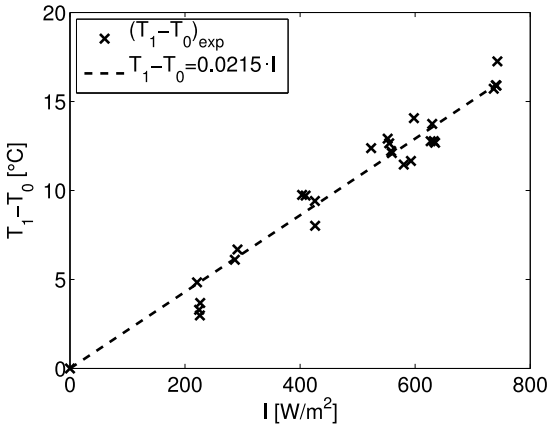

Figure 4.10: Increment of temperature on the solar collector as a function of the solar irradiance on the horizontal plane.

Once the performance of the system at steady state was analysed, the drying conditions that would be obtained in the drying chamber with the solar air heater operating for the reference climate are evaluated.

4.6 Drying conditions

The conditions obtained at the outlet of the solar collector set the drying conditions in an indirect solar dryer. Operating with the lab-scale solar dryer under the reference climate detailed in section 2.3, the conditions obtained at the inlet (0) and at the outlet (1) of the artificial solar air heater are presented in Figure 4.11.

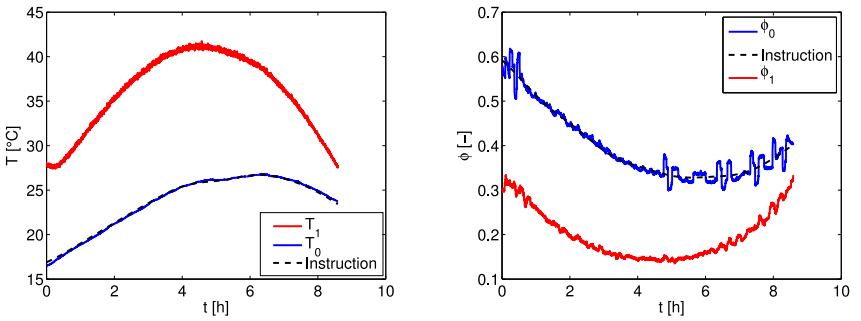

(a) (b)

Figure 4.11: Conditions at the inlet and at the outlet of the solar collector, a) temperature, b) relative humidity.

Figure 4.11a shows the aiflow temperatures at the inlet and at the outlet of the solar collector. The instruction given to the air conditioning system is presented in Figure 4.11 in dashed line. A proper response of the experimental facility following the instruction can be observed in Figure 4.11, as previously discussed in section 2.5. At the beginning of the process, a period of a slight decrement of T_1 is observed. This is due to the preheating of the solar collector during the first 2.5 hours of the day, when it operates under natural convection. The drying process starts 2.5 hours after the sunrise, as stated in section 2.3.2. During those 2.5 hours, the solar collector is exposed to the solar irradiance but the fan is not yet started. When the fan is started, a transition from natural convection to forced convection occurs. The temperature of the absorber plate descends, since the airflow begins to circulate over it, which entails the profile shown at the first minutes of the process. In order to consider this effect, the first 2.5 hours of the solar collector were programmed with the solar irradiance corresponding to the 2.5 first hours of the simulated climate, and operated under natural convection.

Figure 4.11b shows the relative humidity at the inlet (ϕ_0) and at the outlet (ϕ_1) of the solar collector. As in the case of the temperature, the instruction given (in dashed line) corresponds to the relative humidity of the simulated ambient conditions. The instabilities in ϕ_0 are due to the response of the humidifier of the air conditioning system to the PID controller, explained in section 2.5.

The drying conditions considered for the subsequent studies of the drying process result from the conditions at the outlet of the collector presented in Figure 4.11. The temperature and the relative humidity present oscillations due to the experimental measurement of the sensor immersed in the airflow. The characteristic frequency is that of the acquisition system (0.2 Hz). In the case of the relative humidity, another effect is observed, due to the instability of the humidification system. In order to show the drying conditions without the effect of the oscillations around the instruction, showed mainly in the relative humidity, a moving average of the signal is applied. The mean average of the temperature is centred in periods of 10 min and the relative humidity in 20 min. The drying conditions at the inlet of the drying chamber are shown in Figure 4.12.

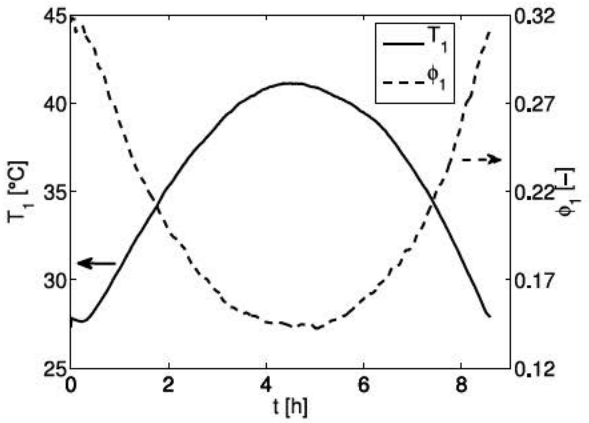

Figure 4.12: Drying conditions.

The drying process occurring downstream of the inlet of the drying chamber depends on the conditions shown in Figure 4.12 and on the interaction between air and product. The maximum evaporation rate that could be obtained in the experimental facility, applying the model presented in Chapter 3 is presented in Figure 4.13a. The accumulated amount of water evaporated is presented in

Figure 4.13b.

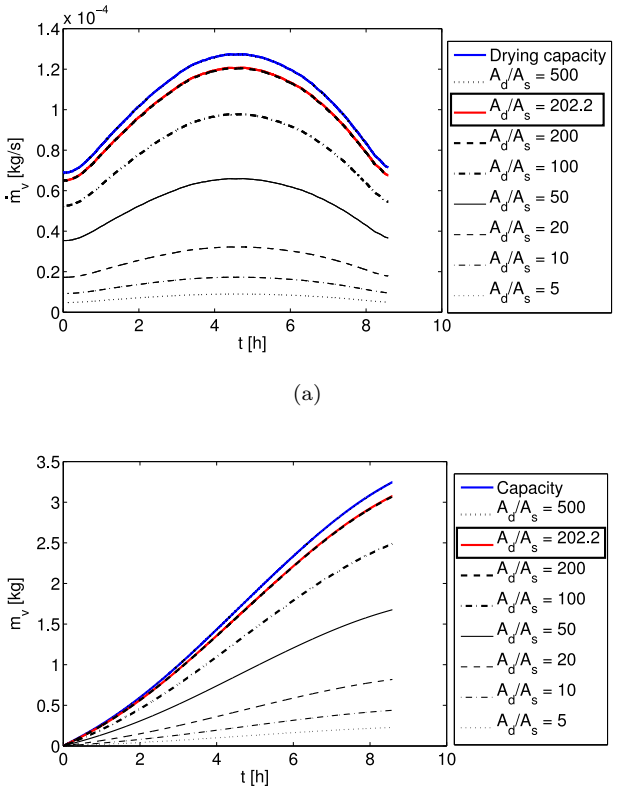

Figure 4.13: a) Maximum evaporation rate obtainable and b) maximum amount of free water evaporated, as a function of time for different aspect ratios in the drying chamber, including the value $A_d/A_s = 202.2$ corresponding to the experimental facility.

Figure 4.13a shows, in a blue solid line, the drying capacity of the experimental facility, for the drying conditions presented in Figure 4.12, neglecting the capacitive terms in the drying chamber, and for evaporation of free water, following the procedure proposed in Chapter 3. The maximum evaporation rate obtained, calculated with equation (3.17), is presented for different aspects ratios in the drying chamber A_d/A_s. For the design of the drying chamber of the experimental facility, the maximum evaporation rate that can be obtained is presented in red solid line. Figure 4.13b shows the actual amount of free water that would be evaporated as a function of time, including the maximum permis-

sible before saturation, in blue line, and for the dimensions of the experimental facility, in red line.

The design of the solar dryer was performed following the design criteria extracted from Chapter 3, obtaining a maximum evaporation rate close to the drying capacity, but within a reasonable range of dimensions. However, note that such study considers the evaporation of free water. The drying process of biological products is controlled by the diffusion of water within the interior of the product (Panchariya *et al.*, 2002). Hence, the actual drying rate that would be obtained in the solar dryer would be lower than the maximum evaporation rate permissible when evaporating free water. The actual drying kinetics of the product considered is analysed in Chapter 5.

4.7 Conclusions

In this chapter, an analysis of the air heating process in the lab-scale solar collector of the experimental facility was presented.

A theoretical model that predicts the performance of the solar collector was developed, showing a proper agreement with the experimental results. The model considering steady state conditions could predict accurately the temperature of the airflow at the outlet of the collector, whereas the prediction of the glass cover temperature was overestimated in 0.75 °C in average and the absorber plate temperature was underestimated in 6.6 °C in average. The model resulted in a collector efficiency factor $F' = 0.85$ and a collector heat loss coefficient $U_L = 6.6$ W/m^2. The model was applied to a process under transient conditions. The comparison with the experimental measurements presented a slight higher error than that of the steady state model.

An experimental analysis was also performed in order to characterize the operation of the lab-scale solar air heater. The typical testing methods for solar collectors were applied, obtaining, for the nominal air mass flow rate $\dot{m}_a = 0.015$ kg/s a collector loss coefficient $U_L = 8.0$ W/m^{2}K, a heat removal factor $F_R = 0.8$ and a collector efficiency factor $F' = 0.9$. The differences with the values obtained from the model ($F' = 0.85$ and $U_L = 6.6$ W/m^{2}K) are slight, despite the hypotheses made in the model.

The characteristic time of the solar collector was also studied, obtaining a value of 981 s for the heating process and 1216 s for the cooling process.

The drying conditions at the inlet of the drying chamber were obtained

based on the solar collector performance. The drying capacity of the airflow was analysed, based on the study presented in Chapter 3. The maximum evaporation rate obtainable for the drying chamber dimensions met the compromise between being close to the drying capacity but within reasonable dimensions. Since the drying capacity and the maximum evaporation rate are based on evaporation of free water, a study on the drying kinetics of the product is crucial, prior the the global analysis of the solar drying process.

Nomenclature

A_c	Collector area [m^2]
A_d	Drying area [m^2]
A_s	Cross section in the drying chamber [m^2]
c_p	Specific heat of the absorber plate [J/kgK]
c_c	Specific heat of the glass cover [J/kgK]
c_{p_a}	Specific heat of the air [J/kgK]
d_h	Hydraulic diameter [m]
F'	Collector efficiency factor [−]
F_R	Collector heat removal factor [−]
h_c	Heat convection coefficient [W/m^2K]
$h_{c_{ca}}$	Heat convection coefficient from the glass cover to the ambient [W/m^2K]
$h_{c_{fc}}$	Heat convection coefficient: airflow to glass cover [W/m^2K]
$h_{c_{ia}}$	Heat convection coefficient: insulation to ambient [W/m^2K]
$h_{c_{pf}}$	Heat convection coefficient: absorber plate to airflow [W/m^2K]
$h_{r_{ca}}$	Heat radiation coefficient from glass cover to ambient [W/m^2K]
$h_{r_{pc}}$	Heat radiation coefficient from absorber plate to glass cover [W/m^2K]
I	Solar irradiance [W/m^2]
k_a	Thermal conductivity of the air [W/mK]
k_c	Thermal conductivity of the glass cover [W/mK]
k_i	Thermal conductivity of the insulation [W/mK]
l_c	Characteristic length of the upper surface of the glass cover [m]
L	Collector length [m]
m_c	Mass of the glass cover [kg]
m_p	Mass of the absorber plate [kg]
$\dot{m}_a$	Air mass flow rate [kg/s]
$\dot{m}_v$	Evaporation rate [kg/s]
Nu	Nusselt number [−]

Pr	Prandtl number [−]
q_b	Heat flux: losses from absorber plate to ambient [W/m^2]
q_{fc}	Heat flux from airflow to glass cover [W/m^2]
q_{pf}	Heat flux from absorber plate to glass cover [W/m^2]
q_{pf}	Heat flux from absorber plate to airflow [W/m^2]
q_t	Heat flux: losses from glass cover to ambient [W/m^2]
q_u	Useful heat flux gained by the airflow, per unit of collector area [W/m^2]
Ra	Rayleigh number [−]
Re	Reynolds number [−]
s	Plate spacing (collector) and tray spacing (drying chamber) [m]
S	Solar irradiance absorbed by the absorber plate [W/m^2]
t	Time [s]
t_c	Glass cover thickness [m]
t_i	insulation thickness [m]
T_a	Temperature of the air along the collector [°C]
T_{amb}	Temperature of the ambient [°C]
T_c	Average temperature of the glass cover [°C]
T_f	Average temperature of the fluid [°C]
T_p	Average temperature of the absorber plate [°C]
T_{p_f}	Final temperature of the absorber plate [°C]
T_{p_i}	Initial temperature of the absorber plate [°C]
T_0	Temperature at the inlet of the solar collector [°C]
T_1	Temperature at solar collector outlet / drying chamber inlet [°C]
U_b	Collector bottom heat loss coefficient [W/m^{2}K]
U_L	Collector heat loss coefficient [W/m^{2}K]
U_p	Absorber plate heat loss coefficient [W/m^{2}K]
U_t	Collector top heat loss coefficient [W/m^{2}K]
V_c	Volume of the glass cover [m^3]
V_p	Volume of the absorber plate [m^3]
W	Width of the dryer [m]
x	Coordinate of the collector in the fluid flow direction [m]

Greek letters

η	Thermal efficiency [−]
ϵ_c	Emissivity of the glass cover [−]
ϵ_p	Emissivity of the absorber plate [−]

μ_a	Dynamic viscosity of the air [kg/ms]
ρ_a	Density of the air [kg/m^3]
ρ_c	Density of the glass cover [kg/m^3]
ρ_p	Density of the absorber plate [kg/m^3]
σ	Stephan-Boltzmann constant [W/m^{2}K^4]
τ_c	Characteristic time of the cooling process [s]
τ_h	Characteristic time of the heating process [s]
ϕ_0	Relative humidity at the inlet of the collector [−]
ϕ_1	Relative humidity at the inlet of the drying chamber[−]
Θ_c	Adimensional temperature during the cooling process [−]
Θ_f	Adimensional temperature during the heating process [−]
$(\tau\alpha)$	Effective transmittance-absorptance product [−]

Subindex

exp	Experimental
mod	Model

References

Akpinar, E. K. & Koçyigit, F. 2010 Experimental energy and exergy analysis of a double-flow solar air heater having different obstacles on absorber plates. *Applied Energy* 87, 3438–3450.

Alta, D., Bilgili, E., Ertekin, C. & Yaldiz, O. 2010 Experimental investigation of three different solar air heaters: Energy and exergy analyses. *Applied Energy* 87 (10), 2953–2973.

Duffie, J. A. & Beckman, W. A. 2006 *Solar Engineering of Thermal processes*, 3rd edn. Hoboken, New Jersey: John Wiley and Sons.

Ekechukwu, O. V. & Norton, B. 1999 Review of solar-energy drying systems III: low temperature air-heating solar collectors for crop drying applications. *Energy Conversion and Management* 40 (6), 657–667.

Energy-Plus 2015 http://energyplus.net/weather, accessed: may 2015.

Forson, F. K., Nazha, M. & Rajakaruna, H. 2003 Experimental and simulation studies on a single pass, double duct solar air-heater. *Energy Conversion and Management* 44, 1209–1227.

Hill, J. E., Jenkins, J. P. & Jones, D. E. 1979 *Experimental Verifications of a Standard Test Procedure for Solar Collectors*. Washington, D.C: National Bureau of Standards.

Hottel, H. C. & Whillier, A. 1958 Evaluation of flat-plate solar-collector performance. *Transactions of the Conference on Use of Solar Energy* 54 (1), 19–41.

Incropera, F. K. & Dewitt, D. P. 1990 *Introduction to heat transfer*, 2nd edn. Indiana, USA: John Wiley and Sons, Purdue University.

Kadam, D. M. & Samuel, D. V. K. 2006 Convective flat-plate solar heat collector for cauliflower drying. *Biosystems Engineering* 93 (2), 189–198.

Karim, M. A. & Hawlader, M. N. A. 2006 Performance evaluation of a v-groove solar air collector for drying applications. *Applied Thermal Engineering* 26 (1), 121–130.

Karsli, S. 2007 Performance analysis of new-design solar air collectors for drying applications. *Renewable Energy* 32 (10), 1645–1660.

Leon, M. A. & Kumar, S. 2007 Mathematical modeling and thermal performance analysis of unglazed transpired solar collectors. *Solar Energy* 81 (1), 62–75.

Montero, I. 2005 Modelado y construcción de un secadero solar híbrido para residuos biomásicos. PhD thesis, Universidad de Extremadura.

Montero, I., Blanco, J., Miranda, T., Rojas, S. & Celma, A. R. 2010 Design, construction and performance testing of a solar dryer for agroindustrial by-products. *Energy Conversion and Management* 51 (7), 1510–1521.

Njomo, D. 1991 Modeling the heat exchanges in a solar air heater with a cover partially transparent to infrared radiations. *Renewable Energy* 1 (5-6), 837–843.

Oztop, H. F., Bayrak, F. & Hepbasli, A. 2013 Energetic and exergetic aspects of solar air heating (solar collector) systems. *Renewable and Sustainable Energy Reviews* 21, 59–83.

Panchariya, P. C., Popovic, D. & Sharma, A. L. 2002 Thin-layer modelling of black tea drying process. *Journal of Food Engineering* 52 (4), 349–357.

Singh, S. & Kumar, S. 2012 Development of convective heat transfer correlations for common designs of solar dryer. *Energy Conversion and Management* 64, 403–414.

Tchinda, R. 2009 A review of the mathematical models for predicting solar air heaters systems. *Renewable and Sustainable Energy Reviews* 13, 1734–1759.

Yeh, H. M. & Lin, C. 1996 The Effect of Collector Aspect Ratio on the collector efficiency of upward-type flat-plate solar air heater. *Energy* 21 (10), 843–850.

CHAPTER

FIVE

Drying kinetics of solar drying of Granny Smith apples

Contents

5.1 Abstract

The thin-layer drying kinetics of Granny Smith apples is studied by means of themogravimetric analysis of the drying process at constant temperatures ranging from 20 °C to 50 °C, using intervals of 5 °C. The experimental drying curves obtained in the TGA were fitted to the Wang-Singh equation, which was found to describe precisely the drying process. A model, capable of predicting the evolution of the moisture ratio of Granny Smith apples during the drying

process under variable drying temperatures, was proposed. The model was validated with experimental TGA measurements of the drying of apples at variable temperatures, typical of solar drying application. Once validated, the model proposed was also applied to the drying of Granny Smith apples in an indirect solar dryer. The comparison of the model prediction with the experimental measurements of the drying of apples at variable drying conditions conducted in the lab-scale solar dryer showed a proper agreement, with low deviations due to the thermal inertia of the apple samples.

5.2 Introduction

In indirect solar dryers, the drying process depends mainly on the drying conditions (air mass flow rate and airflow temperature and relative humidity) in the drying chamber and on the drying kinetics of the product at those conditions. The drying conditions at the inlet of the drying chamber depend on the air heating process in the solar collector, and thus the drying process is highly dependent on the ambient conditions and on the solar irradiance. While the solar drying process is characterized by variable drying conditions, the drying kinetics is generally studied at constant drying conditions.

The thin-layer drying is the procedure of drying one single layer of particles or slices of a product. The thin-layer equations predict the temporal evolution of the moisture content of the samples, based on empirical models of the drying process: Lewis, Page, Henderson and Pabis, Logarithmic, two terms, two terms exponential, Wang and Singh, among others (Akpinar, 2006). These models have been widely used in the study of the drying kinetics or for the determination of the diffusion coefficient of several agricultural products (Celma *et al.*, 2007; Doymaz, 2009; Zhu & Shen, 2014; Bezerra *et al.*, 2015).

Even though the solar drying process is characterised by variable drying conditions, the drying kinetics are generally studied at constant drying conditions. When the drying kinetics obtained at constant drying conditions is applied to the prediction of solar drying processes, it is generally performed by means of mathematical simulation of the heat and mass transfer processes in the drying chamber (Karim & Hawlader, 2005; Janjai *et al.*, 2009) which are simulations of high complexity. To the knowledge of the author, there are no simple models available in the literature to predict the evolution of the moisture loss during the drying process at the variable drying conditions characteristic of solar drying processes.

Regarding the drying kinetics of apples, most of the works are based on the mathematical modelling of the drying curves obtained experimentally, employing the thin-layer equations at constant drying conditions, for different varieties of apples. The tests are typically conducted at different values of constant temperatures, and for different values of a second parameter, such as the sample thickness (Sacilik & Elicin, 2006), the air velocity (Menges & Ertekin, 2006) or the air relative humidity (Zlatanović *et al.*, 2013). Only a few researchers have focused on the drying kinetics of Granny Smith apples. Velić *et al.* (2007) and Vega-Galvez *et al.* (2012) studied the drying kinetics in a range of temperatures between 40 °C and 80 °C. González-Fésler *et al.* (2008) and Doymaz (2009) reported the effect of different pre-treatments on the drying kinetics of Granny Smith apples at 60 °C and 65 °C respectively. However, these studies do not cover the whole range of temperatures of small-scale solar drying, which for Granny Smith application would be lower.

In this chapter, thin-layer drying tests were conducted in a TGA for several constant drying temperatures, obtaining the drying curves for Granny Smith apples. Different thin-layer equations available in the literature were fitted to the experimental drying curves obtained in the TGA. Then, a mathematical model, capable of predicting the sample mass loss under variable temperatures, is proposed and validated using TGA experimental results and experimental measurements obtained in the lab-scale solar dryer.

5.3 Experimental setup

The experiments were conducted employing two different systems: a thermogravimetric analyser (TGA) and the lab-scale indirect solar dryer. The TGA was described in section 2.6.2 and the lab-scale indirect solar dryer was described in section 2.4.

The lab-scale solar dryer can operate at either constant conditions or at the variable conditions corresponding to different climates. The characteristic climate of the harvest season of Granny Smith apples, described in section 2.3, is here used. The solar irradiance on the horizontal plane I in a typical sunny day of the harvest season in the location where the apples are harvested, and the solar irradiance absorbed by the absorber plate S that would be obtained in a typical small-scale solar air heater are shown in Figure 2.3a. The air temperature T_0 and the air relative humidity ϕ_0 at the inlet of the solar collector are shown in Figure 2.3b. For those conditions, and operating with an air mass

flow rate $\dot{m}_a = 0.015$ kg/s in the lab-scale indirect solar dryer, the temperature and relative humidity of the airflow obtained at the inlet of the drying chamber (T_1 and ϕ_1) are presented in Figure 4.12. Those conditions will be employed during the drying process of Granny Smith apples at variable conditions in both the TGA and the indirect solar dryer tests.

The apples used for the tests in the solar dryer are washed, cut into slices of 2.4 mm in thickness and immersed in citric acid in order to prevent oxidation (Doymaz, 2009). The apple samples employed in the tests of the TGA were cylinders of 1 cm in diameter and a thickness of 2.4 mm. The mass of the Granny Smith apples used in the TGA measurements is around 150 mg. Even though the apple samples do not become oxidized in the nitrogen stream employed in the TGA tests, the samples were immersed in citric acid to present the same initial conditions as those of the tests in the solar dryer. For the determination of the drying kinetics, tests at constant temperatures ranging from 20 °C to 50 °C, using intervals of 5 °C, were conducted, covering the whole temperature operating range shown in Figure 4.12.

The average total moisture content of the samples (wet basis), determined for 25 samples dried in a Memmert UFE 500 oven, was 86.7%, with a standard deviation of 0.8%, as stated in section 2.7.

5.4 Mathematical model of the thin-layer drying of Granny Smith apples

In this section, the drying curve for Granny Smith apples was estimated using thin-layer drying equations for a range of temperature between 20 °C to 50 °C, a typical drying temperature range for solar dryers. Based on these results, a mathematical model capable of predicting the evolution of the drying process for variable air temperatures is proposed.

5.4.1 Thin-layer drying equations

The drying process of biological products is governed by the diffusion mechanism of moisture during the falling rate period (Panchariya *et al.*, 2002). There are many equations available in the literature capable of predicting the evolution of the mass of the sample during the falling rate period of the drying process. The drying process is characterized by the moisture ratio, MR, a

dimensionless parameter that quantifies the reduction of the moisture content of the sample during time (Panchariya *et al.*, 2002; Doymaz, 2009; Zlatanović *et al.*, 2013). The moisture ratio is defined as:

$$MR = \frac{M(t) - M_e}{M_0 - M_e} \tag{5.1}$$

where $M(t)$ is the moisture content (wet basis) after a time t, M_e is the equilibrium moisture content and M_0 is the initial moisture content. The moisture ratio MR varies between $MR = 1$, at the beginning of the drying process, and $MR = 0$, once the sample is dried at equilibrium with the drying air.

Different equations based on the thin-layer drying equations available in the literature were used to determine the evolution with time of the moisture ratio of Granny Smith apples dried at a constant temperature of 35 °C. The moisture loss was determined using the TGA and the moisture ratio was calculated using equation (5.1). The results were fitted to eleven different thin-layer drying equations. For the fitting procedure, the moisture ratio considered is between $MR = 1$ and $MR = 0.1$, since after that value, the drying rate decreases drastically and thus the samples are almost dry. Table 5.1 shows the equations proposed by different authors for the prediction of the evolution of the moisture ratio with time, together with the values of the fitting parameters of each equation obtained for the experimental results. The determination coefficient R^2 of the different fittings is also reported in the table.

Based on the results shown in Table 5.1, and considering simplicity and accuracy criteria, the equation selected for the prediction of the moisture ratio is that proposed by Wang & Singh (1978), which is a quadratic equation in the form:

$$MR = 1 + a \cdot t + b \cdot t^2 \tag{5.2}$$

The moisture ratio as a function of time obtained in the TGA for the isothermal process at 35 °C is plotted in Figure 5.1 together with the fitting of Wang and Singh equation. The equation proposed by Wang and Singh described precisely the drying process occurring in the TGA at the temperature of 35 °C for moisture ratio above $MR = 0.1$, nevertheless the model is not capable of predicting properly the drying process for moisture ratios below 0.1.

Several drying processes of Granny Smith apples were conducted in the thermogravimetric analyser for constant temperatures ranging from 20 °C to 50 °C, using temperature intervals of 5 °C. Figure 5.2a shows the evolution

Table 5.1: Fitting parameters of different thin-layer drying equations available in the literature applied to the moisture ratio obtained drying Granny Smith samples in TGA at 35 °C. Valid for $1 \geq \mathrm{MR} \geq 0.1$.

Equation	**Model**	**Parameters**	$\mathbf{R}^2[-]$
$MR = 1 + at + bt^2$	Wang and Singh (Wang & Singh, 1978)	$a = -0.00794$ min^{-1}; $b = 1.28 \cdot 10^{-5}$ min^{-2}	0.9999
$MR = \exp(-kt)$	Lewis (Lewis, 1921)	$k = 0.01074$ min^{-1}	0.9865
$MR = a\exp(-kt^n)$	Page (Page, 1949)	$k = 0.00257$ min^{-n}; $n = 1.32$	0.9961
$MR = a\exp(-kt)$	Henderson and Pabis (Henderson & Pabis, 1961)	$a = 1.078$; $k = 0.0118$ min^{-1}	0.9798
$MR = a\exp(-kt) + c$	Logarithmic (Sacilik & Elicin, 2006)	$a = 1.888$; $k = 0.00441$ min^{-1}; $c = -0.880$	0.9998
$MR = a\exp(-k_1 t) + b\exp(-k_2 t)$	Two terms (Madamba *et al.*, 1996)	$a = 29.82$; $k_1 = 0.00255$ min^{-1}; $b = -28.82$; $k_2 = 0.00236$ min^{-1}	0.9999
$MR = a\exp(-kt) + (1-a)\exp(-kat)$	Two terms exponential (Ertekin & Yaldiz, 2004)	$a = 1.846$; $k = 0.01629$ min^{-1}	0.9952
$MR = a\exp(-kt) + (1-a)\exp(-kbt)$	Diffusion approximation (Togrul & Pehlivan, 2003)	$a = -8.39$; $k = 0.01794$ min^{-1}; $b = 0.9435$	0.9879
$MR = a\exp(-k_1 t) + (1-a)\exp(-k_2 t)$	Verma (Verma *et al.*, 1985)	$a = 4.823$; $k_1 = 0.00295$ min^{-1}; $k_2 = 0.0016$ min^{-1}	0.9998
$MR = a\exp(-k_1 t) + b\exp(-k_2 t) + c\exp(-k_3 t)$	Modified Henderson and Pabis (Karathanos, 1999)	$a = -4.674$; $k_1 = 0.0339$ min^{-1}; $b = 1.678$; $k_2 = 0.0509$; $c = 4.015$ min^{-1}; $k_3 = 0.0215$ min^{-1}	0.9989
$MR = a\exp(-kt^n) + bt$	Midilli (Midilli *et al.*, 2002)	$a = 0.993$; $k = 0.00414$ min^{-n}; $n = 1.13$; $b = -0.00135$ min^{-1}	>0.9999

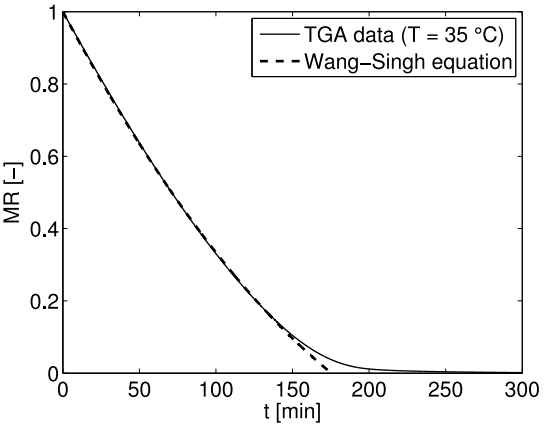

Figure 5.1: Moisture ratio obtained by the TGA at 35 °C and Wang and Singh equation fitting for the moisture ratio above $MR = 0.1$.

of the moisture ratio MR with time t for the different constant temperatures tested. The tendency of the moisture ratio is similar for all the temperatures studied, but there is a strong effect of the temperature on the drying time. This effect is shown in Figure 5.2b, where the drying time t_d needed to obtain a determined value of the moisture ratio is plotted as a function of the drying temperature.

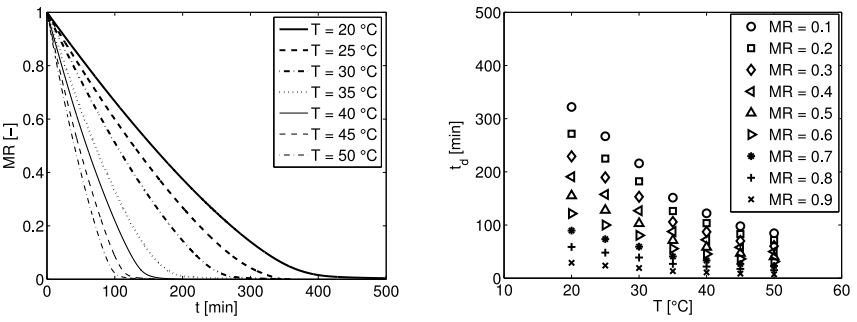

(a) (b)

Figure 5.2: Thin-layer drying of Granny Smith apples in TGA: a) evolution of the moisture ratio with time, b) drying time as a function of temperature.

5.4.2 Mathematical model of the thin-layer drying process of Granny Smith apples at variable temperature

Following the procedure describe in section 5.4.1, the equation proposed by Wang & Singh (1978) (equation (5.2)) was employed to fit the evolution of the experimental moisture ratio with time from $MR = 1$ to $MR = 0.1$, for each temperature. The values of the free parameters a and b in equation (5.2) obtained for each temperature are shown in Figure 5.3a and 5.3b respectively, as a function of the constant temperature employed during the drying process in the TGA. The values obtained for a and b are plotted in Figure 5.3 together with a parabolic fitting, showing a proper agreement of the fitting to the values. The determination coefficients of the fitting are $R^2 = 0.997$ for a and $R^2 = 0.998$ for b. The equations of the parabolic fitting for the parameters of the equation proposed by Wang & Singh (1978) for the temporal evolution of the moisture ratio are:

$$a = -3.44 \cdot 10^{-6} \cdot T^2 - 1.35 \cdot 10^{-4} \cdot T + 1.26 \cdot 10^{-3} \tag{5.3}$$

$$b = 3.75 \cdot 10^{-8} \cdot T^2 - 1.39 \cdot 10^{-6} \cdot T + 1.44 \cdot 10^{-5} \tag{5.4}$$

where a is obtained in min^{-1} and b in min^{-2} for a temperature T in °C.

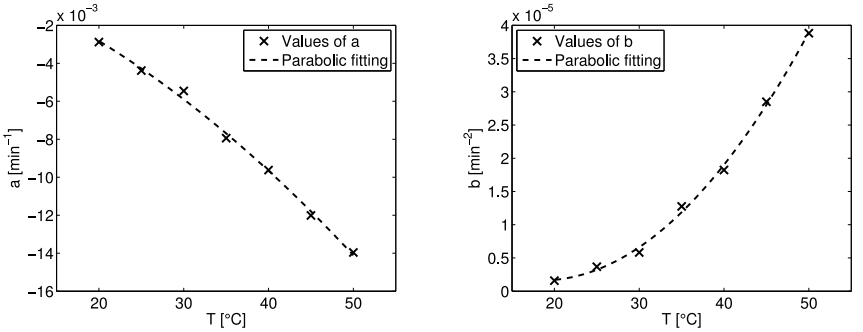

(a) (b)

Figure 5.3: Values of the free parameters of the equation proposed by Wang & Singh (1978) for the TGA measurements.

The values of a and b can be obtained for any temperature using respectively equation (5.3) and equation (5.4). Hence, a model is proposed to estimate the evolution of the moisture ratio during the thin-layer drying process of Granny Smith apples conducted in a TGA under a variable temperature profile.

Considering the reduced size of the sample employed in the TGA tests, the model assumes the thermal inertia of the sample to be negligible. The drying time is discretized in small time intervals dt of 10 ms, and for each time $t = n \cdot dt$ the corresponding drying temperature is determined from the temperature profile. Using equation (5.3) and equation (5.4) the values of a and b are determined for the calculated temperature. Knowing the value of MR estimated by the model at the beginning of the time interval, the values of a and b obtained are employed to determine the decrement of the moisture ratio ΔMR for the time interval dt, considering the temperature constant during that short time period. Therefore, the value of the moisture ratio at the end of the time interval dt is calculated as the value at the beginning of the time interval minus the decrement of the moisture ratio, i.e. $MR(t + dt) = MR(t) - \Delta MR$. The initial condition for the moisture ratio, at the beginning of the drying process, is $t = 0 \rightarrow MR = 1$. The model estimates the evolution of the moisture ratio with time for $MR \geq 0.1$.

5.5 Results and discussion

5.5.1 Validation of the thin-layer drying model

The model proposed for the thin-layer drying of Granny Smith apples at a variable temperature was validated conducting a drying test in the TGA for variable drying temperatures. In order to employ a realistic drying temperature, the temperature measured at the inlet of the drying chamber in the lab-scale indirect solar dryer (Figure 4.12) was used to program the temperature profile in the TGA. The temperature at the inlet of the drying chamber was obtained using the operating conditions discussed in section 2.3. Since the TGA Q 500 employed permits only to program constant heating rates, i.e. linear temperature increases, the temperature measured at the inlet of the drying chamber, shown in Figure 4.12, was divided into 30 linear temperature increases, which were programmed in the TGA. Since the temperature in the TGA cannot be controlled accurately during the cooling process, the test in the TGA ends once the maximum temperature is reached, that is after around 300 min. Nevertheless, the apple sample is totally dried ($MR \rightarrow 0$) before 300 min.

The model proposed in section 5.4.2 was applied to the thin-layer drying process of the Granny Smith apple samples in the TGA, subjected to the temperature profile showed in Figure 4.12. The experimental value of the moisture

ratio obtained in the TGA MR_{TGA} and the estimated value obtained from the model proposed MR_{mod} can be observed in Figure 5.4a. As can be seen in Figure 5.4a, the model follows the trend of the evolution of the moisture ratio of the apples for a drying process with a variable temperature. In fact, the deviation between the model estimation of the drying time t_d and the experimental values is lower than 2.5 min for moisture ratios between 1 and 0.1, as shown in Figure 5.4b. This maximum deviation of 2.5 min corresponds to a maximum relative error of the time estimated by the model of 1.5%. Therefore, the model was proved to predict accurately the evolution of the moisture ratio during a variable temperature thin-layer drying process of Granny Smith apples.

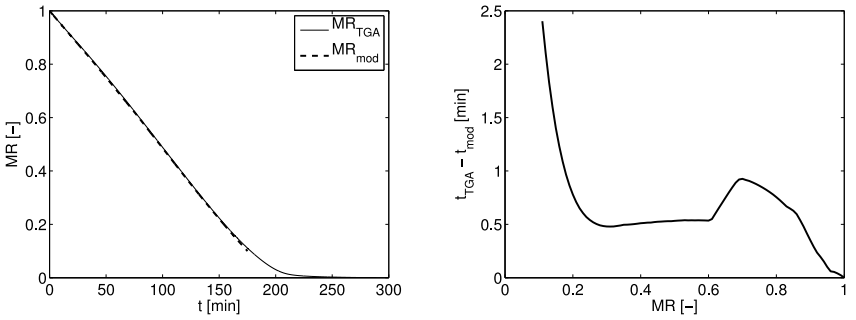

(a) (b)

Figure 5.4: a) Measured and estimated evolution of the moisture ratio with time for the variable temperature drying process in the TGA, b) deviation between the estimated and the measured drying time.

5.5.2 Application of the drying model in an indirect solar dryer

Once validated using TGA measurements, the model was applied to the drying of Granny Smith apples in a solar indirect dryer. In this case, a total mass of around 80 g of slices of apples (2.4 mm of thickness) were dried on the reference tray in the drying chamber. The variation of the sample mass with time was measured with the balance each 5 s. Therefore, the evolution of the moisture ratio with time during the drying process in the indirect solar dryer can be calculated, and a procedure similar to that employed previously for the TGA measurements can be followed. First, several constant temperature drying tests were performed in the indirect solar dryer, using temperatures between 25 °C

and 40 °C in intervals of 5 °C. In this case, for each value of the temperature, the corresponding value of the relative humidity of air was employed, following the weather data for the climate selected, explained in section 2.3, and the drying conditions presented in section 4.6. The evolution with time of the moisture ratio obtained in the solar dryer for each temperature is plotted in Figure 5.5a. An increase in the constant temperature of the drying process decreases significantly the drying time, similar to what was shown for the TGA experiments. The values of the drying time for each moisture ratio and drying temperature can be found in Figure 5.5b.

The moisture ratio curves obtained for each constant temperature in the indirect solar dryer were fitted to a curve as that proposed by Wang & Singh (1978), shown in equation (5.2), determining the fitting parameters a and b. The values of the fitting parameters obtained for each temperature are presented in Figure 5.6, together with their parabolic fitting. The equations of the parabolic fitting of the parameters a and b of the Wang-Singh equation for the thin-layer drying of Granny Smith apples in the solar indirect dryer, considering the climate data presented in Figure 2.3 and the drying conditions presented in Figure 4.12, are:

$$a_{SD} = 4.86 \cdot 10^{-6} \cdot T^2 - 5.38 \cdot 10^{-4} \cdot T + 6.93 \cdot 10^{-3} \tag{5.5}$$

$$b_{SD} = -5.87 \cdot 10^{-9} \cdot T^2 + 7.94 \cdot 10^{-7} \cdot T - 1.37 \cdot 10^{-5} \tag{5.6}$$

where a_{SD} is obtained in min^{-1} and b_{SD} in min^{-2} for a temperature T in °C.

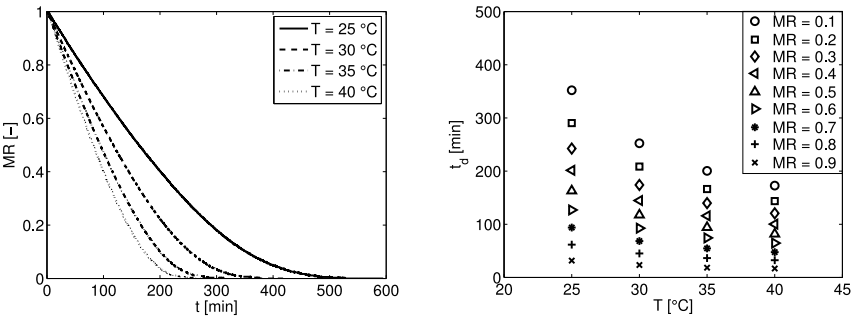

(a) (b)

Figure 5.5: Thin-layer drying of Granny Smith apples in an indirect solar dryer: a) evolution of the moisture ratio with time, b) drying time as a function of temperature.

The model proposed for the thin-layer drying of Granny Smith apples at

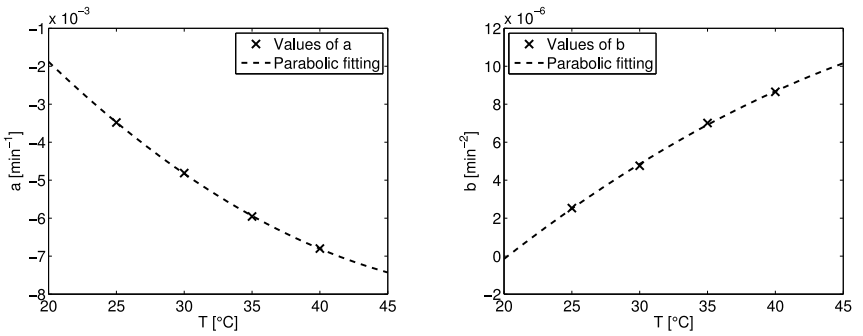

(a) (b)

Figure 5.6: Values of the free parameters of the equation proposed by Wang & Singh (1978) for the indirect solar dryer measurements.

variable temperature was applied to the drying process in the solar indirect dryer. To that end, the values of the parameters a_{SD} and b_{SD} of the Wang-Singh equation for the solar dryer were obtained from equation (5.5) and equation (5.6) for each drying chamber temperature. The drying chamber temperature was that showed in Figure 4.12. Then, using the variable temperature and the parabolic fittings of the parameters a_{SD} and b_{SD} for the solar dryer, the proposed model can be employed to estimate the evolution of the moisture ratio with time during the thin-layer drying of Granny Smith apples.

The values measured in the indirect solar dryer for the moisture ratio are shown in Figure 5.7a, together with the estimation of the model. The experimental curve showed in Figurre 5.7a is the average of 5 different tests. Nevertheless, the tests presented high repeatability, being the maximum standard deviation in the whole MR curve less that 0.01. In each test, 9 slices of apple where dried in the reference mesh detailed in section 2.4.

The model seems to overestimate the performance of the indirect solar dryer, predicting lower drying times than those measured. The maximum deviation between the predicted and the measured drying time for the indirect solar dryer was lower than 20 min, as shown in Figure 5.7b, corresponding to a maximum relative error around 10%. The higher error obtained for the estimations of the model for the drying process occurring in the indirect solar dryer might be attributed to the effect of the thermal inertia of the sample. For the experiments in the indirect solar dryer, the mass of the sample is much larger than the mass used in the TGA tests (approximately 80 g in the indirect solar dryer and just

around 150 mg in the TGA), thus the temperature of the sample might differ from that measured in the air of the drying chamber. The lower temperature of the sample in the indirect solar dryer tests due to thermal inertia would delay the drying process, and might be the cause of the differences observed in Figure 5.7.

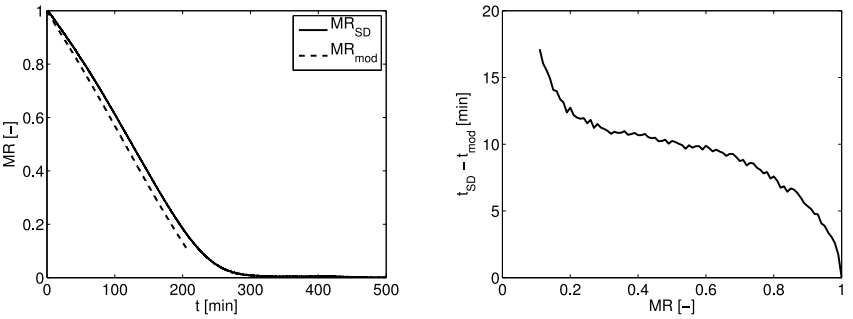

(a) (b)

Figure 5.7: a) Measured and estimated evolution of the moisture ratio with time for the variable temperature drying process in the indirect solar dryer, b) deviation between the estimated and the measured drying time.

The effect of the thermal inertia of the sample on the delay of the drying process in the indirect solar dryer was analysed, performing drying tests, using the atmospheric conditions described in section 2.3 for various air mass flow rates. The nominal air mass flow rate of 0.015 kg/s was increased to 0.020 kg/s and 0.025 kg/s and drying tests were carried out. The process to obtain the estimations of the model proposed for the moisture ratio evolution was repeated for these new values of the air mass flow rate, and the deviations in time between the experimental measurements and the model predictions were quantified. The results are shown in Figure 5.8, where the time deviations for the three different air mass flow rates employed are plotted. The deviations are proved to decrease for higher air mass flow rates, as a consequence of the higher convection coefficient obtained using a higher air velocity, which reduces the effect of thermal inertia of the sample.

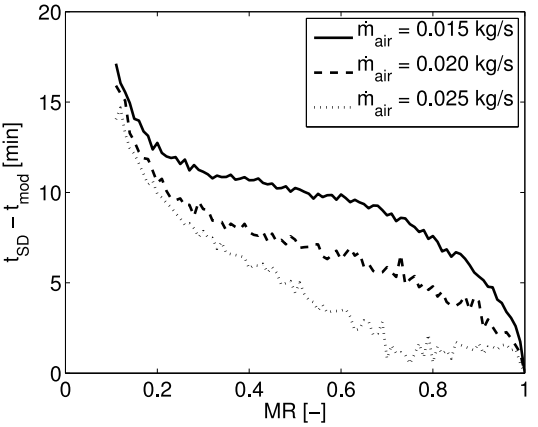

Figure 5.8: Deviation between the estimated and the measured drying time for different values of the air mass flow rate.

5.6 Conclusions

The kinetics of the thin-layer drying process of Granny Smith apples was experimentally analysed by means of thermogravimetric measurements. Drying tests were conducted at different constant drying temperatures in a TGA, obtaining the drying curves of Granny Smith apples as a function of temperature. The Wang-Singh equation was employed to fit the experimental drying curves obtained in the TGA for constant temperatures. A model was proposed, based on the Wang-Singh equation, to predict the evolution of the moisture ratio during the thin-layer drying process of Granny Smith apples under variable temperature profiles. The model was validated using experimental results of the drying of apples in the TGA for a variable drying temperature. The prediction of the model proposed for the evolution of the moisture ratio with variable temperature was in excellent agreement with the experimental measurements obtained in the TGA.

The model was also applied to the drying process of thin slices of Granny Smith apples in an indirect solar dryer. The procedure was replicated, obtaining the parameters of the Wang-Singh equation for the drying conditions presented in the solar drying process. The comparison of the model estimations with experimental measurements carried out in a lab-scale indirect solar dryer shows a proper agreement. Nevertheless, the experimental values of the moisture ratio were delayed compared to the model predictions, a result that can be attributed

to the effect of the thermal inertia of the sample in the indirect solar dryer.

Nomenclature

A_c	Solar collector area [m^2]
a	Free parameter in the Wang-Singh equation [s^{-1}]
b	Free parameter in the Wang-Singh equation [s^{-2}]
dt	Time interval [s]
I	Solar irradiance on the horizontal plane [W/m^2]
$\dot{m}_{air}$	Air mass flow rate [kg/s]
M	Moisture content as a function of time [kg/kg]
M_e	Equilibrium moisture content [kg/kg]
M_0	Initial moisture content [kg/kg]
MR	Moisture ratio [-]
S	Solar irradiance absorbed by the absorber plate [W/m^2]
T	Temperature [°C]
t	Time [s]
t_d	Drying time [s]

Greek letters

ϕ	Relative humidity [-]
ΔMR	Moisture ratio reduction [-]

Subindex

0	Inlet of the collector
1	Outlet of the collector, inlet of the drying chamber
mod	Model
SD	Solar dryer
TGA	Thermogravimetric analyser

References

Akpinar, E. K. 2006 Determination of suitable thin layer drying curve model for some vegetables. *Journal of Food Engineering* 73 (3), 75–84.

Bezerra, C. V., Meller Da Silva, L. H., Corrêa, D. F. & Rodrigues, A. M. C. 2015 A modeling study for moisture diffusivities and moisture transfer coefficients in drying of passion fruit peel. *International Journal of Heat and Mass Transfer* 85, 750–755.

Celma, A. R., Rojas, S., López, F., Montero, I. & Miranda, T. 2007 Thin-layer drying behaviour of sludge of olive oil extraction. *Journal of Food Engineering* 80 (4), 1261–1271.

Doymaz, I. 2009 An Experimental Study on Drying of Green Apples. *Drying Technology* 27 (October 2014), 478–485.

Ertekin, C. & Yaldiz, O. 2004 Drying of eggplant and selection of a suitable thin layer drying model. *Journal of Food Engineering* 63, 349–359.

González-Fésler, M., Salvatori, D., Gómez, P. & Alzamora, S. M. 2008 Convective air drying of apples as affected by blanching and calcium impregnation. *Journal of Food Engineering* 87 (3), 323–332.

Henderson, S. M. & Pabis, S. 1961 Grain drying theory. I. Temperature effect on drying coefficient. *Journal of Agricultural Engineering Research* 6 (3), 169–174.

Janjai, S., Lamlert, N., Intawee, P., Mahayothee, B., Bala, B. K., Nagle, M. & Müller, J. 2009 Experimental and simulated performance of a PV-ventilated solar greenhouse dryer for drying of peeled longan and banana. *Solar Energy* 83 (9), 1550–1565.

Karathanos, V. T. 1999 Determination of water content of dried fruits by drying kinetics. *Journal of Food Engineering* 39, 337–344.

Karim, M. A. & Hawlader, M. N. A. 2005 Mathematical modelling and experimental investigation of tropical fruits drying. *International Journal of Heat and Mass Transfer* 48 (23-24), 4914–4925.

Lewis, W. K. 1921 The rate of drying of solid materials. *Industrial Engineering Chemistry* 13 (5), 427–442.

Madamba, P. S., Driscoll, R. H. & Buckle, K. A. 1996 The thin layer drying characteristics of gralic slices. *Journal of Food Engineering1* 29, 75–97.

Menges, H. O. & Ertekin, C. 2006 Mathematical modeling of thin layer drying of Golden apples. *Journal of Food Engineering* 77 (1), 119–125.

Midilli, A., Kucuk, H. & Yapar, Z. 2002 A new model for single layer drying. *Drying Technology* 20 (7), 1503–1513.

Page, G. 1949 Factors influencing the maximum rates of air drying shelled corn in layers. M. S. Thesis. Purdue University.

Panchariya, P. C., Popovic, D. & Sharma, A. L. 2002 Thin-layer modelling of black tea drying process. *Journal of Food Engineering* 52 (4), 349–357.

Sacilik, K. & Elicin, A. K. 2006 The thin layer drying characteristics of organic apple slices. *Journal of Food Engineering* 73 (3), 281–289.

Togrul, I. T. & Pehlivan, D. 2003 Modelling of drying kinetics of single apricot. *Journal of Food Engineering* 58 (1), 23–32.

Vega-Galvez, A., Ah-Hen, K., Chacana, M., Vergara, J., Martinez-Monzo, J., García-Segovia, P., Lemus-Mondaca, R. & Di Scala, K. 2012 Effect of temperature and air velocity on drying kinetics, antioxidant capacity, total phenolic content, colour, texture and microstructure of apple (var. Granny Smith) slices. *Food Chemistry* 132 (1), 51–59.

Velić, D., Tomas, S. & Bucić-kojić, A. 2007 Study of the Drying Kinetics of " Granny Smith " Apple in Tray Drier. *Agriculturae Conspectus Scientificus* 72 (4), 323–328.

Verma, L. R., Bucklin, R. A., Endan, J. B. & Wratten, F. T. 1985 Effects of drying air parameters on rice drying models. *Transactions of the ASAE* 28, 296–301.

Wang, C. Y. & Singh, R. P. 1978 A single layer drying equation for rough rice. *Transactions of the ASAE* 78 (3001).

Zhu, A. & Shen, X. 2014 The model and mass transfer characteristics of convection drying of peach slices. *International Journal of Heat and Mass Transfer* 72, 345–351.

Zlatanović, I., Komatina, M. & Antonijević, D. 2013 Low-temperature convective drying of apple cubes. *Applied Thermal Engineering* 53 (1), 114–123.

CHAPTER

SIX

Conclusions

In this PhD thesis, a study on the processes involved in indirect solar drying has been presented. The air heating process in the solar collector, and the drying process in the drying chamber were studied separately. An analysis of such processes, and their contribution to the global solar drying process was provided. The work was based on laboratory experiments combined with mathematical modelling of the air heating process and the drying process. In parallel, a fundamental study of such processes, for a general case, has been developed.

A theoretical study on the potential of indirect solar dryers of small-scale was developed. The study considers evaporation of free water, which would settle the maximum evaporation rate obtainable, since the constriction of the drying kinetics of the product is not considered. The study was based on the comparison of the actual amount of water that could be evaporated in the drying chamber, with the drying capacity that the airflow acquires in the solar dryer. The effect of the different parameters that influence the processes involved in the global operation was analysed, selecting the parameters that present a major effect. The study considered a range of variation of the affecting parameters within the characteristic values that are typical of small-scale solar drying.

A simplified model for the calculation of the pick-up efficiency was derived from the numerical simulation of the evaporation of free water in the drying chamber. The deviation of the results of the simplified model compared to the results of the numerical simulation was found to be low. The model was applied for the calculation of the maximum evaporation rate obtainable in the drying chamber, based on a reduced number of parameters, to facilitate the analysis of the effect of such parameters on the process. The main parameters are the air mass flow rate, the collector width and length, the aspect ratio in the drying chamber (drying area to cross section in the airflow direction) and the ambient

conditions. The results showed that the maximum evaporation rate increases with the air mass flow rate, but with a strong dependence on the aspect ratio of the drying chamber. For the nominal case analysed (collector of 1 m length and 0.5 m width), an aspect ratio in the drying chamber between 200 and 300, depending on the air mass flow rate, would be the optimal selection.

A lab-scale indirect solar dryer has been designed, constructed and tested in order to carry out the experiments. The lab-scale solar dryer is capable of reproducing the drying conditions of indirect solar drying processes for different climates, associated with the harvest season of the product to be dried. The experiments were carried out with samples of Granny Smith apples, as an application. A climate characteristic of the harvest season of such variety of apples was characterized, since it establishes the conditions at which the solar drying process occurs.

A characterization of the control system, responsible of the stability of the replication of the solar drying process was conducted. The reproduction of the climatic conditions in the experimental facility was shown to be proper in terms of stability and accurate tracking of the programmed profiles, and thus the solar drying process could be precisely reproduced. A nominal air mass flow rate of 0.015 kg/s was selected, since higher values entail low increments of temperature in the solar collector which, at the climate of the harvest season of Granny Smith apples, would lead to long drying processes.

The air heating process in the solar collector was studied in detail to determine the drying conditions at the entrance of the drying chamber. A mathematical model of the air heating process, capable of describing the collector performance was developed. As a first approximation, the model considered steady state conditions. The model estimates the average temperatures of the absorber plate and the glass cover of the solar collector, and the temperature of the airflow at the outlet of the collector. The model resulted in a collector efficiency factor $F' = 0.85$ and a collector heat loss coefficient $U_L = 6.6$ W/m^{2}K. The results of the temperatures obtained with the mathematical model were compared to experimental measurements carried out in the solar collector of the lab-scale solar dryer, showing a proper agreement. The model predicts accurately the temperature of the airflow at the outlet of the collector, whereas the temperature of the glass cover is overestimated in 0.75 °C in average, and the temperature of the absorber plate is underestimated in 6.6 °C in average. The accurate prediction of the temperature of the airflow at the outlet of the collector is important, since it establishes the drying conditions for the drying

process. The model was then extended, and applied to transient conditions. The results of the model were validated with experimental measurement, showing a slightly higher error than in the case of steady state conditions.

In addition, an experimental analysis of the solar collector operating at the reference climate conditions (Granny Smith harvest season) was carried out. The experimental collector efficiency factor was $F' = 0.9$ and the collector heat loss coefficient $U_L = 8.0$ W/m^{2}K. The differences with the values obtained with the model ($F' = 0.85$ and $U_L = 6.6$ W/m^{2}K) are small despite the hypotheses considered in the mathematical model.

Since the drying process begins immediately after the air heating process, the conditions at the outlet of the collector are the drying conditions, which for solar drying processes are variable with time. The drying kinetics of a product are generally determined at isothermal conditions, and thus it does not suit a solar drying process. A model to predict the drying curve at variable conditions, based on the drying kinetics determined at constant conditions is presented. The drying kinetics of Granny Smith apples was determined using a thermogravimetric analyser (TGA) at constant temperature, and fitted to different thin-layer equations. The Wang-Sing equation was found to be the more suitable equation, based on accuracy and simplicity criteria. Tests at different constant conditions were carried out, within a range of solar drying applications: from 20 °C to 50°C in intervals of 5 °C. Using the developed model, the drying curve at variable temperature was predicted, following the drying temperature provided by the solar air heater. The model results were compared to experimental measurements carried out in the TGA, where the variable drying temperature was programmed. The model was shown to predict with high accuracy the drying curve at variable conditions.

The model was then applied to the estimation of the drying curve in the solar dryer, considering also the air mass flow rate and the variable relative humidity. The free parameters of the Wang-Singh equation were obtained for the drying conditions presented in the solar drying process. The model is able to estimate properly the drying curve obtained experimentally, with a slight deviation due to the thermal inertia of the apple samples. The model links the typical procedure of determination of the drying kinetics at isothermal conditions with the prediction of the solar drying process, in a simple way.

The combination of the different models presented provides with a proper prediction of the global solar drying process, based on simple modelling of the different processes involved. The potential of the dryer might be determined

with a simple expression. The temperature of the airflow at the outlet of the collector can be accurately calculated, establishing the drying conditions. For such conditions, the drying curve can be estimated, based on the drying kinetics of the product, determined at constant conditions.

This PhD thesis is an attempt to contribute to the systematization of the methodology of evaluation of solar drying operations. The procedures presented are a first step to establish a broader research line, focused on the comprehensive analysis of solar drying processes, and strengthened by the development of a versatile experimental facility.

Alphabetical list of references

AENOR 2010 Biocombustibles sólidos. Determinación del contenido de humedad. Método de secado en estufa. Parte 1: Humedad total. Métod de referencia.

Ahmad-Qasem, M. H., Barrajon-Catalan, E., Micol, V., Cárcel, J. A. & Garcia-Perez, J. V. 2013 Influence of air temperature on drying kinetics and antioxidant potential of olive pomace. *Journal of Food Engineering* 119 (3), 516–524.

Akpinar, E. K. 2006 Determination of suitable thin layer drying curve model for some vegetables. *Journal of Food Engineering* 73 (3), 75–84.

Akpinar, E. K. & Koçyigit, F. 2010 Experimental energy and exergy analysis of a double-ow solar air heater having different obstacles on absorber plates.pdf. *Applied Energy* 87, 3438–3450.

Al-Juamily, K. E. J., Khalifa, A. J. N. & Yassen, T. A. 2007 Testing of the performance of a fruit and vegetable solar drying system in Iraq. *Desalination* 209 (1-3 SPEC. ISS.), 163–170.

Alta, D., Bilgili, E., Ertekin, C. & Yaldiz, O. 2010 Experimental investigation of three different solar air heaters: Energy and exergy analyses. *Applied Energy* 87 (10), 2953–2973.

Altobelli, F., Condorí, M., Duran, G. & Martinez, C. 2014 Solar dryer efficiency considering the total drying potential. Application of this potential as a resource indicator in north-western Argentina. *Solar Energy* 105, 742–759.

Belessiotis, V. & Delyannis, E. 2011 Solar drying. *Solar Energy* 85 (8), 1665–1691.

Bezerra, C. V., Meller Da Silva, L. H., Corrêa, D. F. & Rodrigues, A. M. C. 2015 A modeling study for moisture diffusivities and moisture transfer coefficients in drying of passion fruit peel. *International Journal of Heat and Mass Transfer* 85, 750–755.

Boughali, S., Benmoussa, H., Bouchekima, B., Mennouche, D., Bouguettaia, H. & Bechki, D. 2009 Crop drying by indirect active hybrid solar - Electrical dryer in the eastern Algerian Septentrional Sahara. *Solar Energy* 83 (12), 2223–2232.

Buluswar, S., Friedman, Z., Mehta, P., Mitra, S. & Sathre, R. 2014 *50 breakthroughs-Critical scientific and technological advances needed for sustainable global development*. Institue for Globally Transformative Technologies Lawrence Berkeley National Lab.

Cai, J. M. & Chen, S. Y. 2008 Determination of Drying Kinetics for Biomass by Thermogravimetric Analysis under Nonisothermal Condition. *Drying Technology* 26 (12), 1464–1468.

Celma, A. R., Rojas, S., López, F., Montero, I. & Miranda, T. 2007 Thin-layer drying behaviour of sludge of olive oil extraction. *Journal of Food Engineering* 80 (4), 1261–1271.

Chen, D., Zheng, Y. & Zhu, X. 2012 Determination of effective moisture diffusivity and drying kinetics for poplar sawdust by thermogravimetric analysis under isothermal condition. *Bioresource Technology* 107, 451–455.

Contreras, C., Martín-Esparza, M. E., Chiralt, A. & Martínez-Navarrete, N. 2008 Influence of microwave application on convective drying: Effects on drying kinetics, and optical and mechanical properties of apple and strawberry. *Journal of Food Engineering* 88 (1), 55–64.

Daguenet, M. 1989 Les sechoirs solaires, theorie et practique. *Tech. Rep.*. UNESCO.

Damartzis, T., Vamvuka, D., Sfakiotakis, S. & Zabaniotou, A. 2011 Thermal degradation studies and kinetic modeling of cardoon (Cynara cardunculus) pyrolysis using thermogravimetric analysis (TGA). *Bioresource Technology* 102 (10), 6230–6238.

Dissa, A. O., Bathiebo, D. J., Desmorieux, H., Coulibaly, O. & Koulidiati, J. 2011 Experimental characterisation and modelling of thin layer direct solar drying of Amelie and Brooks mangoes. *Energy* 36 (5), 2517–2527.

Doymaz, I. 2009 An Experimental Study on Drying of Green Apples. *Drying Technology* 27 (October 2014), 478–485.

Duffie, J. A. & Beckman, W. A. 2006 *Solar Engineering of Thermal processes*, 3rd edn. Hoboken, New Jersey: John Wiley and Sons.

Ekechukwu, O. V. & Norton, B. 1999*a* Review of solar-energy drying systems II: an overview of solar drying technology. *Energy Conversion and Management* 40 (6), 615–655.

Ekechukwu, O. V. & Norton, B. 1999*b* Review of solar-energy drying systems III: low temperature air-heating solar collectors for crop drying applications. *Energy Conversion and Management* 40 (6), 657–667.

El-Beltagy, A., Gamea, G. R. & Essa, A. H. A. 2007 Solar drying characteristics of strawberry. *Journal of Food Engineering* 78 (2), 456–464.

El-Sebaii, A. A., Aboul-Enein, S., Ramadan, M. R. I. & El-Gohary, H. G. 2002 Experimental investigation of an indirect type natural convection solar dryer. *Energy Conversion and Management* 43 (16), 2251–2266.

Elkhadraoui, A., Kooli, S., Hamdi, I. & Farhat, A. 2015 Experimental investigation and economic evaluation of a new mixed-mode solar greenhouse dryer for drying of red pepper and grape. *Renewable Energy* 77, 1–8.

Energy-Plus 2015 http://energyplus.net/weather, accessed: may 2015.

Erbs, D. G., Klein, S. A. & Duffie, J. A. 1982 Estimation of the diffuse radiation fraction for hourly, daily and monthly-average global radiation. *Solar Energy* 28 (4), 293–302.

Ertekin, C. & Yaldiz, O. 2004 Drying of eggplant and selection of a suitable thin layer drying model. *Journal of Food Engineering* 63, 349–359.

Evin, D. 2012 Thin layer drying kinetics of Gundelia tournefortii L. *Food and Bioproducts Processing* 90 (2), 323–332.

FAO 2006 Dryer construction for solar dried fruit and vegetables production. *Technologies and practices for small agricultural producers* .

Forson, F. K., Nazha, M. & Rajakaruna, H. 2003 Experimental and simulation studies on a single pass, double duct solar air-heater. *Energy Conversion and Management* 44, 1209–1227.

Freire, F., Figuredo, A. & Ferrão, P. 1999 Thermal Analysis and Drying Kinetics of Olive Bagasse. *Drying Technology* 17 (4-5), 895–907.

Fudholi, A., Sopian, K., Ruslan, M. H., Alghoul, M. A. & Sulaiman, M. Y. 2010 Review of solar dryers for agricultural and marine products. *Renewable and Sustainable Energy Reviews* 14 (1), 1–30.

González-Fésler, M., Salvatori, D., Gómez, P. & Alzamora, S. M. 2008 Convective air drying of apples as affected by blanching and calcium impregnation. *Journal of Food Engineering* 87 (3), 323–332.

Henderson, S. M. & Pabis, S. 1961 Grain drying theory. I. Temperature effect on drying coefficient. *Journal of Agricultural Engineering Research* 6 (3), 169–174.

Hill, J. E., Jenkins, J. P. & Jones, D. E. 1979 *Experimental Verifications of a Standard Test Procedure for Solar Collectors*. Washington, D.C: National Bureau of Standards.

Hottel, H. C. & Whillier, A. 1958 Evaluation of flat-plate solar-collector performance. *Transactions of the Conference on Use of Solar Energy* 54 (1), 19–41.

Hunn, B. D. & Calafell, D. O. 1977 Determination of average ground reflectivity for solar collectors. *Solar Energy* 19 (1), 87–89.

Iglesias, I., Carbó, J., Bonany, J. & Montserrat, R. 2009 Varietal Innovation in apples. *Revista de Fruticultura* pp. 13–25.

Incropera, F. K. & Dewitt, D. P. 1990 *Introduction to heat transfer*, 2nd edn. Indiana, USA: John Wiley and Sons, Purdue University.

ITDG & UNIFEM 1995 *Drying. Food Cycle Technology*. London, UK: Intermediate Technology Publications.

Janjai, S., Lamlert, N., Intawee, P., Mahayothee, B., Bala, B. K., Nagle, M. & Müller, J. 2009 Experimental and simulated performance of a PV-ventilated solar greenhouse dryer for drying of peeled longan and banana. *Solar Energy* 83 (9), 1550–1565.

Jannot, Y. & Coulibaly, Y. 1998 The " Evaporative Capacity " As a Performance Index for a solar-drier air-heater. *Solar Energy* 63 (6), 387–391.

Kadam, D. M. & Samuel, D. V. K. 2006 Convective flat-plate solar heat collector for cauliflower drying. *Biosystems Engineering* 93 (2), 189–198.

Kaleta, A., Gornicki, K., Winiczenko, R. & Chojnacka, A. 2013 Evaluation of drying models of apple (var. Ligol) dried in a fluidized bed dryer. *Energy Conversion and Management* 67, 179–185.

Karathanos, V. T. 1999 Determination of water content of dried fruits by drying kinetics. *Journal of Food Engineering* 39, 337–344.

Karim, M. A. & Hawlader, M. N. A. 2004 Development of solar air collectors for drying applications. *Energy Conversion and Management* 45 (3), 329–344.

Karim, M. A. & Hawlader, M. N. A. 2005 Mathematical modelling and experimental investigation of tropical fruits drying. *International Journal of Heat and Mass Transfer* 48 (23-24), 4914–4925.

Karim, M. A. & Hawlader, M. N. A. 2006 Performance evaluation of a v-groove solar air collector for drying applications. *Applied Thermal Engineering* 26 (1), 121–130.

Karsli, S. 2007 Performance analysis of new-design solar air collectors for drying applications. *Renewable Energy* 32 (10), 1645–1660.

Kaya, A., Aydin, O. & Demirtas, C. 2007 Drying Kinetics of Red Delicious Apple. *Biosystems Engineering* 96 (4), 517–524.

Koua, K. B., Fassinou, W. F., Gbaha, P. & Toure, S. 2009 Mathematical modelling of the thin layer solar drying of banana, mango and cassava. *Energy* 34 (10), 1594–1602.

Kumar, M., Sansaniwal, S. K. & Khatak, P. 2016 Progress in solar dryers for drying various commodities. *Renewable and Sustainable Energy Reviews* 55, 346–360.

Lamnatou, C., Papanicolaou, E., Belessiotis, V. & Kyriakis, N. 2012 Experimental investigation and thermodynamic performance analysis of a solar dryer using an evacuated-tube air collector. *Applied Energy* 94, 232–243.

Leon, M. A. & Kumar, S. 2007 Mathematical modeling and thermal performance analysis of unglazed transpired solar collectors. *Solar Energy* 81 (1), 62–75.

Leon, M. A., Kumar, S. & Bhattacharya, S. C. 2002 A comprehensive procedure for performance evaluation of solar food dryers. *Renewable and Sustainable Energy Reviews* 6 (4), 367–393.

Lewis, W. K. 1921 The rate of drying of solid materials. *Industrial Engineering Chemistry* 13 (5), 427–442.

Li, Z. Y. & Kobayashi, N. 2005 Determination of moisture diffusivity by thermo-gravimetric analysis under non-isothermal condition. *Drying Technology* 23 (6), 1331–1342.

Liu, B. Y. H. & Jordan, R. C. 1963 The Long-Term Average Performance of Flat-Plate Solar Energy Collectors. *Solar Energy* 7 (2), 53–74.

Madamba, P. S., Driscoll, R. H. & Buckle, K. A. 1996 The thin layer drying characteristics of gralic slices. *Journal of Food Engineering1* 29, 75–97.

Madhava, M., Rao, P. Srinivasa & Goswami, T. K. 2001 Drying Kinectics of Paddy Using Thermogravimetric Analysis. *Drying Technology* 19 (6), 1201–1210.

Mahapatra, A. K. & Imre, L. 1990 Role of solar-agricultural drying in developing countries. *International Journal of Ambient Energy* 11 (4), 205–210.

Menges, H. O. & Ertekin, C. 2006 Mathematical modeling of thin layer drying of Golden apples. *Journal of Food Engineering* 77 (1), 119–125.

Midilli, A., Kucuk, H. & Yapar, Z. 2002 A new model for single layer drying. *Drying Technology* 20 (7), 1503–1513.

Montero, I. 2005 Modelado y construcción de un secadero solar híbrido para residuos biomásicos. PhD thesis, Universidad de Extremadura.

Montero, I., Blanco, J., Miranda, T., Rojas, S. & Celma, A. R. 2010 Design, construction and performance testing of a solar dryer for agroindustrial by-products. *Energy Conversion and Management* 51 (7), 1510–1521.

Montero, I., Miranda, T., Sepúlveda, F., Arranz, J., Rojas, C. & Nogales, S. 2015 Solar Dryer Application for Olive Oil Mill Wastes. *Energies* 8 (12), 14049–14063.

Njomo, D. 1991 Modeling the heat exchanges in a solar air heater with a cover partially transparent to infrared radiations. *Renewable Energy* 1 (5-6), 837–843.

Oztop, H. F., Bayrak, F. & Hepbasli, A. 2013 Energetic and exergetic aspects of solar air heating (solar collector) systems. *Renewable and Sustainable Energy Reviews* 21, 59–83.

Page, G. 1949 Factors influencing the maximum rates of air drying shelled corn in layers. M. S. Thesis. Purdue University.

Panchariya, P. C., Popovic, D. & Sharma, A. L. 2002 Thin-layer modelling of black tea drying process. *Journal of Food Engineering* 52 (4), 349–357.

Pangavhane, D. R., Sawhney, R. L. & Sarsavadia, P. N. 2002 Design, development and performance testing of a new natural convection solar dryer. *Energy* 27 (6), 579–590.

Passamai, V. & Saravia, L. 1997 Relationship Between a Solar Drying Model of Red Pepper and the Kinetics of Pure Water Evaporation (I). *Drying Technology* 15 (5), 1419–1432.

Pirasteh, G., Saidur, R., Rahman, S. M. A. & Rahim, N. A. 2014 A review on development of solar drying applications. *Renewable and Sustainable Energy Reviews* 31, 133–148.

Ringeisen, B., Barrett, D. M. & Stroeve, P. 2014 Concentrated solar drying of tomatoes. *Energy for Sustainable Development* 19 (1), 47–55.

Romano, G., Kocsic, L. & Farkas, I. 2009 Analysis of energy and environmental parameters during solar cabinet drying of apple and carrot. *Drying Technology* 27 (4), 574–579.

Rosselló, C., Bema, A. & Mulet, A. 1990 Solar Drying of Fruits in a Mediterranean Climate. *Drying Technology* 8 (2), 305–321.

Sacilik, K. & Elicin, A. K. 2006 The thin layer drying characteristics of organic apple slices. *Journal of Food Engineering* 73 (3), 281–289.

Shanmugam, V. & Natarajan, E. 2006 Experimental investigation of forced convection and desiccant integrated solar dryer. *Renewable Energy* 31 (8), 1239–1251.

Shumacher, F. E. 1973 *Small is Beautiful: A study on economics as if people mattered*. Blond & Briggs.

Singh, S. & Kumar, S. 2012*a* Development of convective heat transfer correlations for common designs of solar dryer. *Energy Conversion and Management* 64, 403–414.

Singh, S. & Kumar, S. 2012*b* Testing method for thermal performance based rating of various solar dryer designs. *Solar Energy* 86 (1), 87–98.

Sokhansanj, S. & Jayas, D. S. 2006 Drying of Foodstuffs. In *Handbook of Industrial Drying*, 3rd edn. (ed. A.S Mujumdar), chap. 21, pp. 522–545. Taylor and Francis Group, CRC Press.

Sreekumar, A., Manikantan, P. E. & Vijayakumar, K. P. 2008 Performance of indirect solar cabinet dryer. *Energy Conversion and Management* 49 (6), 1388–1395.

Swetman, T. 2007 Solar drying. *Tech. Rep.*. Practical Action.

Tchinda, R. 2009 A review of the mathematical models for predicting solar air heaters systems. *Renewable and Sustainable Energy Reviews* 13, 1734–1759.

Tiris, C. & Dincer, I. 1995 Investigation of the thermal efficiencies of a solars dryer. *Energy Conservation and Management* 36 (3), 205–212.

Toğrul, H. 2005 Simple modeling of infrared drying of fresh apple slices. *Journal of Food Engineering* 71 (3), 311–323.

Togrul, I. T. & Pehlivan, D. 2003 Modelling of drying kinetics of single apricot. *Journal of Food Engineering* 58 (1), 23–32.

Treybal, R. E. 1980 *Mass-Transfer Operations*, 3rd edn. United States of America: McGraw-hill Book Company.

Vega-Galvez, A., Ah-Hen, K., Chacana, M., Vergara, J., Martinez-Monzo, J., García-Segovia, P., Lemus-Mondaca, R. & Di Scala, K. 2012 Effect of temperature and air velocity on drying kinetics, antioxidant capacity, total phenolic content, colour, texture and microstructure of apple (var. Granny Smith) slices. *Food Chemistry* 132 (1), 51–59.

Velić, D., Planinić, M., Tomas, S. & Bilić, M. 2004 Influence of airflow velocity on kinetics of convection apple drying. *Journal of Food Engineering* 64 (1), 97–102.

Velić, D., Tomas, S. & Bucić-kojić, A. 2007 Study of the Drying Kinetics of " Granny Smith " Apple in Tray Drier. *Agriculturae Conspectus Scientificus* 72 (4), 323–328.

Verma, L. R., Bucklin, R. A., Endan, J. B. & Wratten, F. T. 1985 Effects of drying air parameters on rice drying models. *Transactions of the ASAE* 28, 296–301.

Vijaya, S. V. R., Iniyan, S. & Goic, R. 2012 A review of solar drying technologies. *Renewable and Sustainable Energy Reviews* 16 (5), 2652–2670.

Wang, C. Y. & Singh, R. P. 1978 A single layer drying equation for rough rice. *Transactions of the ASAE* 78 (3001).

Weiss, W. & Buchinger, J. 2004 Establishment of a production, sales and consulting infrastructure for solar thermal plants in Zimbabwe. *Institute for sustainable Technologies* p. 110.

Yeh, H. M. & Lin, C. 1996 The Effect of Collector Aspect Ratio on the collector efficiency of upward-type flat-plate solar air heater. *Energy* 21 (10), 843–850.

Zhu, A. & Shen, X. 2014 The model and mass transfer characteristics of convection drying of peach slices. *International Journal of Heat and Mass Transfer* 72, 345–351.

Zlatanović, I., Komatina, M. & Antonijević, D. 2013 Low-temperature convective drying of apple cubes. *Applied Thermal Engineering* 53 (1), 114–123.

Zomorodian, A., Zare, D. & Ghasemkhani, H. 2007 Optimization and evaluation of a semi-continuous solar dryer for cereals (Rice, etc). *Desalination* 209 (1-3 SPEC. ISS.), 129–135.

Şevik, S. 2014 Experimental investigation of a new design solar-heat pump dryer under the different climatic conditions and drying behavior of selected products. *Solar Energy* 105, 190–205.

List of publications

The results of this PhD thesis have been published in the following papers:

- Blanco-Cano, L., Soria-Verdugo, A., Garcia-Gutierrez, L.M., Ruiz-Rivas, U. Modelling the thin-layer drying process of Granny Smith apples: Application in an indirect solar dryer. *Under review in Applied Thermal Engineering.*

- Blanco-Cano, L., Soria-Verdugo, A., Garcia-Gutierrez, L.M., Ruiz-Rivas, U. 2016. Evaluation of the Maximum Evaporation Rate in Small-Scale Indirect Solar Dryers. ASME Journal of Solar Energy Engineering, 138, 245021-245024.

and presented in the following Conference:

- L. Blanco-Cano, A. Soria-Verdugo, L.M. Garcia-Gutierrez, U. Ruiz-Rivas. Modelling and Design of Indirect Solar Dryers for Batch Drying. Proceedings of the International Conference of Renewable Energies and Power Quality, Bilbao, 2013. Paper No. 542

Other works that the author has published in collaboration during her PhD thesis are:

- Soria-Verdugo, A., Garcia-Gutierrez, L. M., Blanco-Cano, L., Garcia-Hernando, N., Ruiz-Rivas, U. 2014. Evaluating the accuracy of the Distributed Activation Energy Model for devolatilization curves obtained at high heating rates. Energy Conversion and Management, 86, 1045-1049.

- Soria-Verdugo, A., Garcia-Gutierrez, L. M., Blanco-Cano, L., Garcia-Hernando, N., Ruiz-Rivas, U. On the validity of the DAEM Model using low heating rate devolatilatization curves. 8th Conference On Sustainable Development Of Energy, Water And Environment Systems. Dubrovnik, 2013.

- Blanco-Cano, L., Concepcion-Murillo, O., Soria-Verdugo, A., Venegas-Bernal, M., Miranda-Urbina, R., Ruiz-Rivas, U. Evaluación de las posibilidades de secado solar en Nicaragua. VI Congreso Universidad y Cooperación al Desarrollo, Valencia 2013.

- Ruiz-Rivas, U., Blanco-Cano, L., Soria-Verdugo, A., Chinchilla-Sánchez, M. Modelización de bombas manuales para abastecimiento de agua. VI Congreso Universidad y Cooperación al Desarrollo, Valencia 2013

- Martínez-Crespo, J., Chinchilla-Sánchez, M., Bueno-Lorenzo, M., Blanco-Cano, L., Ruiz-Rivas, U. Evaluación del impacto de las asignaturas de cooperación para el desarrollo en la UC3M. VI Congreso Universidad y Cooperación al Desarrollo, Valencia 2013.